A PATIENT-SPECIFIC KNEE MODEL DRIVEN BY IN VIVO KINEMATICS TO BETTER REPRESENT AN ACL-INJURED PEDIATRIC POPULATION

Thesis submitted to the University of Ottawa in partial fulfillment of the requirements for the Master of Science in Human Kinetics

Blake Miller, BSE.ME, EIT

Supervisor: Daniel L Benoit

Committee Members:
Thomas Uchida, PhD
Allison Clouthier, PhD

University of Ottawa
Faculty of Health Sciences
School of Human Kinetics

© Blake Miller, Ottawa, Canada, 2023

Acknowledgements

I would like to first acknowledge the support of my lab mates through this process. I want to thank Céline G with helping to improve my critical thinking and writing ability. Also, I want to thank Farid A for numerous drives to and from the airport, countless laughs, and helping me feel like I belong in this city. Thank you to Claire W, and Nick R, and Teresa F for your early mentorship, you helped me get established early on, at a time when I was working remotely. Thank you, Mike DB, and Chrissy S, for reminding me of the goodness of being a Maritimer. Thank you to Jo G, and Lisa EO, for helping me get set up in the lab, and for being worthy competitors for Uno Fridays. Thank you to Elese SL, Aidan A, and Taylor C, for being my lab mates during the latter part of my degree, being able to mentor all of you through your own research has further reinforced my interest in academia.

Thank you for my thesis advisory committee, Dr. Clouthier, and Dr. Uchida, this project would never have gotten to where it is without your insight. Learning how to articulate my thesis work to experts in my field has been an invaluable skill for me to learn.

Thank you to my parents, who pushed to me to take a leap of faith and join a research lab halfway across the country. Thank you for continuing to push me to continue to do more education, to trade away short-term gain, for a lifetime of learning. Thank you to my partner Ellie, you've been the ligaments to my knee through this process, the one who kept me together through all my tough times.

Thank you to my Fall 2022 biomechanics students who were part of my lab, I had a blast being able to teach you all in person and learning just how many of you had knee injuries, just like myself (seems to be a biomechanics theme…).

Thank you to my supervisor, Dr. Benoit, for your guidance through this process. Thank you for being patient with me, while I moved across the country to start at your lab. Thank you for pushing me to think critically, to think for myself, and most of all, to question everything. Thank you for letting me explore the literature, and find out what truly interests me, rather than simply assigning me a thesis topic, and telling me to complete it. I look forward to further honing these skills during my Doctorate degree.

Finally, thank you to the financial support from the University of Ottawa for providing me with the Admission Scholarship for the duration of my master's degree.

Table of Contents

List of Figures

List of Appendix Figures

List of Tables

Glossary of Terms

Ab/Add	Abduction-Adduction
ACL	Anterior Cruciate Ligament
ACL-D	Anterior Cruciate Ligament- Deficient
ACLi	Anterior Cruciate Ligament Injured
ACL-R	Anterior Cruciate Ligament Reconstruction
AP	Anterior-Posterior Translation
ASIS	Anterior Superior Iliac Spine
CBRU	Clinical Biomechanics Research Unit
CHEO	Children's Hospital of Eastern Ontario
CMJ	Countermovement Jump
CT	Computed Tomography
DoF	Degree of Freedom
DP	Distal-Proximal Translation
DVJ	Drop-Vertical Jump
FACL	Female Anterior Cruciate Ligament
FACLi	Female Anterior Cruciate Ligament Injured
FCON	Female Control
FCONd	Female Control Dominant Limb
FCONnd	Female Control Non-Dominant Limb
Flex/Ext	Flexion-Extension
IE	Internal-External Rotation
IMU	Inertial Measurement Unit
LCL	Lateral Collateral Ligament
MACL	Male Anterior Cruciate Ligament
MACLi	Male Anterior Cruciate Ligament Injured
MCL	Medial Collateral Ligament
MCON	Male Control
MCONd	Male Control Dominant Limb
MCONnd	Male Control Non-Dominant Limb
ML	Medial-Lateral Translation
MRI	Magnetic Resonance Imaging
MSK	Musculoskeletal
PEDI-FABS	Pediatric Functional Activity Brief Scale
PEDI-IKDC	Pediatric International Knee Documentation Committee
PCL	Posterior Cruciate Ligament
PSIS	Posterior Superior Iliac Spine
RMSE	Root Mean Squared Error
SD	Standard Deviation
SPM	Statistical Parametric Mapping
STAPLE	Shared Tools for Automatic Personalized Lower Extremity Modelling
TLEM	Twente Lower Extremity Model

General Abstract

Purpose: Pediatrics and adolescents are at a higher risk to suffer an anterior cruciate ligament (ACL) injury in comparison to their adult counterparts. As well, the rate of injury is increasing. While some of this increased injury rate may be attributed to increased participation in sport, it remains unknown why only some children suffer an ACL injury. Traditionally, surface marker-based motion-capture would be used to determine this difference; however, due to the presence of soft tissue artifact, marker translation may exceed the physiological range of the knee itself. Using OpenSim, the range of motion of the knee was constrained to allow for soft tissue artifact to be reduced. Therefore, the two objectives of this thesis are 1) to create and validate a new OpenSim knee model, and 2) to use this knee model to determine whether differences in knee kinematics and ligament lengths exist between ACL injured and non-injured control pediatrics.

Methods: Manuscript 1 (Chapter 5), focused on the first objective of creating and validating a new OpenSim knee model. Thirty-two healthy pediatric females performed squats, countermovement jumps, and drop-vertical jumps. OpenSim models were made and scaled to each participant and featured a 6-degree-of-freedom knee. Each knee was allowed to move in a manner dictated by published in vivo biplanar fluoroscopy studies. These resultant biplanar fluoroscopy-constrained knee kinematics were then compared to another series of in vivo constraints: bone pin-constrained kinematics. Finally, the length of the four main ligaments of the knee were tracked and compared to existing literature on healthy ligament lengths from extension to deep flexion.

Manuscript 2 (Chapter 6) sought to answer the second question: Are there differences in kinematics and ligament lengths between ACL-injured and uninjured control participants? Forty ACL-injured (20 male, 20 female) and 40 uninjured control (20 male, 20 female) participants completed a countermovement jump, which drove inverse kinematics for the OpenSim model

created in Manuscript 1. Knee kinematics and ligament lengths were compared between male injured to male control, and female injured were compared to female control. To isolate the effect of injury, males were not compared to females.

Results: Starting with Manuscript 1, the squat task had the best agreement between biplanar fluoroscopy and bone pin kinematics, during periods of low knee flexion. At high flexion, the ACL length was shorter than literature data, for all tasks. For Manuscript 2, during the countermovement jump, female control participants obtained greater knee flexion and internal rotation when compared to female ACL-injured participants. For males, there were only small differences in countermovement jump kinematics. For ligament lengths, female controls had longer posterior cruciate ligament lengths, whereas for males, male ACL-injured participants presented with longer ligament lengths for all 4 ligaments.

Conclusion: The thesis results identified how to use deep flexion biplanar fluoroscopy constraints to minimize soft tissue artifact. In comparison to previously established knee bone pin constraints, the biplanar fluoroscopy knee relied more on internal-external rotation and anterior-posterior translation to obtain the required bone positions in OpenSim. This additional anterior-posterior translation also led to the increased shortening of the ACL, as the linear distance between ligament insertion points decreased. Next, this thesis identified small differences in kinematics between ACL-injured and control pediatric females during a countermovement jump, where control participants obtained greater knee flexion in the preparatory and landing phase of the task. Few differences in kinematics were found in males. Differences in ligament lengths between injured and control groups were based on differences in knee kinematics, or by participant anthropometrics; taller participants had longer ligaments.

1.0 Rationale

The anterior cruciate ligament (ACL) is the most injured ligament in the knee (Majewski et al., 2006) with rising injury rates in the pediatric population (Arbes et al., 2007; Beck et al., 2017; Frank & Gambacorta, 2013; Herzog et al., 2017; Shea et al., 2004). There is a lack of understanding as to why ACL injury rates are rising in this population which could be elucidated with a better understanding of the mechanics of the tissue during high-risk activity. This is complicated by the complexity of the ligament and the inherent difficulty in measuring the length and strain of the ACL due to its location in the body.

Several methods to measure strain in the ACL have been used in literature, such as in vivo (live participant), in vitro (cadaver-based), and in silico (computer simulation). For in vivo studies, it is both difficult and invasive to measure ACL behaviours in live participants as the typical method for measurement involves the surgical placement of a strain gauge on the anterior-medial bundle of the ACL (Cerulli et al., 2003). In contrast, cadaver studies allow the measurement of all internal ligament properties but are limited by both the age of the cadaver (e.g., typically older population) and by their level of intactness at the time of testing (Krosshaug, 2005). Finally, computer-based simulation software such as OpenSim (Delp et al., 2007) or AnyBody (AnyBody Technologies, Denmark) allow for simulation of dangerous conditions that could lead to an ACL injury such as an extreme external rotation of the knee (Neumann, 2010).

Several studies have reported strong agreements in results calculated using both OpenSim and AnyBody (Ghezelbash et al., 2020; Trinler et al., 2019). From a publication count point of view, a search of terms "OpenSim" yielded 402 article results on PubMed whereas "AnyBody modelling" only yielded 205 article results. This increase in publication count may be due to the

open-source nature of OpenSim and the ease of access of the program itself and set guidelines for optimal model design and use (Hicks et al., 2015). With the goal of making a model that may be used by individuals with a variety of technical backgrounds, OpenSim is the preferred software. However, OpenSim is not without its own limitations.

The drawback to most OpenSim models is that most existing models were created for an adult population with no prior injuries. As well, most default OpenSim models use cadaver-based data to infer knee motion during the calculation of inverse kinematics (Rajagopal et al., 2016), which is an issue as cadavers are often from an older population. These are all limitations when trying to model both a pediatric population and a pediatric population with an ACL injury as knee kinematics will likely change in response to the loss of the ACL (Zabala et al., 2015).

As the calculation of inverse kinematics is often the first step to other operations in OpenSim, it is crucial that the calculated knee kinematics are as accurate as possible. Therefore, this thesis proposes the creation of a new knee model, one designed specifically for a pediatric population with an ACL injury, as to our knowledge, there are no existing models for this specific group. The new knee model used in vivo data, rather than the cadaver data that drives the Walker knee model (Walker et al., 1988), which is used in the popular Rajagopal full-body model (Rajagopal et al., 2016). This new knee model will then be used to accurately test for differences between ACL-D and control (CON) pediatric participants, with the goal of highlighting any knee kinematic changes that may have resulted from an ACL injury. Both male and female participants will be used. However, due to physiological differences between the two sexes, injury comparisons will be sex specific (Del Bel et al., 2018; Otsuki et al., 2021).

2.0 Literature Review

2.1 Pediatric ACL injury risk

ACL injuries in the pediatric population are on the rise illustrated by an increase of 37% in ACL tears between 2002 and 2014 (Herzog et al., 2017). The rates of pediatric ACL injuries have also significantly increased in comparison to adults over the same period (2007-2011) (Herzog et al., 2018). This is coupled with a reported one-in-three chance of a secondary tear following ACL reconstruction surgery for patients who return to sport (Dekker et al., 2017; Paterno et al., 2014). Additionally following an ACL tear and reconstruction the risk of early onset osteoarthritis severely increases for adolescents (Dekker et al., 2017; Majewski et al., 2006).

Several factors have been proposed as to why the rates of ACL injuries are increasing in the pediatric population. One such factor is the increased participation in physical activity at younger ages (Costa et al., 2017; Ladenhauf et al., 2013), noting that physical activity affects skeletal development (Carsen et al., 2021). Another risk factor in the pediatric population is the changes the body goes through during puberty (Hewett et al., 2012; Shea et al., 2004), such as changes in how the muscles activate in reaction to external forces to ensure joint stability, also known as neuromuscular control (Hewett, et al., 2004; Hewett et al., 2005). Poor neuromuscular control can lead to the inability of muscles to compensate for forces at the joint which can result in the ligaments experiencing higher loads (Alentorn-Geli et al., 2009; Withrow et al., 2008). To better understand how an ACL injury and/or puberty can affect the stability of the knee, it is important that we first understand the mechanics of the pediatric knee itself.

2.2 The functional role of knee ligaments

The knee is a complex joint that includes four main ligaments: the anterior cruciate ligament (ACL), the posterior cruciate ligament (PCL), the medial collateral ligament (MCL) and

the lateral collateral ligament (LCL). All four ligaments serve to restrict tibiofemoral motion, but each ligament has a more specific function. From a mechanical perspective, the primary function of the ACL is to prevent excessive anterior translations of the tibia relative to the femur while the primary function of the PCL is to prevent excessive posterior translations of the tibia (Neumann, 2010). The secondary function of the ACL and PCL is to resist extreme internal and external rotation (Woo et al., 2006). The primary function of the MCL is to resist knee adduction moments with a secondary function of resisting external rotation. Finally, the primary function of the LCL is to resist knee abduction moments with a secondary function to resist internal rotation (Neumann, 2010). In addition to their inherent structural importance in resisting excessive tibiofemoral motion, the four knee ligaments also contain mechanoreceptors which contribute to proprioception (feedback of joint position to the muscles) of the knee itself (Neumann, 2010). Of the four main ligaments, the ACL is the most likely to be injured (Majewski et al., 2006). When the ACL is torn the remaining ligaments often endure higher loads especially for internal-external rotation movements of the knee (Amis, 2017).

Overall, the ligaments of the knee are crucial structural components which are stiff enough to prevent excessive separation between the femur and tibia during normal uninjured motion. As well, the healthy ligaments can undergo various amounts of strain and cyclic loading before failure. However, there are few studies that have been able to define true in vivo strain of the ligaments and the exact failure mechanics of the ACL are still relatively speculative (Renstrom et al., 2008). This is likely due to the difficulty of measuring strain through traditional engineering methods such as through the placement of a strain gauge directly onto the surface of the ACL (Cerulli et al., 2003). Instead, estimations of ligament strain have been based on the change in femoral and tibial insertion points of the ligaments (Smale et al., 2019). For this method to be an effective

approximation of ligament strain, accurate knee kinematics are required. There are three methods to determine knee kinematics: through in vivo (live) testing, in vitro (cadaver) testing, and in silico (computer simulation) testing.

2.3 In Vivo Knee Motion

In vivo data comes directly from a live participant instead of being calculated (in silico) or obtained from a cadaver (in vitro). To obtain valid in vivo motion of how the tibia moves in relation to the femur we must be able to look past the skin. While knee flexion and extension may be easily discernible by the human eye, the remaining 5 degrees of freedom (abduction-adduction (ABD-ADD), internal-external rotation (IE), medial-lateral translation (ML), anterior-posterior translation (AP), and distal-proximal translation (DP)) are far less evident and difficult to measure due to the presence of soft tissue artifact (Leardini et al., 2005). Existing literature has highlighted the two main methods of obtaining in vivo knee motion: using intercortical bone pins and using biplanar fluoroscopy (Gasparutto et al., 2017).

2.3.1 Intercortical bone pins

To circumvent the errors of soft tissue artifact and the subsequent error of calculating femur and tibia motion based on surface-based markers, intercortical bone pins (attached to marker clusters) can be tapped directly into the femur and tibia bones under the presence of localized anesthetic (Benoit et al., 2006). Early studies involving bone pins focused on reporting true in vivo knee kinematics instead of simple skin marker-based kinematics which were prone to error (Lafortune et al., 1992). More recent works focused more on the frontal-plane kinematics of the knee during cutting tasks (Benoit et al., 2006). Benoit et al. (2006) provided an in-depth examination of the error obtained when comparing skin-based markers to intercortical bone pin markers and found the results as displayed in Table 1.

Table 1: Recreation of table of maximum absolute rotational and translational error between skin-based markers and intercortical bone pin markers for a cutting task as reported by Benoit et al. (2006). Only the maximum values were taken from the original table as Benoit et al. (2006) reported both side cuts and a walking task at foot strike, mid-stance and toe-off. The following abbreviations are used: Flex/Ext = Flexion-extension, Abd/Add = Abduction-adduction, Int/Ext = internal-external rotation, Med/Lat = medial-lateral translation, Ant/Post = anterior-posterior translation, Dist/Comp = distraction-compression, 1 SD = 1 standard deviation.

Rotations (Mean ± SD) [degrees]			Translations (Mean ± SD) [mm]		
Flex/Ext	Abd/Add	Int/Ext	Med/Lat	Ant/Post	Dist/Comp
4.2 (2.7)	13.1 (9.8)	3.3 (1.8)	13.9 (10.1)	16.1 (8.9)	8.3 (6.2)

From Table 1, with rotational errors as high as 13.1 degrees for abduction-adduction and translational errors as high as 16.1 mm for anterior-posterior translation, additional steps must be taken to mitigate soft-tissue artifact. While the usage of bone pins does provide an effective method to circumvent soft tissue artifact, it is also an invasive method. The installation of the bone pins into the target site requires surgery which could cause discomfort and could affect natural knee motion (Gasparutto et al., 2017).

2.3.2 Biplanar fluoroscopy

The second method of obtaining in vivo data is using biplanar fluoroscopy where two different planes of x-rays using multiple exposures to provide time-sequenced images. Selvik. (1989) presented a summary of the history of using x-rays to track joint motion which ran parallel with the founding of x-ray technology. Early studies focused on tracking basic objects with two x-ray beams with specific "calibration cages" (Selvik., 1989). As well, early studies used implanted tantalum balls to track changes in knee kinematics during different loading conditions and to measure knee flexion angles (Karrholm et al., 1988). However, these studies were unable to track dynamic motion of the knee which likely due to the computing ability of the time of the study. Later studies (Tashman & Anderst, 2003; Tashman et al., 2004) addressed the issue of capturing dynamic motion with biplanar fluoroscopy via high-speed video radiography using implanted tantalum beads and combined with computed tomography (CT) which is used to identify the bone

shapes that will be tracked from the radiograph. However, these studies still relied on surgical methods such as the implantation of tantalum beads into the bone to define an anatomical reference system.

More recent studies have continued the protocol defined by Tashman et al. (2004) but have moved away from the invasive surgical installation of tantalum beads. Instead, recent studies have focused on utilizing software to define anatomical coordinate systems (Deneweth et al., 2010; Gray et al., 2019; Miranda et al., 2013; Miyaji et al., 2012; Murakami et al., 2016). These studies have used CT scanning of participants' bones to define anatomical coordinate systems and then overlayed the bones onto the frames captured by the biplanar fluoroscopy. This provides a non-invasive method to accurately determine knee motion while still obtaining accurate results. This method can also be used to estimate knee ligament lengths by determining the distance between ligament insertion points (Li et al., 2004; Park et al., 2006). While the process of biplanar fluoroscopy is still somewhat invasive due to the exposure to ionizing radiation on the area of focus (Johnson et al., 2001), this process does not require the invasive surgery that is involved with implantation of bone pins.

Overall, in vivo studies provide the most accurate data of how the knee moves but due to the obvious ethical constraints, these studies cannot be designed to intentionally injure the participant (such as removing the participant's ACL) and then continue testing, as to examine changes that have occurred. Cadaver models and computer simulations can be used to bridge this gap.

2.4 In Vitro Knee Motion

Using cadaver models, it is possible to simulate various conditions that would not be deemed ethical for a live participant. Examples of this could be the removal of a ligament in the knee or subjecting the knee to immense loads that would cause injury. Typical cadaver studies involve the placement of a knee cadaver in an apparatus designed to move the knee into flexion and extension while the motion is measured (Woo et al., 1999). Motion can be measured through the implantation of bone pins (Walker et al., 1988), specific loads (Markolf et al., 2004), or through traditional motion capture (Blaha et al., 2003). Such studies allow for the direct measurement of knee kinematics as well as the direct measurement of ligament mechanics. It is also possible to simulate conditions that could lead to a ligament rupture or to simulate conditions where the ACL has been completely removed from the knee.

Despite the wide variety of tests that can be performed on cadaver models, they are not without their limitations. Cadavers typically come from an older population which may not make them suitable to model a younger population due to changes in bone geometry and muscle composition from aging (Larsson & Karlsson, 1978). As well, it is difficult to simulate true knee motion with most apparatuses that are designed for cadaver testing as knee motion is driven by musculature and not external hinges. To achieve "natural knee motion", linear motors for all muscles that cross the knee would be required and not just the quadriceps and hamstrings (Markolf et al., 2004). To circumvent the physical limitations of the apparatuses for cadaver studies, another approach is to digitize and simulate such models via musculoskeletal modelling software.

2.5 Computer-Based Musculoskeletal modelling

Computer-based musculoskeletal (MSK) modelling involves the process of approximating the physiological characteristics of the human skeleton as a series of individual bodies. The concept of multibody dynamics has its foundations in Newtonian physics but given the vast number of calculations required, the complexity (number of rigid bodies present) of models has been limited by computational power. In addition to the calculation of multibody kinematics (to approximate joint angles and translations), force-generating musculature can be added to obtain the dynamics of the system (such as individual joint loading). The most widely used model for muscle approximation is the Hill-type muscle model (Hill, 1938) which requires numerous calculations to estimate the amount of force generated by the muscle. This model depends on several factors such as the length and velocity of the muscle as well as the muscle's activation (Zajac, 1989). However, despite the numerous calculations that must be performed, previous studies have designed software to offload these calculations to a computer program through software such as OpenSim (Delp et al., 2007).

2.5.1 Common musculoskeletal models used in OpenSim

A musculoskeletal model is required to perform calculations in OpenSim. An OpenSim musculoskeletal model consists of a tree of bodies linked by joints and constraints. As well, bodies are visually represented by bone geometry. The more bodies present, the more complicated a simulation can become as more bodies must be tracked (Hicks et al., 2015). In addition to body segments, muscles are often included which are represented as linear actuators that span physiological insertion points (Delp et al., 2007). The current online OpenSim musculoskeletal model repository (SimTK) features models with varying numbers of muscles. For example, in the gait2354 model (Anderson & Pandy, 2001) there are 23 degrees of freedom and 54 muscles

present. This model simplifies muscle groups (the quadriceps, hamstrings, etc.) down to fewer muscles. Due to the removal of several muscles, the model is also more computationally efficient. On the other end of this spectrum is the Rajagopal model (Rajagopal et al., 2016) where there are 30 degrees of freedom and 80 muscles present. With nearly double the number of muscles, the computation time for a simulation is increased by 11% (as reported by the authors) but allows for the simulation of more lower body muscles (all four quadriceps and all hamstrings, and so on). These models are modifiable by the user such that knee ligaments can be added to further constrain the knee (Lenhart et al., 2015; Marra et al., 2015; Smale et al., 2019; Xu et al., 2015). However, to obtain meaningful data such as changes in ligament length or knee joint kinematics, simulations of multibody dynamics over a time series must be performed.

2.5.2 Simulation methods in OpenSim

The most common starting point for simulations via OpenSim is through the usage of inverse kinematics (Hamner et al., 2012). Inverse kinematics are calculated with knowledge of the position of one rigid body with respect to another. This can be calculated using either position and orientation data from inertial measurement units (IMUs) or through the placement of spherical markers directly onto the body collected using marker-based motion capture. Currently, marker-based motion capture systems such as Vicon (Oxford Metrics, Oxford, UK) are still preferred over IMU systems due to their increased accuracy (Brodie et al., 2008). Using the spherical marker-based approach, the inverse kinematics function in OpenSim attempts to fit a scaled rigid-body model to supplied marker motion paths. This can then be used to calculate inverse kinematics which results in joint angles and translations over time. This resultant data can then be used with the addition of force plate data to infer joint moments (Robertson, 2004), or be used in static optimization to approximate muscle activation and the corresponding muscular forces. Finally,

using the instantaneous pose of the rigid bodies, point kinematics can be calculated using the *analysis operation* to track the position of a point on one rigid body in reference to a point on another rigid body throughout a trial. By placing a point on the origin and insertion centroids of a ligament, this method can be used to approximate the changes in ligament length (Li et al., 2004; Park et al., 2006). Then by tracking each point with respect to a known fixed-point such as the origin of a laboratory reference frame, the ligament length can be estimated as the distance between the two points throughout the entire trial (Smale et al., 2019). It is important to note that this approach provides an approximation of ligament length and as this method is directly dependent on inverse kinematics. Any error associated with inverse kinematics will carry forward into any further calculations (Hicks et al., 2015). Therefore, to obtain the best estimations of ligament lengths, inverse kinematics errors such as soft tissue artifact from the usage of surface markers must be minimized (Andersen, 2009; Benoit et al., 2006).

To counter the issue of soft tissue artifact, the skin marker data obtained in vivo in addition to bone pin or x-ray data can be directly implemented into OpenSim. For example, the Rajagopal model (Rajagopal et al., 2016) utilizes constraints derived from the Walker knee model which used 23 cadaver knees instrumented with bone pins (Walker et al., 1988). The usage of the Walker knee allows for the knee flexion angle to be related to the remaining 5 degrees of freedom (DoF) at the knee while ensuring that the remaining 5 DoF remain constrained during inverse kinematics. While this method vastly simplifies the complex kinematics of the knee, the alternative of "unlocking" all DoF at the knee (removing all range-of-motion constraints) results in highly unphysiological motion (Smale et al., 2019). Therefore, the optimal solution may be somewhere in between these two methods (locking and unlocking the DoFs).

2.5.3 Modifying the modelled range of motion for the knee

Instead of completely locking DoF of the knee (turning it into a pin joint) or unlocking the knee (allowing the tibia to move freely through space in reference to the femur) the kinematics can also be restricted to physiological ranges. This method was performed previously, where depending on the knee flexion angle, upper and lower bounds were defined for the remaining 5 DoF at the knee (Potvin, 2016). The upper and lower bounds were based on bone pin ranges of motion derived from gait and cutting tasks (Benoit et al., 2006). By limiting the range of motion for each DoF depending on the knee flexion angle, the knee ROM becomes bounded, as the inverse kinematics simulation is free to move the knee in all 6 DoF, but the knee will not be allowed to move in ways that defy physiology of a healthy participant. However, this method has two drawbacks. Firstly, it is more computationally expensive to assign ranges to each DoF instead of using an ideal knee joint, such as a pin joint (Hicks et al., 2015). As well, this method was previously established for cutting tasks with low knee flexion (approximately 40 degrees) and has not been verified for high knee flexion tasks (Potvin, 2016). To extend the curves that define the relationships between knee flexion angle past the 40 degrees used in Potvin. (2016), a curve fit must be done on the available in vivo data from literature.

There have been few studies that have examined the relationships between higher knee flexion and the remaining 5 DoF at the knee using biplanar fluoroscopy imaging combined with CT-fitted bones. Such studies included 15 healthy adults performing gait up to 80 degrees knee (Gray et al., 2019), 5 where healthy young adults performing squats up to 140 degrees of knee flexion (Murakami et al., 2016) and finally, a study with 7 young healthy adults performing single-legged lunges up to 135 degrees of knee flexion (Qi et al., 2013). The results of these studies indicate a wide range of secondary knee motions where the range of motion changes throughout knee flexion.

This contrasts with the Walker knee model used in OpenSim, which applies a single value of each secondary knee motion based on knee flexion. However, it remains unknown whether this data can be added as constraints into OpenSim and whether it can be used during inverse kinematics simulations. To test this, several dynamic tasks with squatting components should be simulated through inverse kinematics.

2.6 Dynamic Tasks

To simulate high knee flexion range of motion, tasks such as squatting are useful. However, tasks that include a squat and a landing component such as countermovement jumps or drop-vertical jumps can be practical for ACL injury research as landings with full knee extension are a common ACL injury mechanism (Paterno et al., 2010). To validate a new knee model, it should be capable of modelling a simple squat to progressively complicated tasks such as a drop-vertical jump with reasonable physiological agreement (Lund et al., 2012).

2.6.1 Bilateral Squats Task

Squats are a commonly used task during mid-stage ACL rehabilitation (Bynum et al., 1995; Wright et al., 2015) as they are a closed-kinetic-chain task involving multiple joints that must work in unison to successfully complete the task (Salem et al., 2003). The squat task is broken up into two distinct phases. In the first stage the participant lowers down flexing at their knees and flexing their hips resulting in the activation of the hamstrings and the gastrocnemius to drive the knee flexion. In the second phase the participant stands back up by extending at their knees and hips. Overall, the squat itself is a simple task which poses less of a threat to the ACL in comparison to landing tasks such as a countermovement jump or a drop-vertical jump.

2.6.2 Countermovement Jumps

Countermovement jumps (CMJs) are a popular rehabilitation task involving both a squat and a jump which are two common movements in sport (Costley et al., 2021; Dai et al., 2021). Such examples in sport could be a 3-pointer in basketball or a vertical leap to catch a ball in football or baseball. This dynamic task involves multiple joints working in unison to successfully complete the task. The CMJ itself is broken up into six distinct phases: First, a stage where the participant is at rest; then an unweighting phase occurs where the participant lowers their centre of mass and flexes at their knees and hips. Following this, the third phase involves braking in which the downwards linear velocity returns to zero whilst potential energy is stored in the springlike components of the lengthened quadriceps. Then, the explosive propulsive phase occurs in which the participant accelerates upwards by rapidly extending at their knees and hips. Following the propulsive phase, the participant remains in the air during the flight phase in which they follow a vertical parabolic trajectory. Finally, the participant lands in the landing phase in which the linear velocity rapidly returns to zero resulting in a spike in ground reaction force (Chavda et al., 2018).

2.6.3 Drop-Vertical Jumps

A drop-vertical jump (DVJ) is a commonly used task in ACL rehabilitation (Hewett et al., 2005) as it requires both stability and adequate neuromuscular control to successfully complete the task (Kemp & Benoit, 2020; Romanchuk & Benoit, 2019). The DVJ consists of the following steps: first, the participant steps off a raised platform. Then, they land with two feet onto an in-ground force plate (one foot on each force plate; "drop landing") immediately performing a maximal vertical jump and finally landing back onto the force plates with one foot on each plate ("jump landing") (Hewett et al., 2005). While the DVJ is a common task for ACL rehabilitation, it also has greater variance than a simple squat task due to the presence of a landing phase.

2.7 Pediatric knee modelling

In summary, there is a need to create a better OpenSim model to represent both an ACL-injured participant and a pediatric participant. Given the variability amongst these participants due to the presence of an ACL injury or simply the effect of puberty, it is essential that any new model must allow for a wide potential range of motion at the knee while remaining biofidelic. A knee model incorporating the range of motion limits identified through in vivo studies for all degrees of freedom can serve as the basis for further analysis of the pediatric and ACL-injured population during dynamic tasks.

3.0 Objectives and Hypotheses

3.1 Study Objective

The overall objective of this thesis was to improve the estimation of knee joint rotations and translations during movements with deep knee flexions by developing, implementing, and applying a novel 6DoF knee joint constrained to move within the ranges of motion identified through in vivo studies The model will be applied in OpenSim (Delp et al., 2007) and used to estimate the kinematics of adolescent participants during a variety of dynamic tasks. If the model is shown to be valid (*Study 1*), the second main objective will be to compare the knee kinematics and ligament lengths between ACL-deficient (ACL-D) and non-injured control (CON) adolescent participants during clinically relevant dynamic tasks (*Study 2)*.

3.2 Research questions and hypotheses

Question 1) Does a knee joint kinematic model derived from biplanar fluoroscopy data and applied through the OpenSim modeling framework yield physiological knee ligament lengths during dynamic tasks?

The concept of a partially unlocked knee model was previously created in our lab (Potvin, 2016; Smale et al., 2019). The model used by Potvin. (2016), and Smale et al. (2019) was designed specifically for a cutting task and used bone pin data to infer in vivo kinematics up to 45 degrees of knee flexion (Benoit et al., 2007). Since it is well-established that the knee will continue to rotate and translate as it continues to flex, in vivo data for higher range of motion tasks may be required to extend the knee model (Gray et al., 2019; Murakami et al., 2016; Qi et al., 2013). Therefore, when comparing the previous bone pin constraints to the high flexion biplanar fluoroscopy constraints, it was hypothesized that the bone pin constrained knee would abduct significantly more than the biplanar fluoroscopy constrained knee (H1a_study 1). Secondly as the biplanar fluoroscopy constrained knee data from Qi et al. (2013) involved a deep knee flexion, it was hypothesized that the biplanar fluoroscopy constrained knee would have greater posterior translation of the femur and greater external rotation, as seen with other fluoroscopy literature (Murakami et al., 2016) (H1b_study 1).

To validate the knee of the new OpenSim model, the resultant ligament lengths were compared to existing literature featuring in vivo biplanar fluoroscopy on healthy ligament lengths during high knee flexion (Li et al., 2004; Park et al., 2006). Using CON participants, knee kinematics and ligament lengths were simulated for three high knee flexion tasks to determine the versatility of the model (Lund et al., 2012). Finally, it was hypothesized that the more complex of the high knee flexion tasks would have the greatest root mean squared error between calculated and literature ligament lengths (H1c_study 1).

Question 2) Do knee kinematics differ between ACL-injured and non-injured adolescents during countermovement jumps when assessed using a 6-DoF OpenSim knee model?

It is unclear how the presence of an ACL injury will affect the kinematics of the knee as previous studies did not apply in approaches to mitigate soft tissue artifact (Andriacchi & Dyrby, 2005; Beck et al., 2017; Chaudhari et al., 2008; Frank & Gambacorta, 2013; Georgoulis et al., 2003; Solomonow et al., 1987). By using the updated partially unlocked knee model constrained with in vivo constrains, kinematic and ligament length differences were explored between ACL-D participants and healthy CON participants. This was done with the assumption that the partially unlocked knee model was sensitive enough to detect potential differences between groups. To quantify potential differences between ACL-D and CON participants, the CMJ task was performed instead of a squat. The CMJ included a landing component which was more representative of the dangerous loading conditions that could lead to an ACL injury (Hewett et al., 2004). All six knee degrees of freedom were analyzed as well as the resultant changes in ligament length. It was reported by Andriacchi et al. (2005) that IE rotation and AP translation were altered due to the presence of an ACL injury in an adult population during normal gait. Several other studies have reported similar findings in the adult population showing that the presence of an ACL injury reduces AP and ML translation ROM (Li et al., 2006; Scarvell et al., 2005). As well, numerous studies have documented knee abduction as a major contributor to an ACL injury (Ford et al., 2010; Hewett et al., 2009; Levine et al., 2013). Therefore, it was hypothesized that FACL and MACL participants will have significantly smaller knee translations and rotations then their control counterparts as seen in literature for young adult participants (Yamazaki et al., 2010) (H1a_study2). Additionally, due to ligament lengths being calculated based on knee kinematics, it was also hypothesized that ACL-injured participants would have less change in simulated ligament length than healthy control participants (H1b_study2).

4.0 Methods

4.1 General Methodology

This thesis made use of data collected from a larger study involving the collaboration between University of Ottawa Clinical Biomechanics Research Unit (CBRU) and the Children's Hospital of Eastern Ontario (CHEO). The research program followed a test-retest design whereby ACL-deficient (ACL-D) and healthy control (CON) participants completed a series of isometric strength, functional movement, and endurance-based tasks. Additionally participants completed a series of patient-reported outcome forms as to assess knee function (PEDI-IKDC, (Kocher et al., 2011)), activity level (PEDI-FABS, (Fabricant et al., 2013)), level of sport performance (Tegner Activity Level Scale, (Lysholm & Tegner, 2007)), and stage of puberty (Tanner Stage, (Marshall & Tanner, 1969; Marshall & Tanner, 1970)). ACL-D patients were recruited through CHEO where they were referred to the program by orthopaedic surgeons. These participants were tested prior to their surgery (T1) approximately eight to twelve months following ACL reconstruction (ACL-R) surgery following clearance for return-to-play by their attending orthopaedic surgeon (T2) and one year after their T2 visit (T3). For this thesis the focus will be on participants who were tested prior to their surgery (T1). Both male and female ACL-D participants will be considered and compared to control participants, who have not sustained an ACL injury. Uninjured control participants were recruited from the Ottawa/Gatineau region with the requirement that the participants have been actively participating in an organized sport as an attempt to match the activity level of the ACL-D group. As well, controls were matched with the ACL-D group based on height, weight, age, Tanner stage (puberty stage), limb dominance and activity level. The exclusion criteria for the control group were a history of lower body injuries within the last year. This study was approved by both the CHEO (17/74X) and University of Ottawa (H09-17-10) ethics committees.

4.2 Participants for the study

For the first question proposed in addition to root mean squared error (RMSE) calculation, the objective was to check for significant differences between bone pin and biplanar fluoroscopy constraints for the proposed model. An a-priori test for a two-tailed paired-samples (matched pairs) t-test was performed on G* Power (Faul, 2007). To determine the required number of participants, effect size, an α value (type I error, false positive probability) and statistical power ($1 - \beta$, where β is the type II error, false negative probability) are required. The α-value was set at 0.05 and a power value of 0.8 was chosen while the effect size was set at 0.7 which is a medium effect size per Cohen's definition (Cohen, 1992). This effect size was based on the average effect size reported by Khuu et al. (2016) which was a study that examined kinematic differences between limbs during squats, for young adult females. With these values, 39 participants were required. Each of these participants required a custom knee joint model.

For the second study, the objective was to measure the kinematic differences and ligament lengths for male ACL-D vs. male CON, and female ACL-D vs. female CON. This resulted in four groups in total. Therefore, using G* Power, an a-priori test for a two-way ANOVA, with four groups, an effect size of 0.5, an α error probability of 0.05, and a power of 0.95, the required sample size was 76 (19 participants per group). Participants were required from each of the four following groups: male ACL-injured (MACL), female ACL-injured (FACL), male control (MCON), female control (FCON).

4.3 Participant preparation for data collection

The following lower body anthropometrics were collected: the distance between their left and right anterior superior iliac spine (ASIS), the distance between their left and right PSIS, their left and right leg length (defined as the distance from the ASIS to the medial malleolus), the length of

the tibia (the distance from the tibial condyle to the lateral malleolus), as well as the knee and ankle width, and thigh and shank circumferences were measured. These anthropometric measurements served as reference values during the scaling process for OpenSim. Following this, participants completed a five-minute warmup on a stationary bike and then began the kinematic tasks.

Full body kinematics were recorded by placing 84 retroreflective markers (14 mm diameter) on anatomical landmarks according to a hybrid-cluster marker set (Figure A 9.1) adapted from Mantovani & Lamontagne. (2017). Marker trajectories were recorded at 200 Hz using a 10-camera infrared motion analysis system (8 Vero and 2 Vantage cameras; Vicon, Oxford, UK) and its supporting software (Nexus, v2.8, Vicon, Oxford, UK). Force plate data (Bertec 4060, FP4608-08, Bertec Corp., Columbus, OH, USA) were simultaneously collected using Nexus at 1000 Hz, as well as electromyography data (not used in this study).

4.4 Movement protocol

Once the marker set was placed and the participants had time to warm up on the bike, they were asked to perform a squat, a CMJ, and a DVJ task in addition to several other functional and strength assessments (which were not included in this thesis). For the squat, participants were instructed to look forward and place their hands on their heads and go into a controlled squatting motion as far down as they comfortably felt like going while maintaining a constant speed throughout the entire task. For the CMJ, the participants were instructed to place one foot on each force plate with the goal of jumping as high as they could by performing a countermovement (squat-like motion) prior to the jump. No specific depth of the countermovement was requested. Participants were instructed to look forward for the entire task with their hands on their head. Finally, for the DVJ task, participants were asked to step off a bench and land on a set of force plates and then jump as high as they could and finally land back on the same force plates. The

bench was raised to the height of their tibial lateral condyle. In total, five successful squats, CMJs, and DVJs were required; a successful attempt was denoted as one where balance was maintained throughout the entire trial.

The kinematic data was then labelled offline using Nexus Version 2.7 and the marker trajectory and force plate data was then saved as a c3d file for further analysis using custom MATLAB code to calculate the whole-body kinematic data. This kinematic data and the force plate data was then input for the inverse kinematics function in OpenSim (Delp et al., 2007).

4.5 OpenSim model

There have been several other OpenSim models that make use of knee ligaments such as the Xu model (Xu et al., 2015). This model was previously used by Potvin. (2016) in which the partially unlocked knee was first used for a cutting task. This model utilized bone pin constraints taken from Benoit et al. (2006) in which intercortical pins were tapped directly into the femur and tibia of young healthy adults. Following this, the Rajagopal model was introduced, which included additional redundant muscles and physiological wrapping surfaces for muscle paths (23 DoF, 80 muscles) (Rajagopal et al., 2016). Then, Smale et al. (2019) added knee ligaments to the Rajagopal model. Therefore, the OpenSim model which was used for this work was a modified Rajagopal model (23 DoF, 80 muscles) (Rajagopal et al., 2016).

The modified version of the Rajagopal model included a partially unlocked knee model as seen in a previous work from our lab (Potvin, 2016; Smale et al., 2019). However, unlike Potvin. (2016) and Smale et al. (2019), this model utilized full lower-body high-resolution bones, and biplanar fluoroscopy knee constraints instead of bone pin constraints. High resolution bones were MRI bone geometry taken from existing literature (TLEM bone geometry set) (Modenese & Renault,

2021). Figure 4.1 shows the distribution of bones taken from the STAPLE pipeline as well as the default OpenSim geometry.

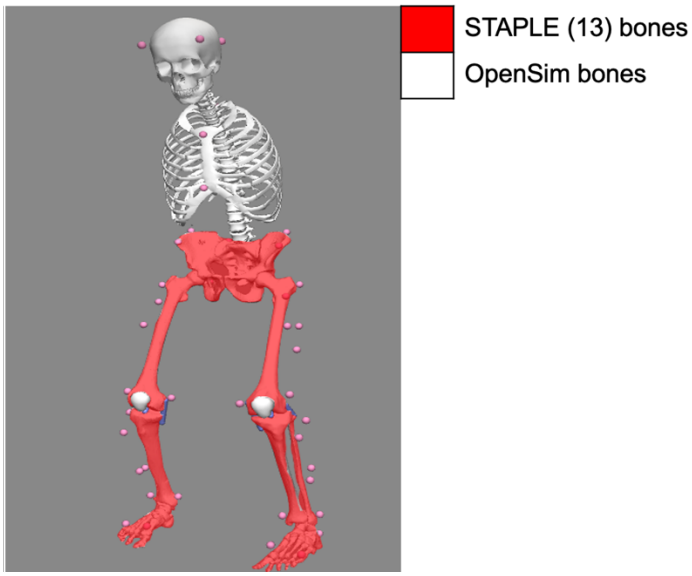

Figure 4.1: The modified Rajagopal model used in this thesis, which features a combination of high-resolution STAPLE pipeline bones in red (from the TLEM set) and low-resolution bones from the default OpenSim set (in white).

Secondly, using the partially unlocked knee model, knee flexion-extension angles were related to the remaining 5 DoF at the knee via biplanar fluoroscopy constraint from literature. The biplanar fluoroscopy curves presented in Qi et al. (2013) were used as the baseline for defining the relationships between knee flexion angle and the remaining 5-DoF at the knee. Qi et al. (2013) was chosen as it featured young healthy male and female adults performing single-legged-lunges in which participants obtained knee flexion angles as high as 150 degrees flexion. However, Qi et al. (2013) did not report the relation between distal-proximal translation vs. knee flexion. Therefore, curves for distal-proximal translation vs. knee flexion were based on the reported data of Gray et al. (2019) a study involving healthy adults performing gait in front of a mobile biplanar fluoroscopy setup. In contrast to the Walker knee from the Rajagopal model which simply relates knee flexion to a single value for the other 5 DoF, the standard deviation of the curves from Qi et

al. (2013), and Gray et al. (2019) provided a range of potential outputs as previously performed by Potvin. (2016) and Smale et al. (2019).

All knee kinematics reported by Qi et al. (2013) were from healthy motion which did not result in an injury. This proved that there can be a range of healthy values (translations, rotations) for any knee flexion. This outcome directly contrasts Walker et al., 1988 which used a polynomial equation to relate knee flexion to a single value for each of the remaining 5 knee. To allow variation between participants in all six degrees of freedom at the knee, data from Qi et al. (2013) and Gray et al. (2019) was used to relate knee flexion to the remaining 5 degrees of freedom.

Next, ligament lengths were determined by using the point kinematics analysis option. The point kinematics function tracks a point in space throughout a specific simulated task such as the inverse kinematics simulation of a CMJ. Ligament insertion points were determined based on one participant's MRI. Then, OpenSim markers were placed on the centroid of the ligament insertions (Li et al., 2004; Park et al., 2006; Smale et al., 2019). Next, the location of each insertion point was related to the OpenSim default parent-axis location of the knee (midpoint between the femoral condyles). The OpenSim GUI was then used to identify marker locations on the lower-body bones in the newly modified Rajagopal model. Finally, the model was scaled to each participant based on their standing reference trial.

4.6 Data analysis

Knee kinematics: To implement the partially unlocked knee model in OpenSim, the remaining knee ROM were set depending on the knee flexion angle calculated from inverse kinematics. Using an updated version of pre-existing code (Potvin, 2016), an upper bound and lower bound were calculated for each DoF depending on the knee flexion angle. For example, when the knee is at 30

degrees flexion then the knee internal-external rotation angle would be between 0 and 12 degrees of rotation (Qi et al., 2013). The range of motion was calculated for each frame of the simulation depending on the previous frame's knee flexion angle. Then, inverse kinematics were computed for a single frame using the range of motion defined by the prior frame's knee flexion angle. This allowed for the model's knee markers to be moved over a range of values as to minimize the error between experimental and theoretical marker placement (least squares error) (Delp et al., 2007). This process was performed for the entire series of frames. The result of this inverse kinematics simulation was a .mot file containing all joint angles of the model as a time series. A visual representation of this process can be seen in Figure 4.2, which is a section of Figure A 5.13.

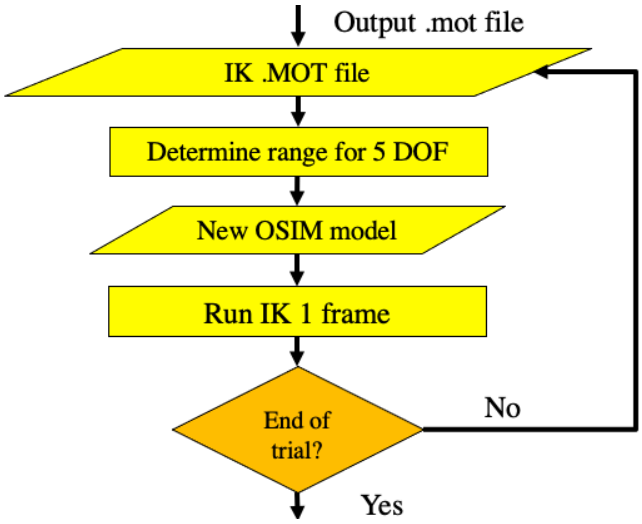

Figure 4.2: A section of the processing code to calculate knee kinematics for the 6-DoF knee. The first step of this code section is to receive an input .mot file, the resultant of running inverse kinematics for a 1-DoF knee. Then, the code steps through one frame at a time, and depending on the knee flexion angle, the upper and lower bounds of each remaining DoF are interpolated from plots from Qi et al. (2013) (seen in Figure 4.2), or Gray et al. (2019). Then, the upper and lower bound of each DoF are assigned to OpenSim as such: [lower, upper]. Finally, inverse kinematics is run for one frame at a time. This process repeats until all frames have been completed.

The resultant kinematics were processed twice, once with the new biplanar fluoroscopy constraints from Qi et al. (2013) and Gray et al. (2019) and then once with the previously used bone pin constraints from Benoit et al. (2006). From here on, these will be known as the biplanar fluoroscopy knee constraints and the bone pin knee constraints respectively.

Ligament length: Finally changes in ligament lengths were calculated using the resultant .mot file using the point kinematics function. A point was placed on each of the ligament insertion points (8 in total, 2 for each ligament) and the change in distance between the two points represented the change in ligament length over the entire trial.

Analysis of Results: We compared the knee joint kinematics and ligament lengths using the new model from *study 1* and then between groups in *study 2*. Resultant knee kinematics and ligament lengths were low pass filtered at 6 Hz (Kim et al., 2018) and time normalized based on knee flexion angle. As all three tasks involved a squatting and standing component and the first instant where the knee flexed past five degrees will be used as the start of the normalized trial. As the participant was standing still at the start of each task, there was minimal risk of trimming important dynamic data. Then, the end of the normalized trial was defined as the instant when the participant extended their knee past five degrees of flexion. Each trial was normalized to a 100% cycle.

4.7 Statistics for the studies

Study 1 (Chapter 5): A two-tailed paired-samples t-test was done to determine whether there were differences in the knee kinematics between biplanar fluoroscopy (Gray et al., 2019; Qi et al., 2013) and bone pin (Benoit et al., 2006; Potvin, 2016) constraints of each model. Given that the bone pin task from Benoit et al. (2006) was a cutting task, involving high knee abduction, it was hypothesized that the bone pin constrained knee would abduct significantly more than the biplanar fluoroscopy constrained knee (H1a_study 1). Secondly, as the biplanar fluoroscopy constrained knee data from Qi et al. (2013) involved a deep knee flexion, it was hypothesized that the biplanar fluoroscopy constrained knee would have greater posterior translation of the femur and greater external rotation, as seen with other fluoroscopy literature (Murakami et al., 2016) (H1b_study 1). To examine the entire trial, and not just the mean value, statistical parametric mapping (SPM) was

used (Pataky, 2010). This test was carried out using a paired-samples t-test, with the addition of statistical parametric mapping to examine the entire trial.

Root mean squared error (RMSE) was calculated between resultant ligament lengths from the biplanar fluoroscopy constrained knee and existing literature ligament lengths (Li et al., 2004; Park et al., 2006). Given that ligament lengths depended directly on the resultant inverse kinematics, it was hypothesized that the more complicated tasks would have worse agreement between calculated and existing literature lengths, as literature lengths were taken from a slow one-legged lunge (Li et al., 2004; Park et al., 2006). It was hypothesized that the squat task would have the lowest RMSE, followed by the countermovement jump, and finally, the drop-vertical jump (H1c_study 1).

All time-series kinematics and ligament lengths were tested for normality, to determine whether a parametric or non-parametric t-test will be used. To adjust for the risk of type 1 error, due to the numerous t-tests being performed, a Bonferroni *p*-value correction was applied, based on the number of comparisons. Finally, effect sizes (Cohen's *d*) were calculated and averaged over regions of significance (Cohen, 1992). Significant effects were those where $p < 0.05$.

Study 2 (Chapter 6): Knee kinematics were first analysed using statistical parametric mapping (Pataky, 2010), a 2x2 ANOVA with participant sex and injury status as factors. This was first performed to determine whether sex or injury status could effectively differentiate our groups, as well as the interaction between sex and injury status. From Figure A 6.15-16, it was found that injury was consistently a significant factor, while sex was inconsistently a factor. Therefore, to isolate the effect of injury, independent samples t-tests were performed for knee kinematics and ligament lengths, for female ACL injured (FACL) versus female control (FCON), and male ACL injured (MACL) versus male control (MCON) participants. To correct for potential type 1 error, a

Bonferroni correction was used to adjust the required significance threshold, based on the number of comparisons. Finally, effect sizes (Cohen's *d*) (Cohen, 1992) were calculated and averaged over regions of significance. All statistics were calculated using MATLAB. It was hypothesized that FACL and MACL participants will have significantly less knee translations and rotations compared to their control counterparts, due to perceived pain and instability (Yamazaki et al., 2010) (H1a_study2). Due to the reduced range of motion, it was hypothesized that the lengths of the lateral and medial collateral ligaments (LCL and MCL) and posterior cruciate ligament (PCL) will be shorter for the FACL and MACL groups, in comparison to the CON groups (H1b_study2). This hypothesis was made with knowledge that the LCL, MCL, and PCL reach their maximum length at high knee flexion (Li et al., 2004; Park et al., 2006).

These two studies shall be presented in the following two chapters, with Chapter 5 for *study 1* and Chapter 6 for *study 2*. Chapters 5 and 6 are self-contained manuscripts. Chapter 7 presents the general discussion and conclusion for this thesis.

5.0 Manuscript 1

Title: A new OpenSim adolescent knee model bounded by in vivo kinematic ranges to assess knee motion during high flexion dynamic tasks

Blake S. Miller[1], Céline I. Girard[2], Michael J. Del Bel[3], Daniel L. Benoit[2,3]

[1]School of Human Kinetics, University of Ottawa

[2]Department of Mechanical Engineering, University of Ottawa

[3]School of Rehabilitation Sciences, University of Ottawa

5.1 Abstract

Background: There is a lack of readily available OpenSim models that can accurately simulate a pediatric population with a knee injury, such as an anterior cruciate ligament (ACL) injury. As the presence of a knee injury will affect knee joint kinematics and limb symmetry, it is crucial that any new model must be able to simulate physiologically valid kinematics and ligaments lengths for a healthy control population first. Therefore, the purpose of this study is to design a new OpenSim model that can output knee joint kinematics and ligament lengths that fall within a physiological bound.

Methods: Thirty-two female control (CON) pediatric females (age = 13.0 ± 1.8 years, height = 162.3 ± 8.1 cm, mass = 52.2 ± 12.0 kg, Tanner stage = 3.0 ± 1.0) with no prior history of knee injuries performed three bilateral motion tasks: a squat, a countermovement jump (CMJ), and a drop-vertical jump (DVJ). Anatomical and cluster marker positions were collected and inputted directly into OpenSim to drive the inverse kinematics function and point kinematics function. A 6-degree-of-freedom (DoF) knee with biplanar fluoroscopy-derived constraints was compared to previously published in vivo bone pin constraints. Knee ligament lengths were compared to previous in vivo literature, via root mean squared error.

Results: The biplanar fluoroscopy-constrained knee consistently rotated more externally, abducted less, and translated more posteriorly when compared to the bone pin knee, for all three tasks. The DVJ task had the most significant difference between limbs followed by the CMJ and then the squat. For ligament lengths, the ACL fell outside 1 standard deviation (SD) of literature during knee flexion greater than 80 degrees. The squat had the highest total ligament length RMSE (71.2 mm), followed by the DVJ (58.9 mm) and CMJ (58.7 mm).

Conclusion: The newly created partially unlocked knee model outputted physiological knee kinematics and ligament lengths. The use of in vivo constraints on range of motion aided in producing physiological knee kinematics while also allowing for variation between participants. Therefore, given the sensitivity of the model it should be capable of simulating kinematics for a pediatric group with lower body injuries.

5.2 Introduction

Sports-based knee injuries are common amongst the pediatric population, with one of the most debilitating being the injury of the anterior cruciate ligament (ACL). ACL injury rates are rising in the pediatric population significantly more than their adult counterparts (Arbes et al., 2007; Beck et al., 2017; Frank & Gambacorta, 2013; Herzog et al., 2017; Shea et al., 2004). This is further complicated by a lack of research into the pediatric population when considering ACL injuries and by the complexity of the knee. It is inherently difficult to measure its complex internal forces without using more advanced imbedded means (Fregly et al., 2012). Instead, it is possible to obtain an estimate of the kinematics and dynamics of the knee using musculoskeletal modelling software.

Simulation software such as OpenSim (Delp et al., 2007) allows for simulation of a wide variety of physiological conditions. As almost all force and muscle-related simulations rely on the results of the inverse kinematics function, small errors incurred at this step have the potential to rapidly increase over several simulations (Hicks et al., 2015; Uchida & Seth, 2022). Therefore, it is crucial that the inverse kinematics function of OpenSim is performed with minimal error.

One such form of potential error from using the inverse kinematics function is the degrees of freedom at each joint. When modelling the knee as a 1-DoF, the flexion-extension hinge joint removes all frontal plane kinematics which ignores key factors that often lead to knee injuries such as high knee valgus (Hewett et al., 2005). On the contrary, the knee joint cannot be fully unlocked as this will produce unphysiological motions (Potvin, 2016).

The drawback to computer simulation software, such as OpenSim is that most existing models were created for an adult population. As well, model outputs are sensitive to the quality of input data. Additionally, most default OpenSim models use cadaver-based data to infer knee motion

(Rajagopal et al., 2016) during the calculation of inverse kinematics. This is an issue when trying to model pediatric populations as knee kinematics will likely change with age and with varying lower-limb injuries (Larsson & Karlsson, 1978). Therefore, a new model must be developed that can accurately represent an ACL-injured pediatric population. Before the model can be used to simulate participants with an ACL injury, it must first be validated on healthy control participants.

As knee kinematics may be altered due to the presence of a knee pathology such as an ACL injury, it is crucial that the resultant inverse kinematics at the knee are as accurate as possible while remaining in a physiological range. This can be achieved by simulating a bilateral squat followed by the countermovement jump (CMJ) as it involves a squat in addition to the increased complexity of a landing task. Finally, the drop-vertical jump (DVJ) can be simulated as it is also one of the most common tasks used to assess ACL injury risk (Hewett et al., 2005).

The objective of this study was therefore to develop a new model and assess the validity of the resulting kinematic outputs and ligament lengths for squat, CMJ, and DVJ tasks. Ideally the model will be evaluated during relevant and increasingly complex tasks (Lund et al., 2012). Our tasks were chosen since the complexity of movement increases from squat, to CMJ, to DVJ and they are commonly used to assess performance during ACL rehabilitation (Wright et al., 2015). To minimize variation between participants, only females were used as it is well-established that kinematic and dynamic differences exist between males and females (Del Bel et al., 2018; Otsuki et al., 2021; Romanchuk et al., 2020). There is also a lack of literature on female-specific kinematics. As the purpose of this model is to represent pediatric participants with knee injuries, it is also crucial that a pediatric sample is being used for the data set. Kinematic and ligament results for an adult population cannot be simply extrapolated to pediatrics with the assumption that they are small adults. It is well documented that various physiological and neuromuscular changes

occur over the course of puberty (Hewett et al., 2004; Shea et al., 2004). Therefore, it is crucial that when attempting to make clinical decisions with regards to a pediatric population, both a pediatric data set and the proper pediatric model are required.

5.3 Methods

5.3.1 Participants

Thirty-two uninjured adolescent female participants (age = 13.0 ± 1.8 years, height = 162.3 ± 8.1 cm, mass = 52.2 ± 12.0 kg, Tanner stage = 3.0 ± 1.0) were included in the study. Participants were included if they actively participated in organized sport, had no history of any previous lower extremity injury in the past six months, and had no prior traumatic knee injury (i.e., meniscal tear, ligament rupture/tear) including any diseases/illnesses that would impact the neuromuscular function. All participants read and signed a letter of informed consent approved by the local research ethics board. Participants completed a series of self-assessment forms that assessed their pubertal stage (Marshall & Tanner, 1969), sport exposure (Fabricant et al., 2014), activity level (Tegner activity scale (Lysholm & Tegner, 2007)), and subjective knee function (HSS-Pedi-IKDC) in English (Kocher et al., 2011) or French (Del Bel et al., 2020).

5.3.2 Protocol

Participants were outfitted with tight-fitting spandex long-sleeve shirts, and shorts and had their height and weight taken, as well as several other anthropometric measurements (leg length, leg width, shank length, ankle width, anterior and posterior superior iliac spine distances), followed by electrode placement on the quadriceps, hamstrings, gastrocnemii, and gluteus medius, for both limbs (16 channels, Trigno Wireless System, Delsys, USA). Following this, participants warmed up for 5 minutes on a stationary bicycle (Monark 828E, Vansbro, Sweden) and then performed various isometric hip, knee, and ankle strength measurements using an isokinetic dynamometer

(System 4 Pro, Biodex Medical Systems, USA). Following this, participants had 84 retroreflective markers (14 mm in diameter) placed on anatomical landmarks and in cluster sets adapted from a hybrid marker set (Mantovani & Lamontagne, 2017). Kinematic data was sampled at 200 Hz using infrared cameras (8 Vero and 2 Vantage, Vicon, Nexus, Oxford, UK). Kinetic data was sampled at 1000 Hz with 2 Bertec force plates (Bertec Corp., Columbus, USA). Participants completed several bilateral tasks including squats, countermovement jumps (CMJ) and drop-vertical jumps (DVJ), with the squat being the simplest task, the DVJ being the most complex, and the CMJ being somewhere in between.

For the squat task, participants were asked to place their hands on their heads and then perform a deep bilateral squat (maximum knee and hip flexion) to the best of their ability (Kemp & Benoit, 2020). For the CMJ task, participants were instructed to squat with both legs with the goal of then jumping as high as they could following the squat. For the DVJ task, participants were asked to step off a platform and land on the force plates and immediately jump vertically with both legs, all in one smooth motion (Kemp & Benoit, 2020). The squat and CMJ tasks were time normalized to 100 points, starting with the first instance in which the participant squatted past 5 degrees of knee flexion and ending when the participant stood up past 5 degrees of knee flexion. For the DVJ, the trial started when the participant stepped off the platform and both legs were at less than 5 degrees knee flexion as this indicated they were midair falling towards the plate. The trial ended when the participant stood up past 5 degrees of knee flexion for the final time.

5.3.3 The Partially Unlocked Knee Model

The model which was used in this study was created using the STAPLE pipeline which allows for the addition of custom bones into an OpenSim model (Modenese & Renault, 2021). All lower body bones (pelvis and below) were taken from the STAPLE pipeline, using the TLEM 2.0 bone

set (Carbone et al., 2014). The torso, spine, and skull were loaded in from the generic OpenSim bone dataset (Delp et al., 2007).

In addition to having more realistic bone geometry, this new model also has a "partially" unlocked 6-degre-of-freedom knee. The range of motion for the five remaining degrees of freedom were defined based on the knee flexion angle. This approach was first done by Potvin. (2016), and then by Smale et al. (2019), in which intercortical bone pin constraints from Benoit et al. (2006) were used. However, it should be noted that Benoit et al. (2006) had young healthy participants performing gait, single legged hopping, and side cutting tasks, which were all at lower knee flexion (less than 60 degrees flexion). However, for high flexion (greater than 60 degrees flexion) tasks such as squats, CMJ, and DVJ, different constraints from high flexion tasks may be a better fit.

The knee flexion angle was related to knee abduction-adduction (Ab/Add), internal-external rotation (IE), anterior-posterior (AP), distal-proximal (DP) and medial-lateral (ML) translation, based on the mean and standard deviations reported by the bone pin constraints (Benoit et al., 2006) and existing biplanar fluoroscopy constraint studies (Gray et al., 2019; Qi et al., 2013). It should be noted that in our approach as the knee flexion angle changes throughout the movement trial, the remaining 5 DoF of the knee are updated in every frame within the physiologically bounded limits through the entire trial (Figure A 5.13).

To update the remaining 5 DoF, custom MATLAB (2021a, MathWorks Inc, Natick, USA) code (Figure A 5.13) was written to run the default OpenSim inverse kinematics function (Delp et al., 2007), one frame at a time. Before each inverse kinematics frame ran, the range of motion of each of the remaining 5 DoF were set for the model based on linear interpolation of knee flexion angle. As part of our preliminary testing, sensitivity analyses were conducted on both marker weighting and on the bounds themselves as only 1 standard deviation was used for the upper and

lower bounds (see Appendix A 5.14 – A 5.17 for the standard deviation sensitivity plots). In short, resultant knee rotations were more sensitive to marker weightings while knee translations were more sensitive to the bound size. From Appendix A 5.18-5.20 with low anatomical marker weights of ω_{marker} = 1, the resultant kinematic and ligament length waveforms were noisy. Additionally, with high marker weights of ω_{marker} = 1000, limb asymmetries appeared due to marker registration error. Therefore, ω_{marker} = 100 was used, as even ω_{marker} = 10 produced a noisy signal.

In addition to the calculation of inverse kinematics for the entire trial, the location of four knee ligament insertion points were tracked using the point kinematics option of the analysis function in OpenSim. The location of the insertion points for the knee ligaments was based on a single participant's MRI where insertion points were placed on the centroid of each insertion location (Li et al., 2004; Park et al., 2006). With the location of both insertion points known, the length of the ligament could be estimated as the distance between the two points. Finally, kinematics and ligament lengths were time normalized across trials to allow the calculation of average values for each participant.

5.3.4 Statistical Analysis

A two-tailed paired-samples t-test was done to determine whether there were differences in the knee kinematics between biplanar fluoroscopy (Gray et al., 2019; Qi et al., 2013) and bone pin (Benoit et al., 2006; Potvin, 2016) constraints of each model. Given that the bone pin task from Benoit et al. (2006) was a cutting task involving high knee abduction, it was hypothesized that the bone pin constrained knee would abduct significantly more than the biplanar fluoroscopy constrained knee (H1a). Secondly, as the biplanar fluoroscopy constrained knee data from Qi et al. (2013) involved a deep knee flexion, it was hypothesized that the biplanar fluoroscopy

constrained knee would have greater posterior translation of the femur and greater external rotation as seen with other fluoroscopy literature (Murakami et al., 2016) (H1b). To examine the entire trial and not just the mean value, statistical parametric mapping was used (Pataky, 2010). This test was carried out using a paired-samples t-test with the addition of statistical parametric mapping to examine the entire trial.

Root mean squared error (RMSE) was calculated and visually inspected between resultant ligament lengths from the biplanar fluoroscopy constrained knee and existing literature ligament lengths (Li et al., 2004; Park et al., 2006). Given that ligament lengths depended directly on the resultant inverse kinematics, it was hypothesized that the more complicated tasks would have worse agreement between calculated and existing literature lengths, as literature lengths were taken from a slow one-legged lunge (Li et al., 2004; Park et al., 2006). It was hypothesized that the squat task would have the lowest RMSE, followed by the countermovement jump, and finally, the drop-vertical jump (H1c).

5.4 Results

5.4.1 Kinematic data

The resultant right and left knee kinematics were plotted for squats in Figure 5.1 and Figure 5.2, for CMJ in Figure 5.3 and Figure 5.4, and for DVJ in Figure 5.5 and Figure 5.6.

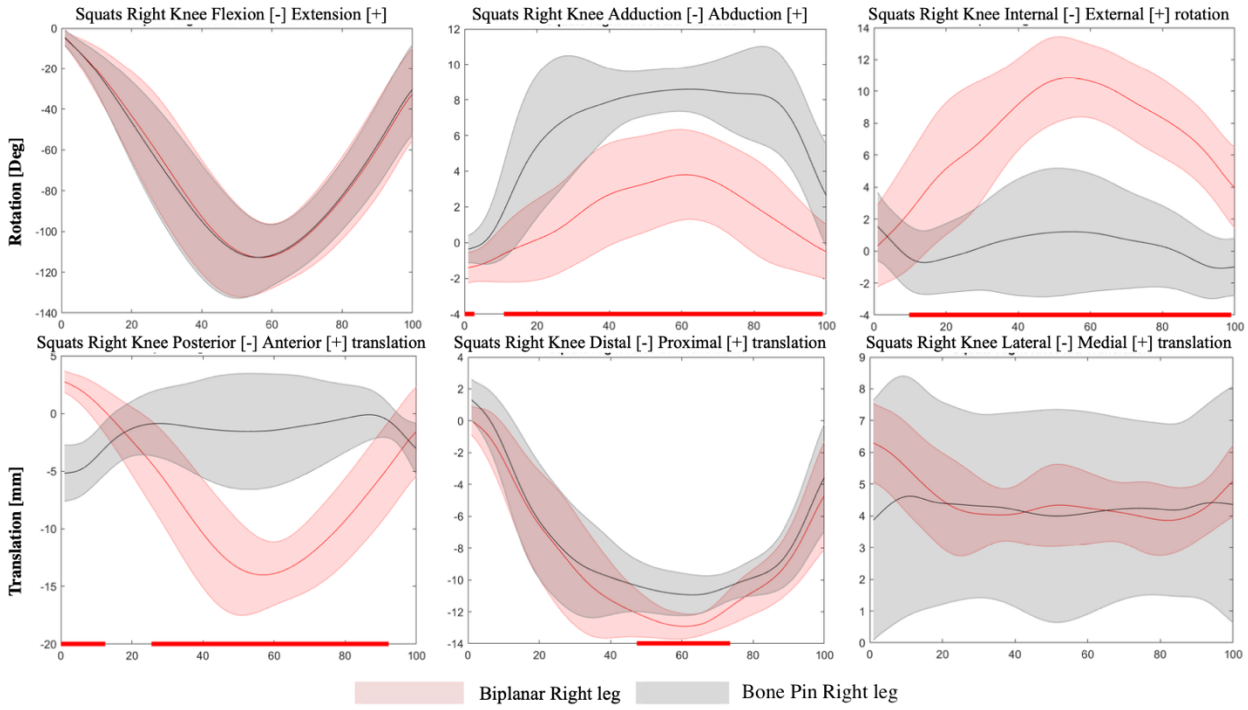

Figure 5.1: Rotation and translation right knee motions for the biplanar fluoroscopy (red) and bone pin (grey) constrained limbs during a squat, time normalized to 0-100% of the movement cycle. Red horizontal bars at the bottom of each plot represent significance between constrained limbs.

During squats for the right knee: the bone pin knee abducted significantly more from 1-3% task (p=0.011, d= 1.24) and from 11-100% task (p<0.001, d=2.14), the biplanar fluoroscopy knee externally rotated significantly more from 38-91% task (p<0.001, d=1.59), the biplanar fluoroscopy knee started more anteriorly translated, from 1-5% task (p=0.01, d=2.12), and then translated significantly more posteriorly from 33-85% task (p<0.001, d=2.07), finally, the biplanar fluoroscopy knee translated significantly more distally from 47-73% task (p<0.001, d=1.64) (Figure 5.1).

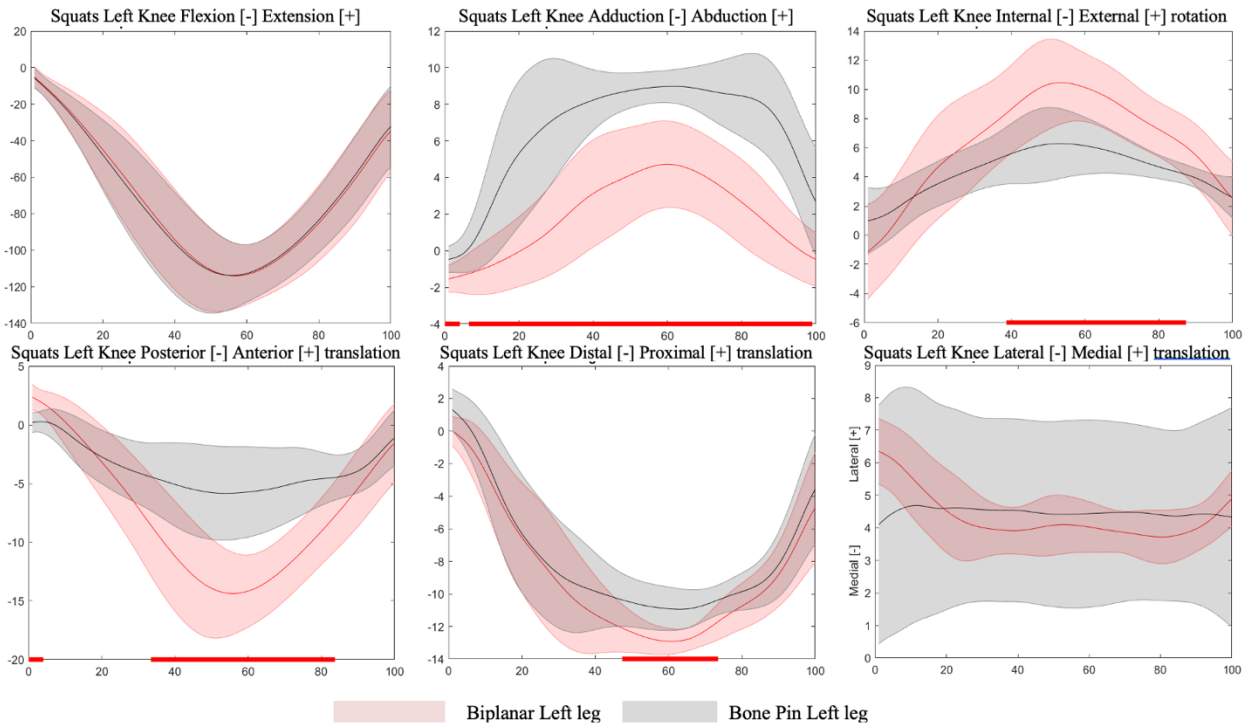

Figure 5.2: Rotation and translation left knee motions for the biplanar fluoroscopy (red) and bone pin (grey) constrained limbs during a squat, time normalized to 0-100% of the movement cycle. Red horizontal bars at the bottom of each plot represent significance between constrained limbs.

During squats for the left knee: the bone pin knee abducted significantly more from 1-4% task (p=0.012, d= 1.34) and from 7-100% task (p<0.001, d=2.16), the biplanar fluoroscopy knee externally rotated significantly more from 39-87% task (p<0.001, d=1.64), the biplanar fluoroscopy knee started more anteriorly translated, from 1-4% task (p=0.01, d=1.92), and then translated significantly more posteriorly from 33-84% task (p<0.001, d=1.94), finally, the biplanar fluoroscopy knee translated significantly more distally from 49-73% task (p<0.001, d=1.46) (Figure 5.2).

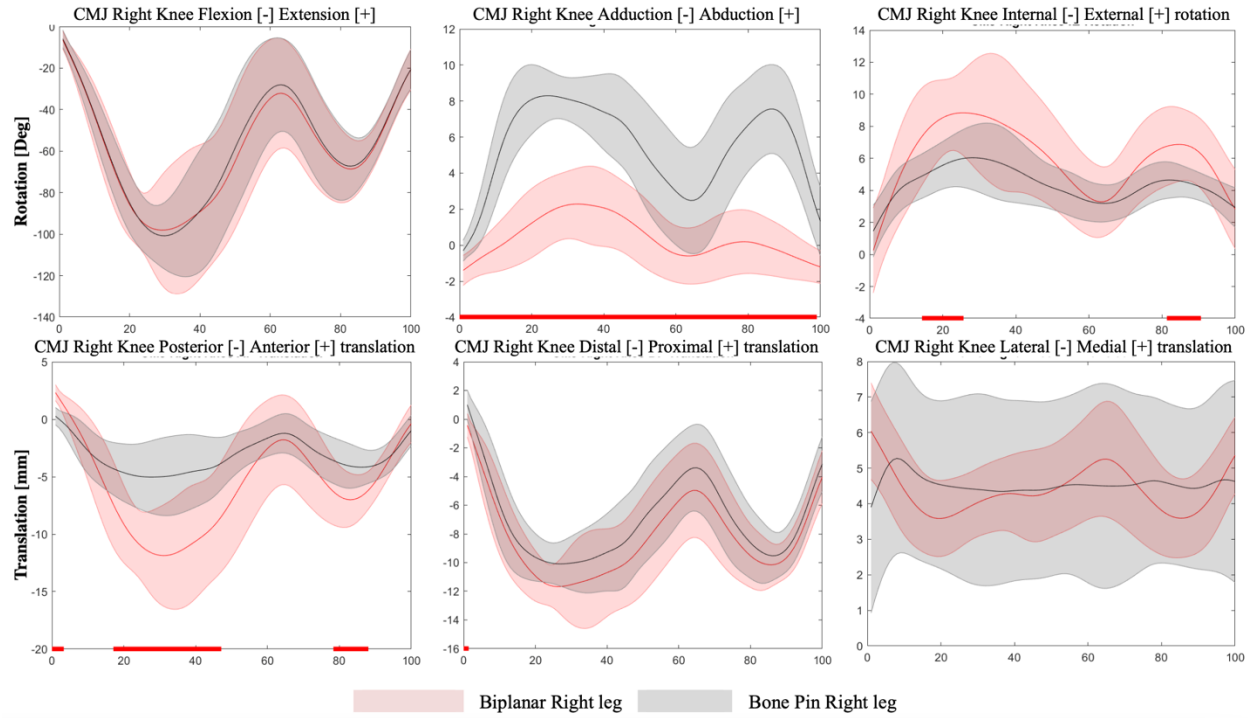

Figure 5.3: Rotation and translation right knee motions for the biplanar fluoroscopy (red) and bone pin (grey) constrained limbs during a CMJ, time normalized to 0-100% of the movement cycle. Red horizontal bars at the bottom of each plot represent significance between constrained limbs.

During CMJs for the right knee: the bone pin knee abducted significantly more during the entire task (p<0.001, d=2.59), the biplanar fluoroscopy knee rotated more externally from 14-26% task (p=0.001, d=1.35) and 81-91% task (p=0.003, d=1.27), the biplanar fluoroscopy knee started the task more anteriorly translated, from 1-3% task (p=0.009, d=2.40), then translated more posteriorly from 17-47% task (p<0.001, d=1.60) and 78-88% task (p=0.001, d=1.30), finally, the biplanar fluoroscopy knee started more distal, from 1-3% task (p=0.012, d=1.34) (Figure 5.3).

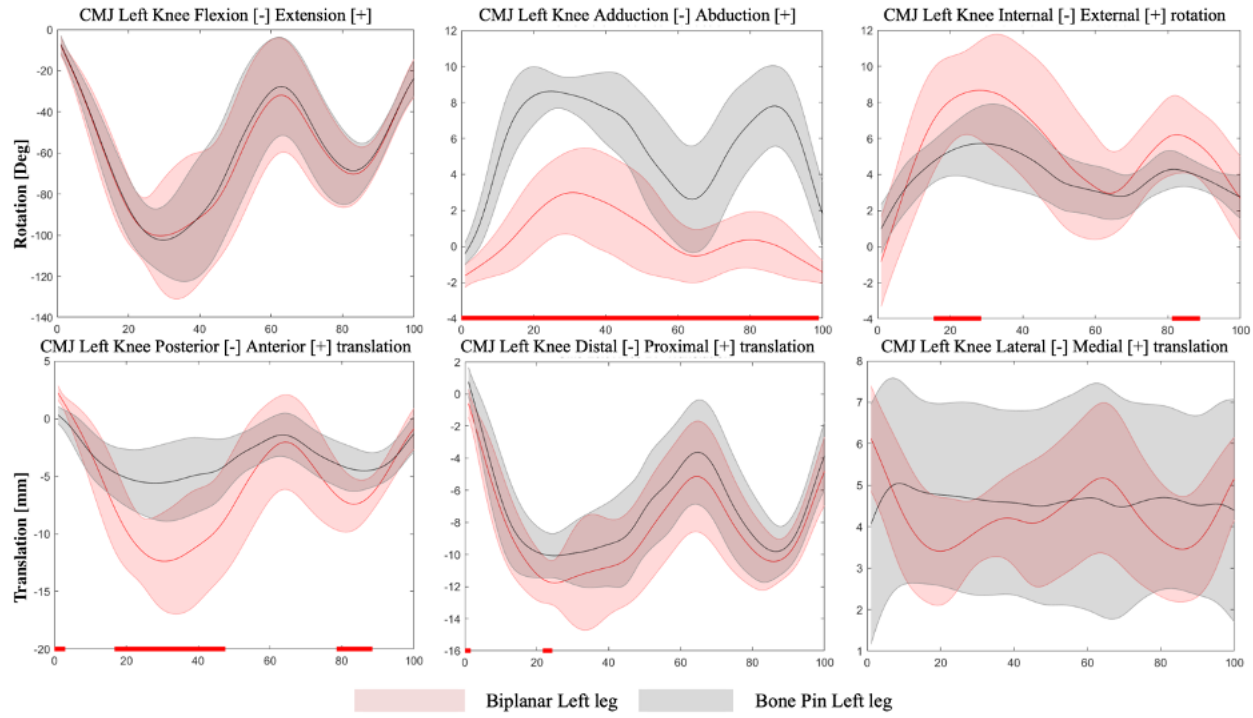

Figure 5.4: Rotations and translation left knee motions for the biplanar fluoroscopy (red) and bone pin (grey) constrained limbs during a CMJ, time normalized to 0-100% of the movement cycle. Red horizontal bars at the bottom of each plot represent significance between constrained limbs.

During CMJs for the left knee: the bone pin knee abducted significantly more during the entire task (p<0.001, d=2.63), the biplanar fluoroscopy knee rotated more externally from 15-29% task (p=0.001, d=1.31) and 81-91% task (p=0.005, d=1.27), the biplanar fluoroscopy knee started the task more anteriorly translated, from 1-3% task (p=0.01, d=2.29), then translated more posteriorly from 17-48% task (p<0.001, d=1.61) and 79-88% task (p=0.001, d=1.38) and the biplanar fluoroscopy knee translated more distally from 1-3% task (p=0.011, d=1.30) and from 22-24% task (p=0.01, d=1.29) (Figure 5.4).

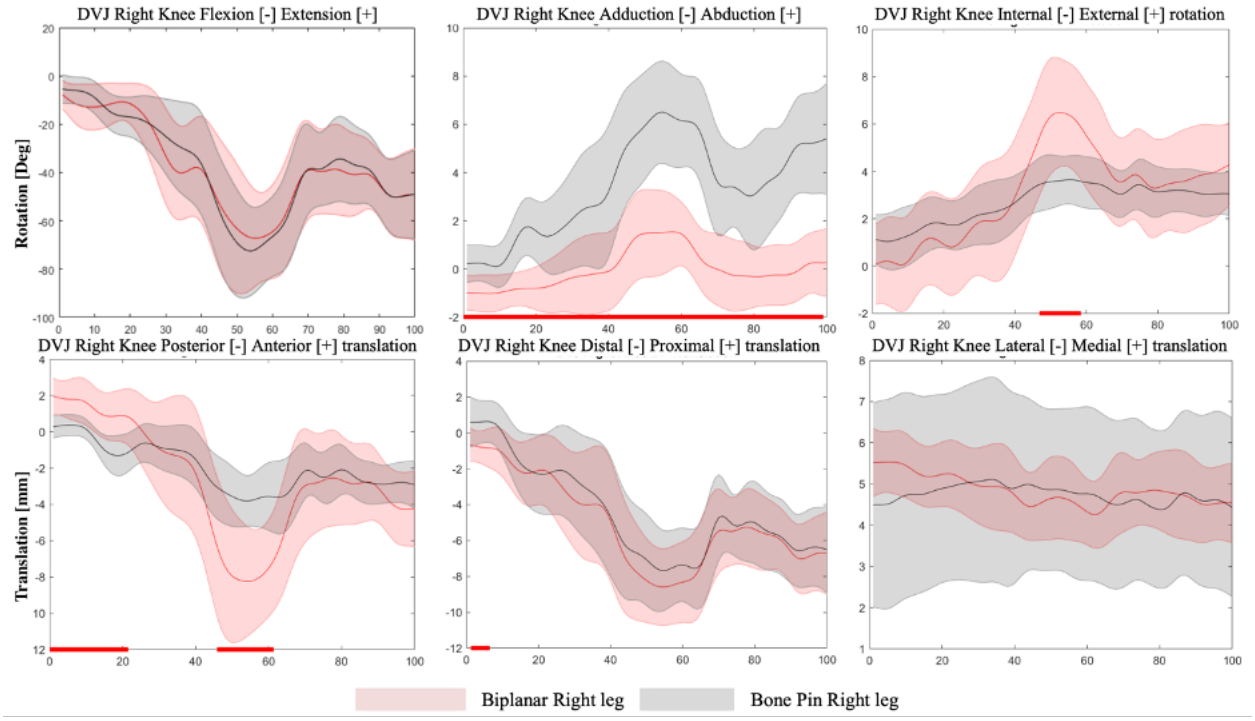

Figure 5.5: Rotation and translation right knee motions for the biplanar fluoroscopy (red) and bone pin (grey) constrained limbs during a DVJ, time normalized to 0-100% of the movement cycle. Red horizontal bars at the bottom of each plot represent significance between constrained limbs.

During DVJs for the right knee: the bone pin knee abducted significantly more during the entire task (p<0.001, d=2.15), the biplanar fluoroscopy knee rotated more externally from 46-58% task (p=0.001, d=1.42), the biplanar fluoroscopy knee started the task more anteriorly translated, from 1-22% task (p<0.001, d=1.68), then translated more posteriorly from 46-61% task (p<0.001, d=1.67), finally, the biplanar fluoroscopy knee translated more distally from 1-7% task (p=0.004, d=1.25) (Figure 5.5).

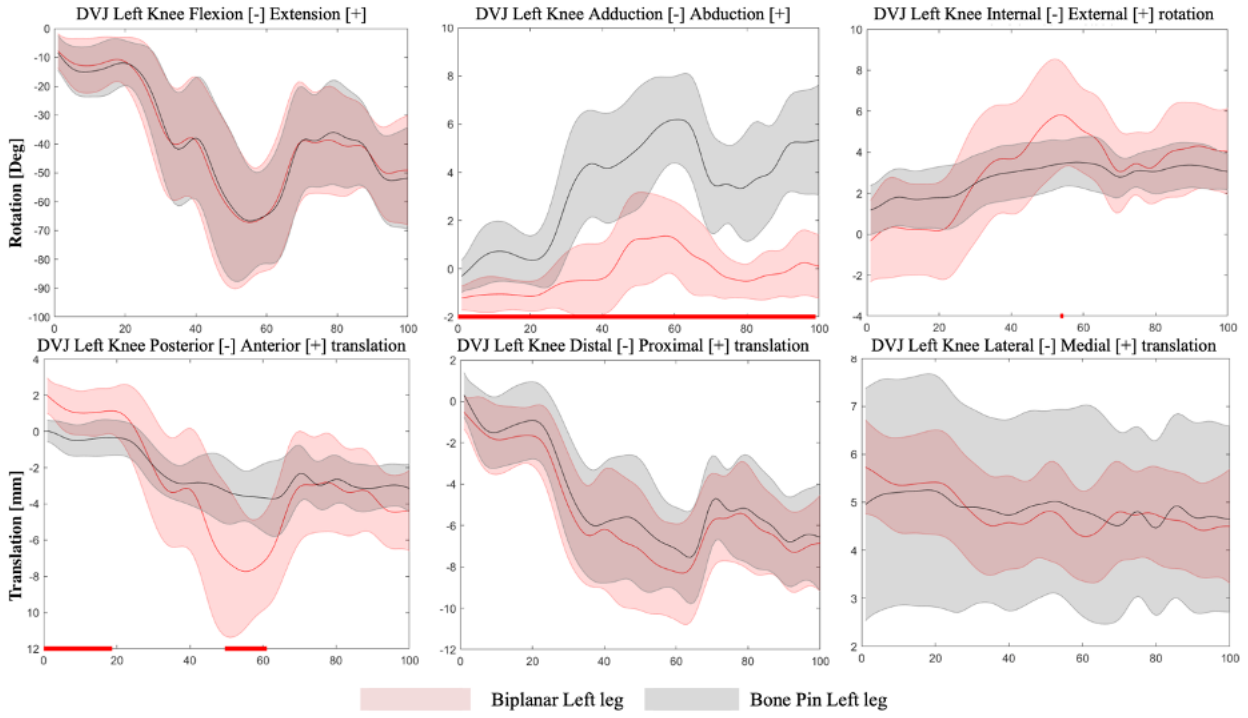

Figure 5.6: Rotation and translation left knee motions for the biplanar (red) and bone pin (grey) constrained limbs during a DVJ, time normalized to 0-100% of the movement cycle. Red horizontal bars at the bottom of each plot represent significance between constrained limbs.

During DVJs for the left knee, the bone pin knee abducted significantly more during the entire task (p<0.001, d=2.23), the biplanar fluoroscopy knee rotated more externally from 55-56% task (p=0.012, d=0.99) and the biplanar fluoroscopy knee started the task more anteriorly translated, from 1-18% task (p<0.001, d=1.54), then translated more posteriorly from 50-60% task (p<0.001, d=1.57) (Figure 5.6).

5.4.2 Ligament lengths

Ligament lengths were plotted for the squat task in Figure 5.7 and Figure 5.8, the CMJ task in Figure 5.9 and Figure 5.10, and the DVJ task in Figure 5.11 and Figure 5.12.

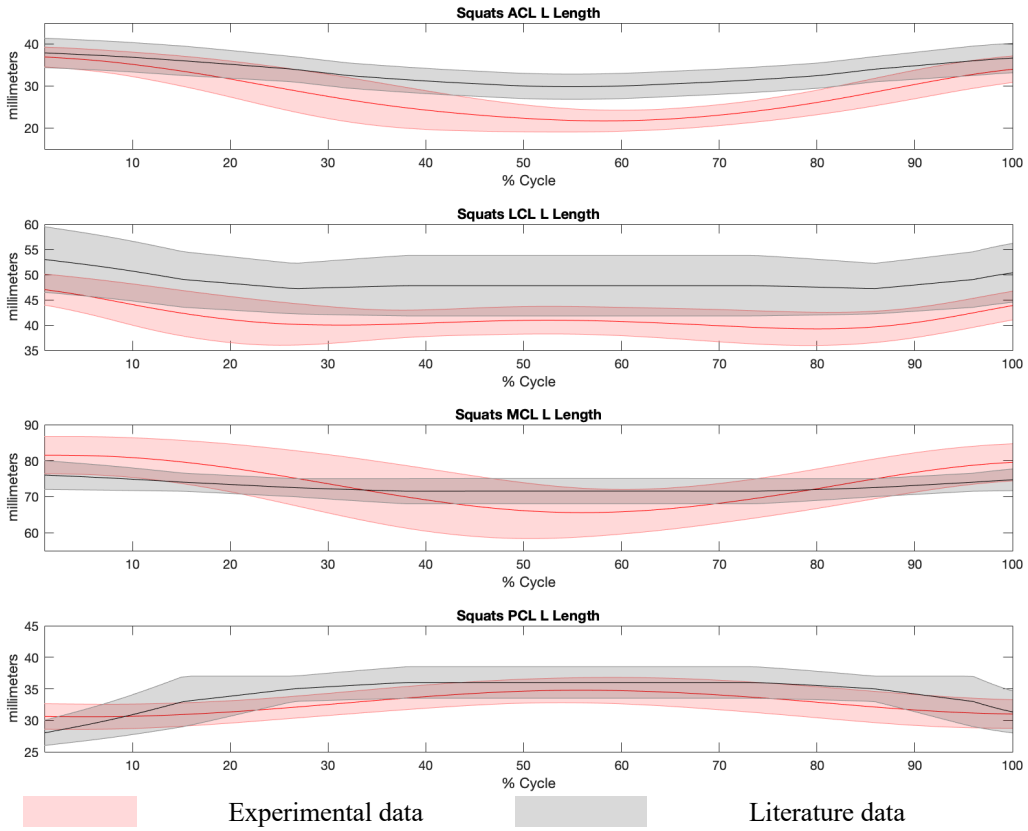

Figure 5.7: Mean and ± 1 standard deviation ligament lengths, for the ACL, LCL, MCL and PCL for the left limb, during a time-normalized Squat task.

During squats for the left knee: ACL mean experimental length diverged from the 1 SD bounds of literature length (Li et al., 2004) from 20-93% of the cycle, LCL mean experimental length diverged from the 1 SD bounds of literature data (Park et al., 2006) from 5-100% of the cycle, MCL mean experimental length diverged from the 1 SD bounds of literature data (Park et al., 2006) from 1-27% cycle, 44-69% cycle, and 86-100% cycle, and PCL mean experimental length diverged from the 1 SD bounds of literature data (Li et al., 2004) from 1-3% cycle, 23-35% cycle, and 76-89% cycle (Figure 5.7).

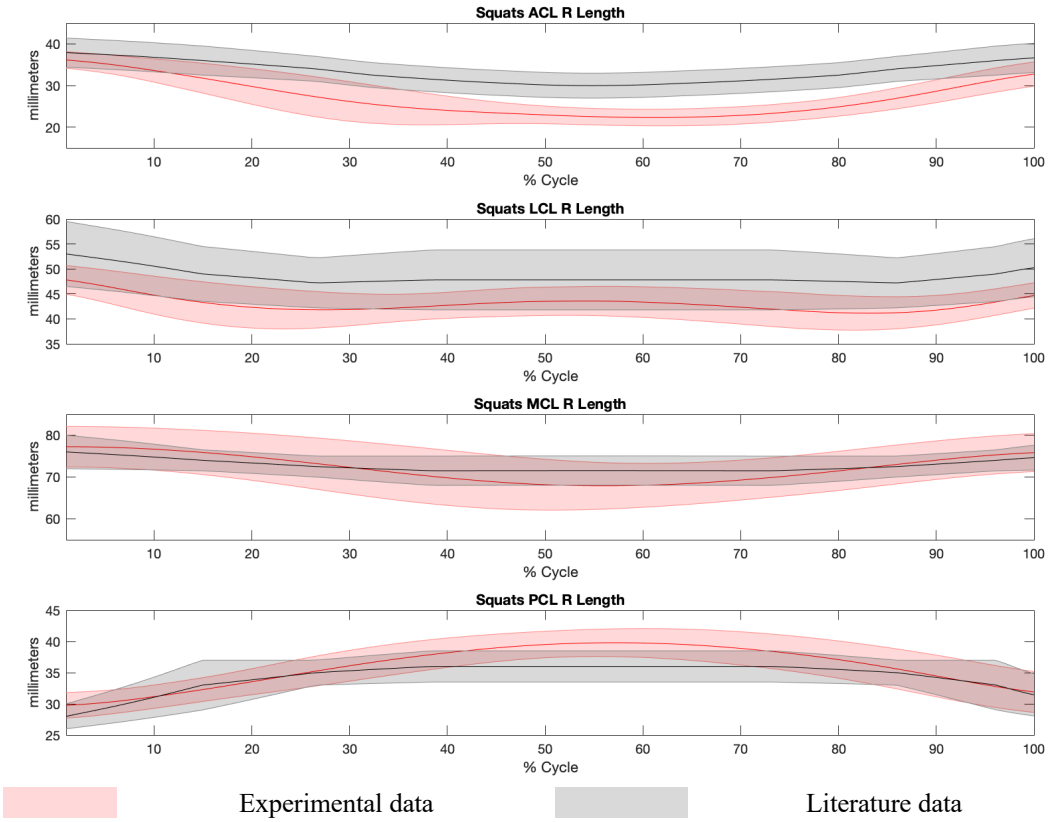

Figure 5.8: Mean and ± 1 standard deviation ligament lengths, for the ACL, LCL, MCL and PCL for the right limb, during a time-normalized Squat task.

During squats for the right knee: ACL mean experimental data diverged from the 1 SD bounds of literature data (Li et al., 2004) from 13-100% of the cycle, LCL mean experimental data diverged from the 1 SD bounds of literature data (Park et al., 2006) from 15-25% of the cycle and 77-96% of the cycle, MCL mean length did not diverge from the 1 SD bounds of literature data (Park et al., 2006), and PCL mean experimental length diverged from the 1 SD bounds of literature data (Li et al., 2004) from 4-72% cycle (Figure 5.8).

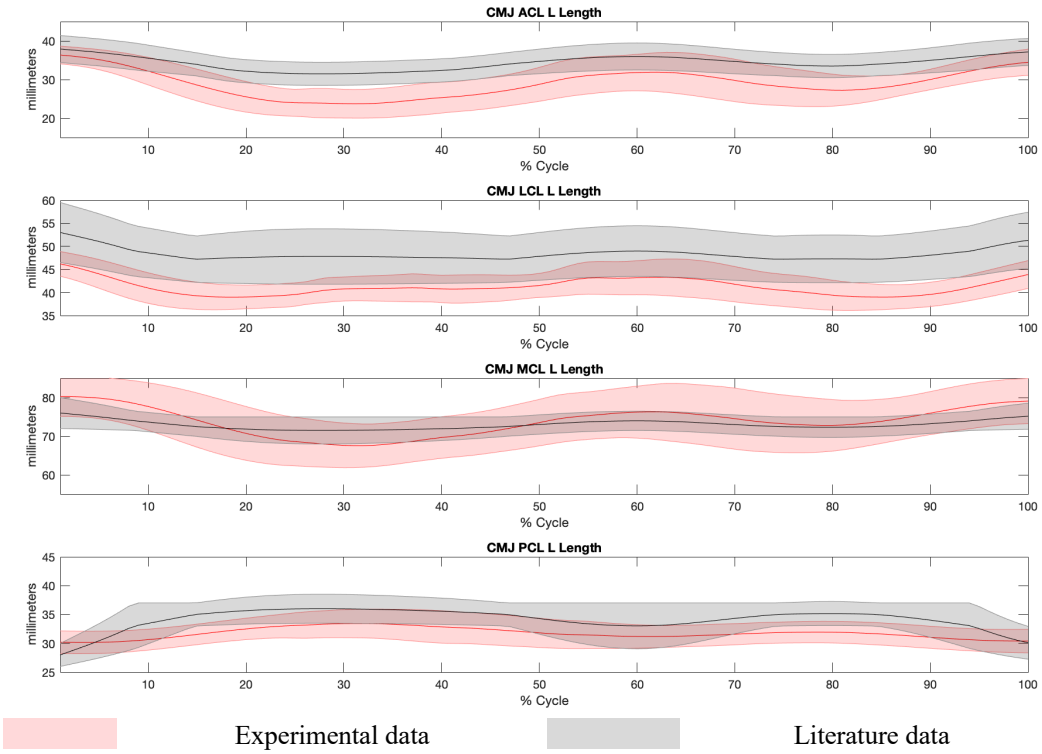

Figure 5.9: Mean and ± 1 standard deviation ligament lengths, for the ACL, LCL, MCL and PCL for the left limb, during a normalized CMJ task.

During CMJs for the left knee: ACL mean experimental length diverged from the 1 SD bounds of literature data (Li et al., 2004) from 10-95% of the cycle, LCL mean experimental length diverged from 1 SD bounds of literature data (Park et al., 2006) from 3-53% and 68-100% of the cycle, MCL mean experimental length diverged from 1 SD bounds of literature data (Park et al., 2006) from 1-13% and 90-100% of the cycle, and PCL mean experimental length diverged from the 1 SD bounds of literature (Li et al., 2004) from 1-2%, 12-30%, 40-50%, and 70-90% of the cycle (Figure 5.9).

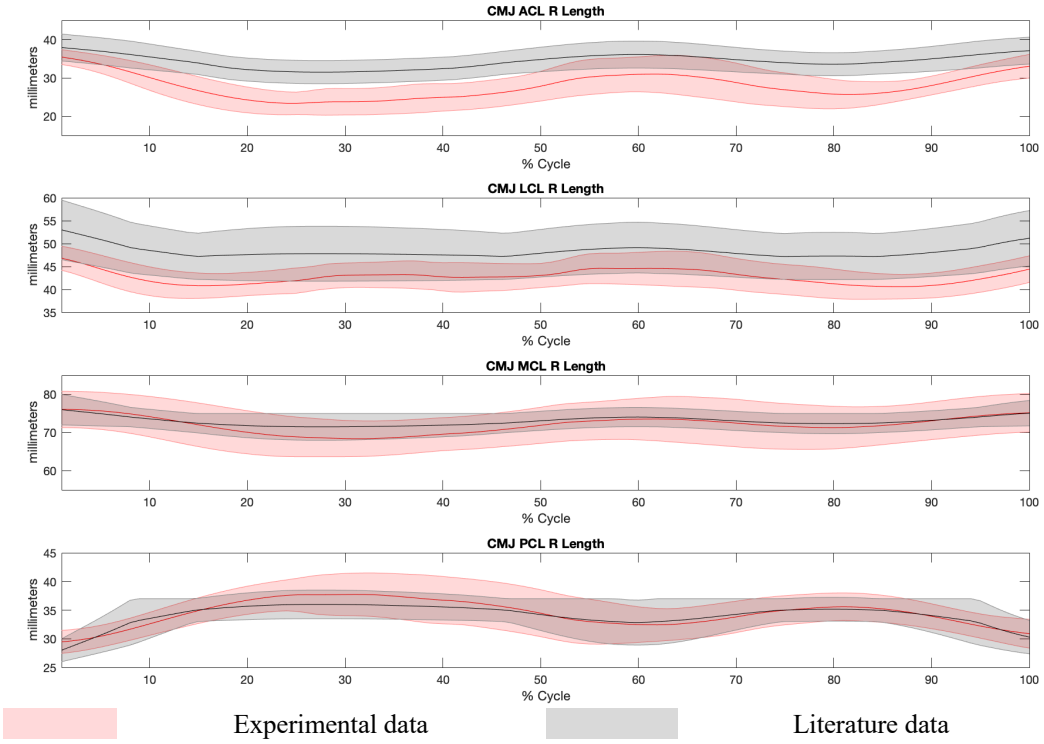

Figure 5.10: Mean and ± 1 standard deviation ligament lengths, for the ACL, LCL, MCL and PCL for the right limb, during a normalized CMJ task.

During the CMJ for the right knee: ACL mean experimental length diverged from the 1 SD bounds of literature data (Li et al., 2004) from 5-100% of the cycle, LCL mean experimental length diverged from 1 SD bounds of literature data (Park et al., 2006) from 5-23% and 75-100% of the cycle, and MCL and PCL lengths did not fall outside the 1 SD bounds of literature data for the entire cycle (Figure 5.10).

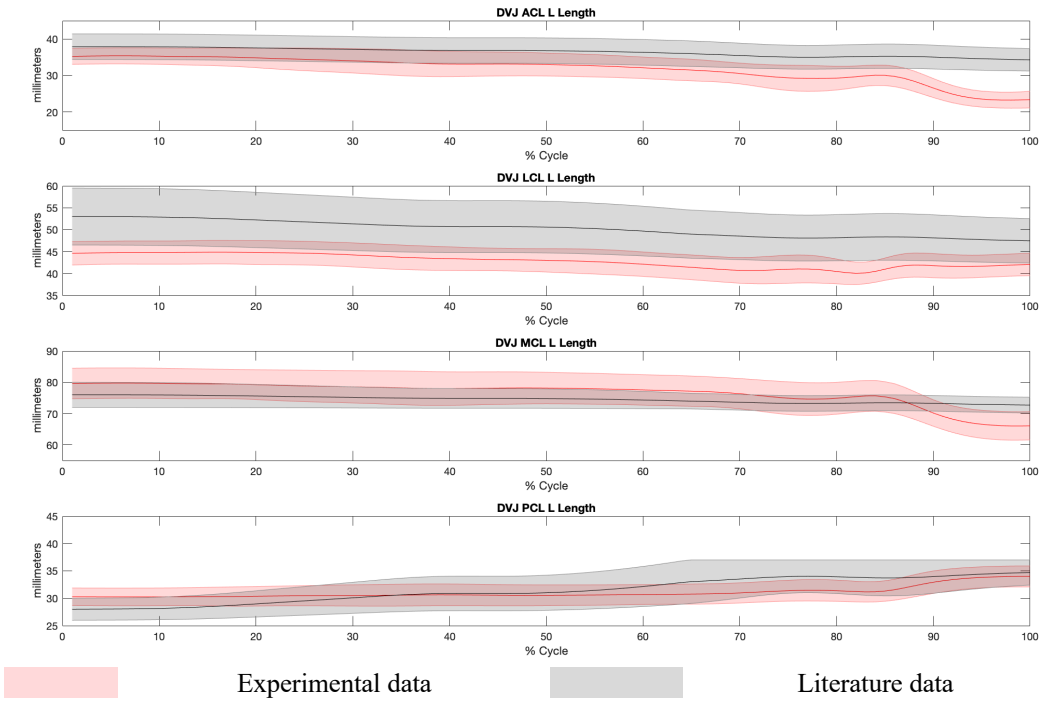

Figure 5.11: Mean and ± 1 standard deviation plots of the four major knee ligament lengths, for the left limb, during a normalized DVJ task.

During DVJs for the left knee, ACL mean experimental length diverged from literature data (Li et al., 2004) from 55-100% cycle, LCL mean experimental data diverged from literature data (Park et al., 2006) for the entire cycle, MCL mean experimental data diverged from 1 SD of literature data (Park et al., 2006) from 81-100% cycle, and PCL mean experimental data did not diverge from literature data (Li et al., 2004) (Figure 5.11).

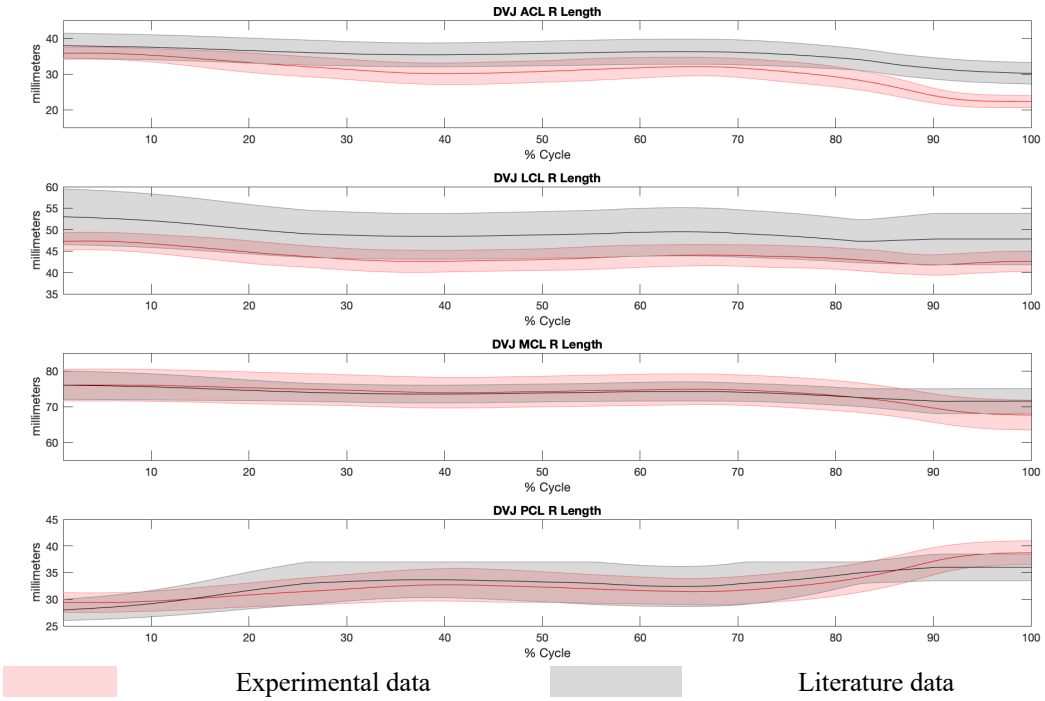

Figure 5.12: Mean and ± 1 standard deviation plots of the four major knee ligament lengths, for the right limb, during a normalized DVJ task.

During DVJs for the right knee, ACL mean experimental length diverged from literature data (Li et al., 2004) from 25-100% cycle, while LCL, MCL, and PCL lengths remained within 1 SD of literature bounds (Li et al., 2004; Park et al., 2006) (Figure 5.12).

In addition to plots of ligament lengths, Table 5.1 includes the resultant RMSE calculations between literature and experimental ligament lengths. Of the three tasks, the squat had the highest total RMSE and the highest ligament RMSE (LCL left leg). The CMJ task had the lowest total RMSE and the lowest ligament RMSE (PCL right leg).

Table 5.1: Root mean squared error values, in millimeters, for ligament length comparisons between literature, and our resultant data for the entire trial. All three tasks were included, with both left and right limbs, for all four major ligaments in the knee. The highest and lowest RMSE values are highlighted. Total RMSE was the sum of all RMSE values for each task, including both legs, and all four ligaments.

	Squats [mm]		CMJ [mm]		DVJ [mm]	
Limb:	L	R	L	R	L	R
ACL	11.9	13.1	10.0	11.9	10.0	9.6
LCL	14.5	10.9	12.9	10.2	14.2	10.5
MCL	8.5	4.0	4.8	2.7	6.8	2.4
PCL	4.2	4.2	4.7	1.5	3.1	2.3
Task RMSE	Total = 71.3		Total = 58.7		Total = 58.9	

5.5 Discussion

The objectives of this study were to: i) determine whether an OpenSim model could simulate knee ligament lengths that were within one standard deviation of published literature (Hicks et al., 2015), and ii) ensure that for bilateral tasks that knee kinematic constraints were similar. The third and final objective was to observe how the model would perform in more complex movements; therefore three tasks of increasing complexity were simulated. It was found that knee kinematics were similar for the squat and CMJ task while differences were found for the DVJ task. As well, it was found that ligament lengths remained within 1 SD for most of the trial with only some exceptions such as the ACL during high knee flexion.

5.5.1 Knee kinematics

Of the three tasks, squatting produced the worst agreement between the biplanar fluoroscopy and bone pin knee. During the squat task, the biplanar fluoroscopy knee underwent more rotation and AP translation to obtain the optimal position of the tibia relative to the femur. In contrast, the bone pin knee underwent larger abduction to optimize bone placement. This was due to the constraints which were placed on the knee joint as the biplanar fluoroscopy constraint had greater range of motion for external rotation and AP translation (Qi et al., 2013), aligning with other in vivo deep-flexion studies (Hamai et al., 2013; Murakami et al., 2016). Likewise, the bone pin data

from Benoit et al. (2006) presented a greater range of motion for knee abduction-adduction as a side cut task was used which aligned with other in vivo cutting tasks (Miranda et al., 2013). This result confirmed hypotheses H1a and H1b that the bone pin knee would abduct more and the biplanar fluoroscopy knee would translate more posteriorly and rotate more externally. Few differences in kinematics occurred between biplanar fluoroscopy and bone pin knees for ML and DP translation which was due to the range of motion being similar between knee constraints.

Following the squat, the CMJ task produced the second-best agreement between knee constraints. As well, the CMJ task produced greater kinematic variability than the squat suggesting that participants were squatting to various depths to obtain a maximum jump. The CMJ task followed the same pattern as the squat task where the biplanar fluoroscopy knee rotated more externally and translated more posteriorly to obtain the required segment position (also confirming hypotheses H1a and H1b). The two knee constraints produced similar kinematic outcomes for ML and DP translation; however, large effect sizes (greater than 2) were found between abduction-adduction and IE rotation. Effect sizes were larger than those found in the squatting task suggesting that the CMJ task is more sensitive to the knee constraint being used. As the CMJ has a squat and a landing phase a combination of knee constraints could potentially be used.

The DVJ task was the last of the three tasks and had the best agreement between knee models. However, the DVJ task produced the highest variation across participants. High variation in knee flexion-extension was observed with both biplanar fluoroscopy and bone pin models which is a function of the highly variable nature of the task (Mok et al., 2016). Like the squats and CMJ, the biplanar fluoroscopy knee rotated more externally to obtain the correct tibial position while the bone pin knee abducted confirming hypotheses H1a and H1b. There was more agreement between constraints for all translations when compared to the squats and CMJ. This is due to the DVJ being

performed at a lower knee flexion angle in which either constraint can be used. The DVJ task was highly variable throughout all six degrees of freedom during the deceleration phase of the DVJ.

5.4.2 Ligament lengths

The assurance that ligament lengths were within 1 standard deviation of well-prescribed literature lengths was the second method to determine whether the created OpenSim model could produce physiological results. Of all tasks, the squat had the highest total RMSE followed by the DVJ and finally the CMJ. This directly opposed the hypothesis H1c, that the squat would have the lowest RMSE. This was likely due to the RMSE associated with the ACL length.

Of the four ligaments, the ACL was the ligament that had the most error during simulation. The model produced ACL lengths that fell outside the 1 SD bounds of literature data whenever the model passed 80 degrees of knee flexion and at its peak the ACL was 10 mm shorter than literature data. The ACL had the highest RMSE scores for the CMJ and squat tasks while the MCL had the highest RMSE score for squat. The error in ACL length is likely due to how it was simulated using linear point kinematics. The ACL length was simulated as the point kinematic distance between the ligament's origin and insertion points and at high knee flexion, the ACL will be slack and bend rather than compress (Neumann, 2010). Therefore, the linear distance between the two insertion points may be less than 25 mm whereas the actual ACL will be longer (Hewett et al., 2012; Iwahashi et al., 2008; Yoo et al., 2010).

Due to the number of tendon and ligament attachment points in the lateral knee such as the biceps femoris, anterolateral ligament and popliteus tendon, it is difficult to identify where the LCL inserts into the femur and fibula (Servant et al., 2004). Therefore, as the LCL RMSE was the greatest across all tasks which could infer there could be potential error in identifying the ligament

insertion points on an MRI and then extrapolating its position to an OpenSim model. Despite the high RMSE, the mean LCL length remains within 1 SD of literature data for a portion of each task.

For most of the tasks, the MCL and PCL lengths remained within 1 SD of ligament length data from existing literature (Li et al., 2004; Park et al., 2006). This further proves the worth of the model as it can still produce physiological ligament lengths at high knee flexion when ligaments like the PCL, are at the greatest risk for injury (Neumann, 2010). Overall, the model was able to output physiological ligament lengths for three of the four main knee ligaments and partial physiological ligament lengths for the ACL.

5.5.2 Limitations

The model used a combination of both high-resolution lower body bones from the STAPLE pipeline (Modenese & Renault, 2021) and low-resolution upper body bones from the OpenSim repository (Beck et al., 2017). These bones are not specific to the participant and may present potential challenges when placing markers exactly on the right location due to anatomical differences between participants. While marker registration error was minimized (marker positions shifted, as to reduce total RMSE during scaling) as to fall within the bounds outlined in previous literature (Hicks et al., 2015) it is impossible to ensure the optimal registration of markers on an OpenSim model without an optimization approach (Uchida & Seth, 2022).

5.6 Conclusion

This study demonstrated that a 6-DoF OpenSim knee model can be driven by in vivo kinematic constraints derived from the literature during deep knee flexion positions and output physiological joint ligament lengths. This was the first study to apply the kinematics constraint approach to various high knee-flexion tasks as well as being the first design specifically using

adolescent data. Instead of using complex optimization approaches to fix the knee, relatively simple constraints on knee range of motion were applied, based on the knee flexion angle. Despite the simple approach, the resultant kinematics were like previous studies with far more complex models (Schmitz & Piovesan, 2016; Smale et al., 2019; Xu et al., 2015). In contrast to optimization methods which may rely on bone geometry, this approach can be used if reliable knee flexion angles can be collected. Since knee flexion angles are typically the most reliable knee degree of freedom to collect using cluster-marker-based motion capture (Gray et al., 2019), our approach could be used for any OpenSim model and is not limited to the specific STAPLE-bone model which was used in this work.

The partially unlocked knee model was able to output knee ligament lengths that mostly agreed with literature except for ACL length at high knee flexion. With regards to ACL length disagreement, this only occurred during high knee flexion, not during low knee flexion where the ACL is the most likely to tear (Hewett et al., 2012).

This study was the first to apply a partially unlocked knee model to a deep-squatting task in addition to a pediatric population. With this model, various knee injury pathologies can now be compared with the confidence that the resultant differences between groups are due to true kinematics and not due to noise. As well, the addition of this model to the OpenSim repository will allow for further validation amongst other researchers.

5.7 Appendix

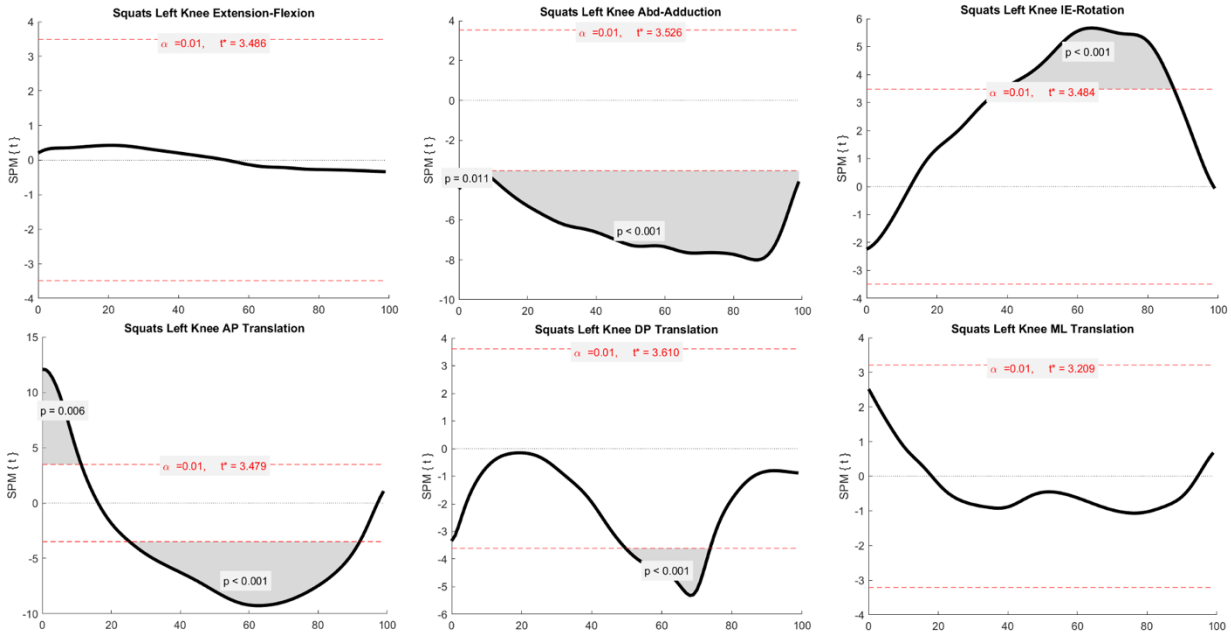

Figure A 5.2: Statistical parametric mapping of two-tailed paired-samples t-test values for the left knee during squat task, between biplanar and bone pin constraints for all six kinematic degrees of freedom, over the entire 100% of the cycle. Areas of significance are in dark grey, critical t-values to obtain a significant difference are also highlighted with red dashed lines.

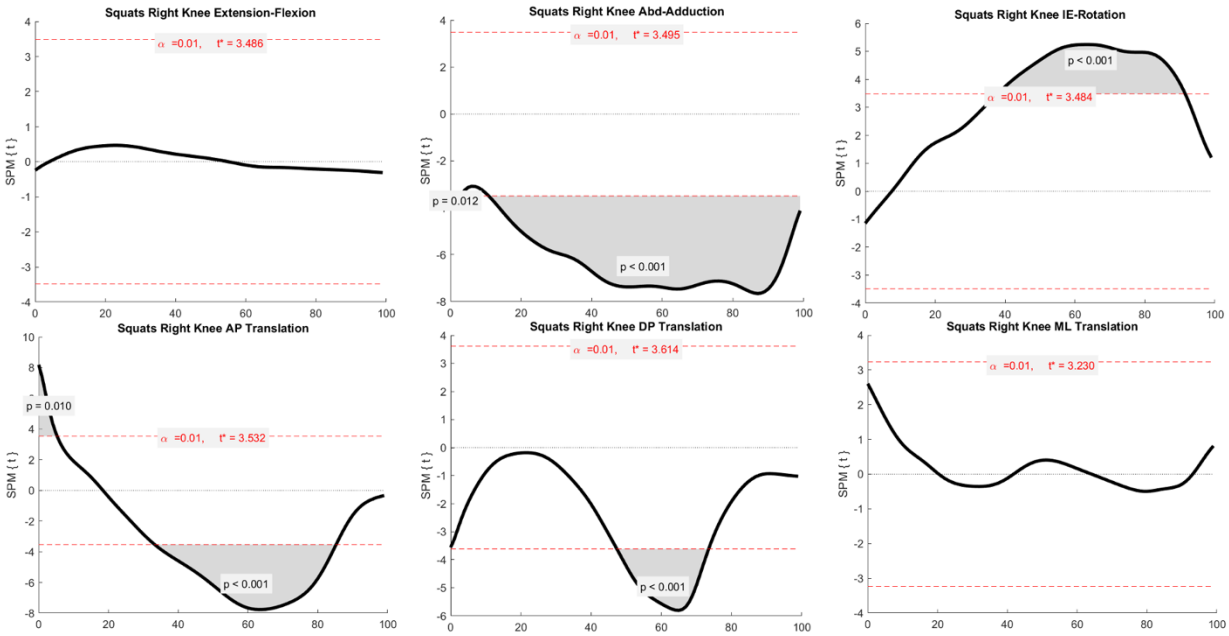

Figure A 5.2 Statistical parametric mapping of two-tailed paired-samples t-test values for the right knee during squat task, between biplanar and bone pin constraints for all six kinematic degrees of freedom, over the entire 100% of the cycle. Areas of significance are in dark grey, critical t-values to obtain a significant difference are also highlighted with red dashed lines.

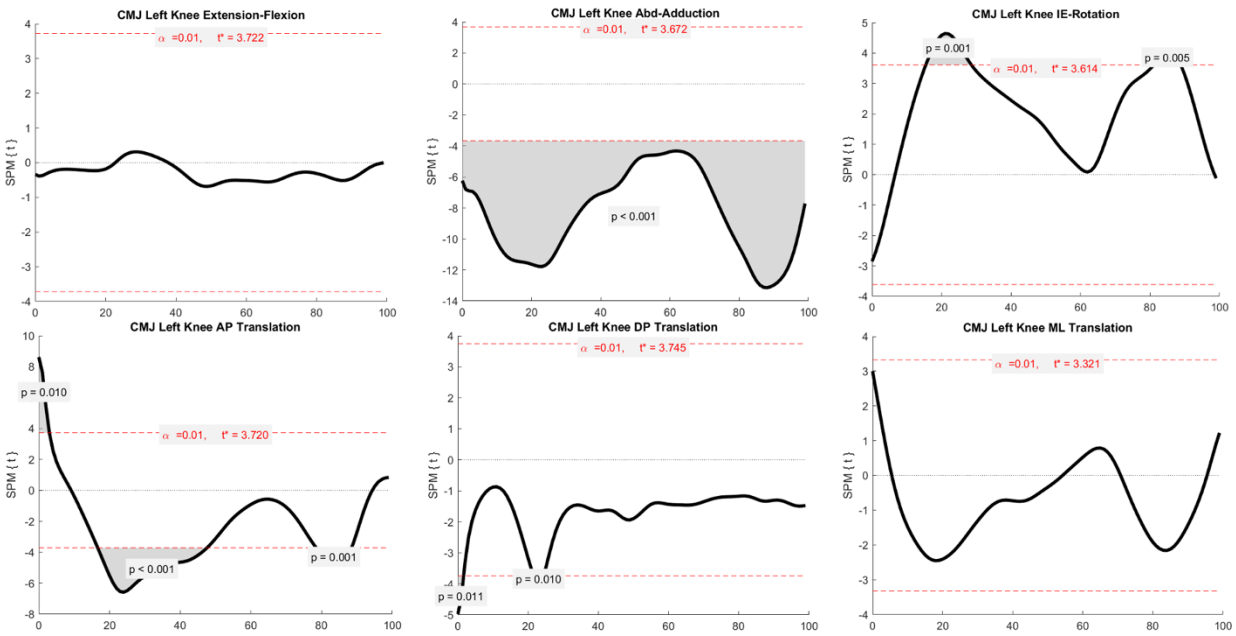

Figure A 5.3: Statistical parametric mapping of two-tailed paired-samples t-test values for the left knee during the CMJ task, between biplanar and bone pin constraints for all six kinematic degrees of freedom, over the entire 100% of the cycle. Areas of significance are in dark grey, critical t-values to obtain a significant difference are also highlighted with red dashed lines.

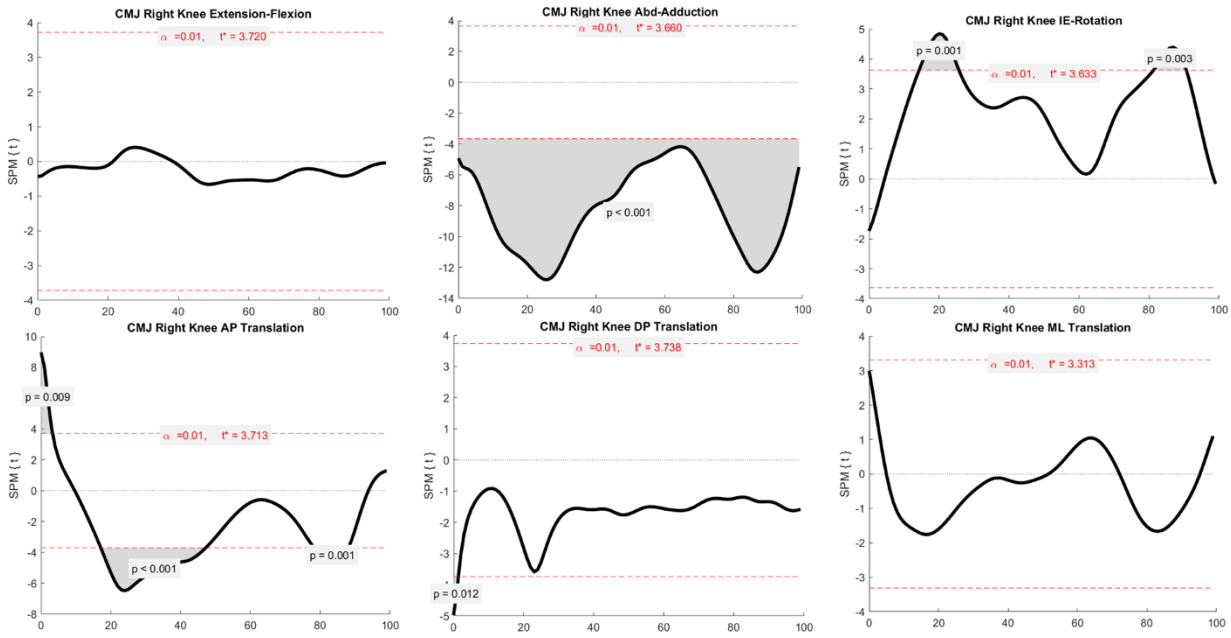

Figure A 5.4: Statistical parametric mapping of two-tailed paired-samples t-test values for the right knee during the CMJ task, between biplanar and bone pin constraints for all six kinematic degrees of freedom, over the entire 100% of the cycle. Areas of significance are in dark grey, critical t-values to obtain a significant difference are also highlighted with red dashed lines.

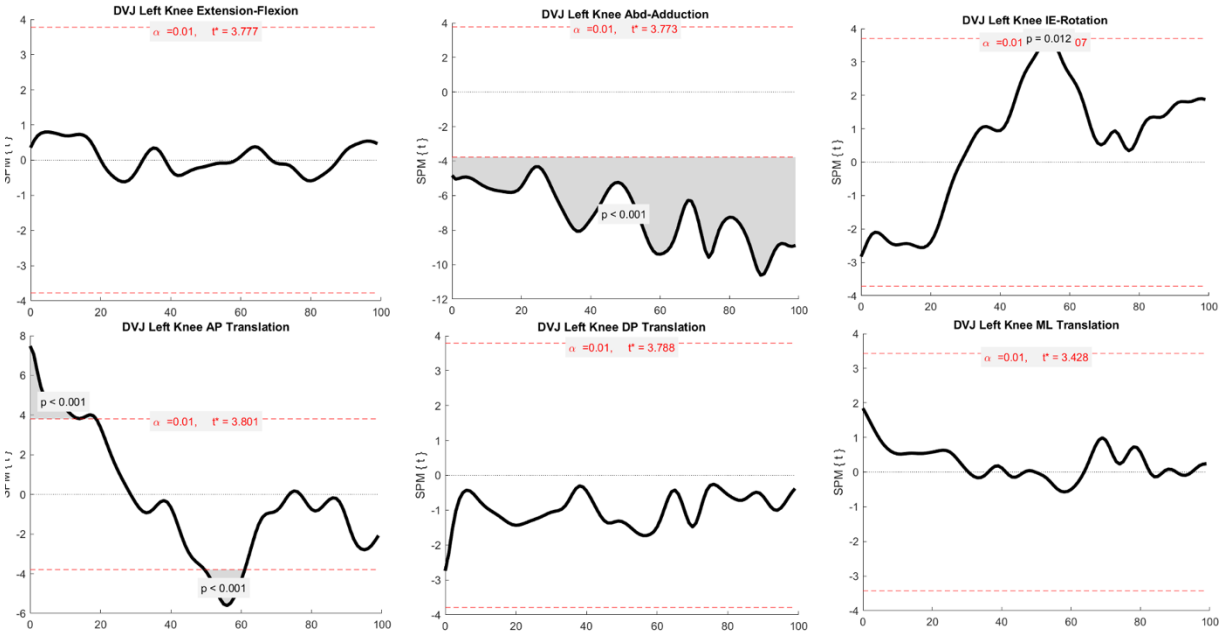

Figure A 5.5: Statistical parametric mapping of two-tailed paired-samples t-test values for the left knee during the DVJ task, between biplanar and bone pin constraints for all six kinematic degrees of freedom, over the entire 100% of the cycle. Areas of significance are in dark grey, critical t-values to obtain a significant difference are also highlighted with red dashed lines.

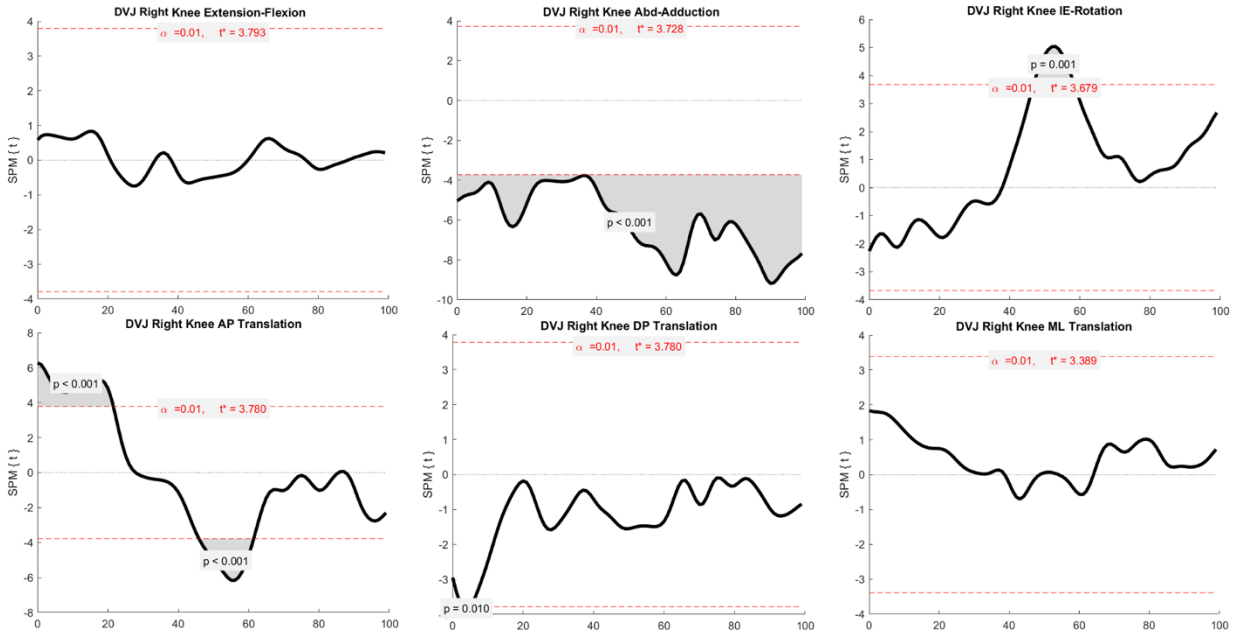

Figure A 5.6: Statistical parametric mapping of two-tailed paired-samples t-test values for the right knee during the DVJ task, between biplanar and bone pin constraints for all six kinematic degrees of freedom, over the entire 100% of the cycle. Areas of significance are in dark grey, critical t-values to obtain a significant difference are also highlighted with red dashed lines.

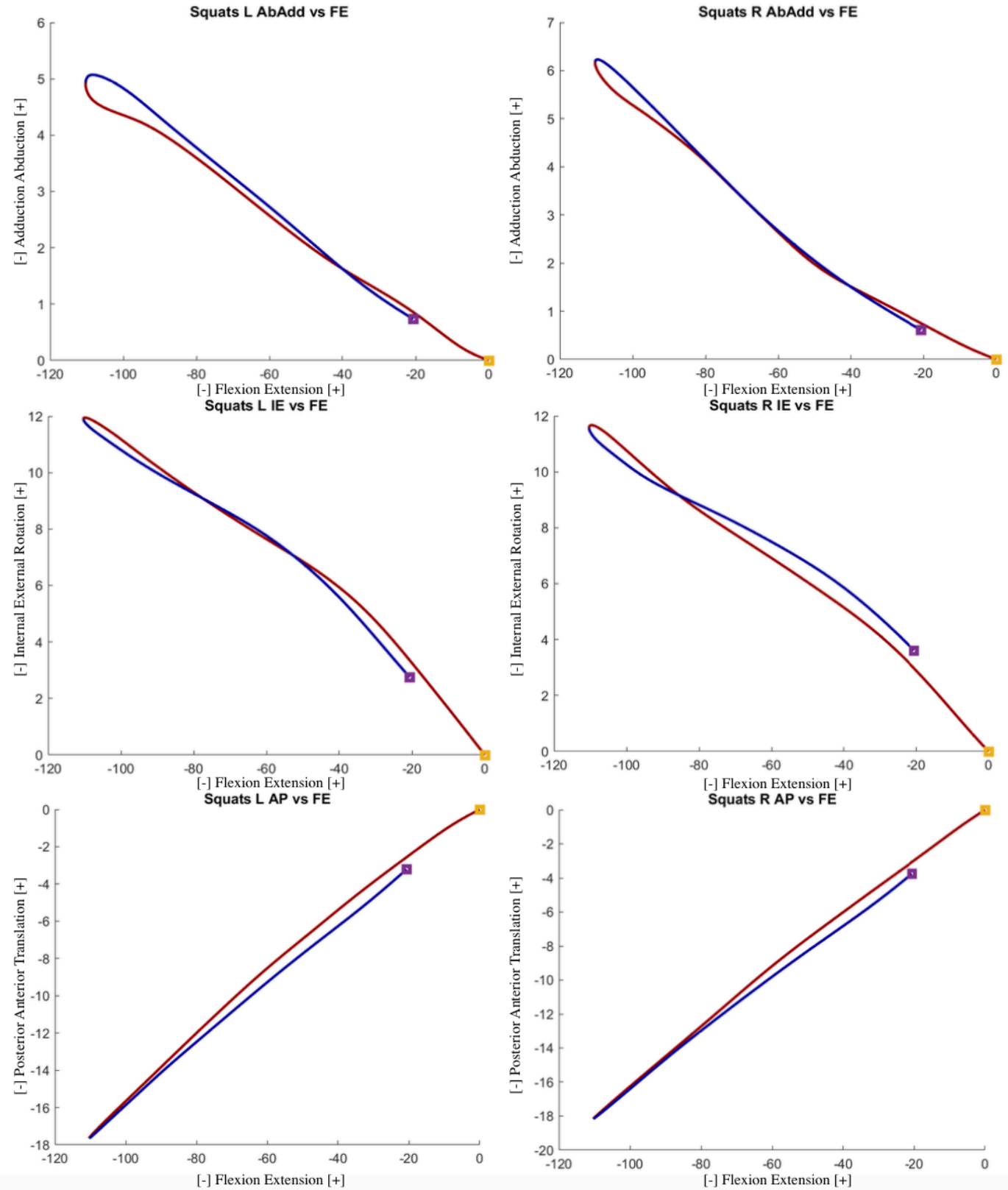
Squats L AbAdd vs FE
[-] Adduction Abduction [+]
[-] Flexion Extension [+]
Squats R AbAdd vs FE
[-] Adduction Abduction [+]
[-] Flexion Extension [+]
Squats L IE vs FE
[-] Internal External Rotation [+]
[-] Flexion Extension [+]
Squats R IE vs FE
[-] Internal External Rotation [+]
[-] Flexion Extension [+]
Squats L AP vs FE
[-] Posterior Anterior Translation [+]
[-] Flexion Extension [+]
Squats R AP vs FE
[-] Posterior Anterior Translation [+]
[-] Flexion Extension [+]

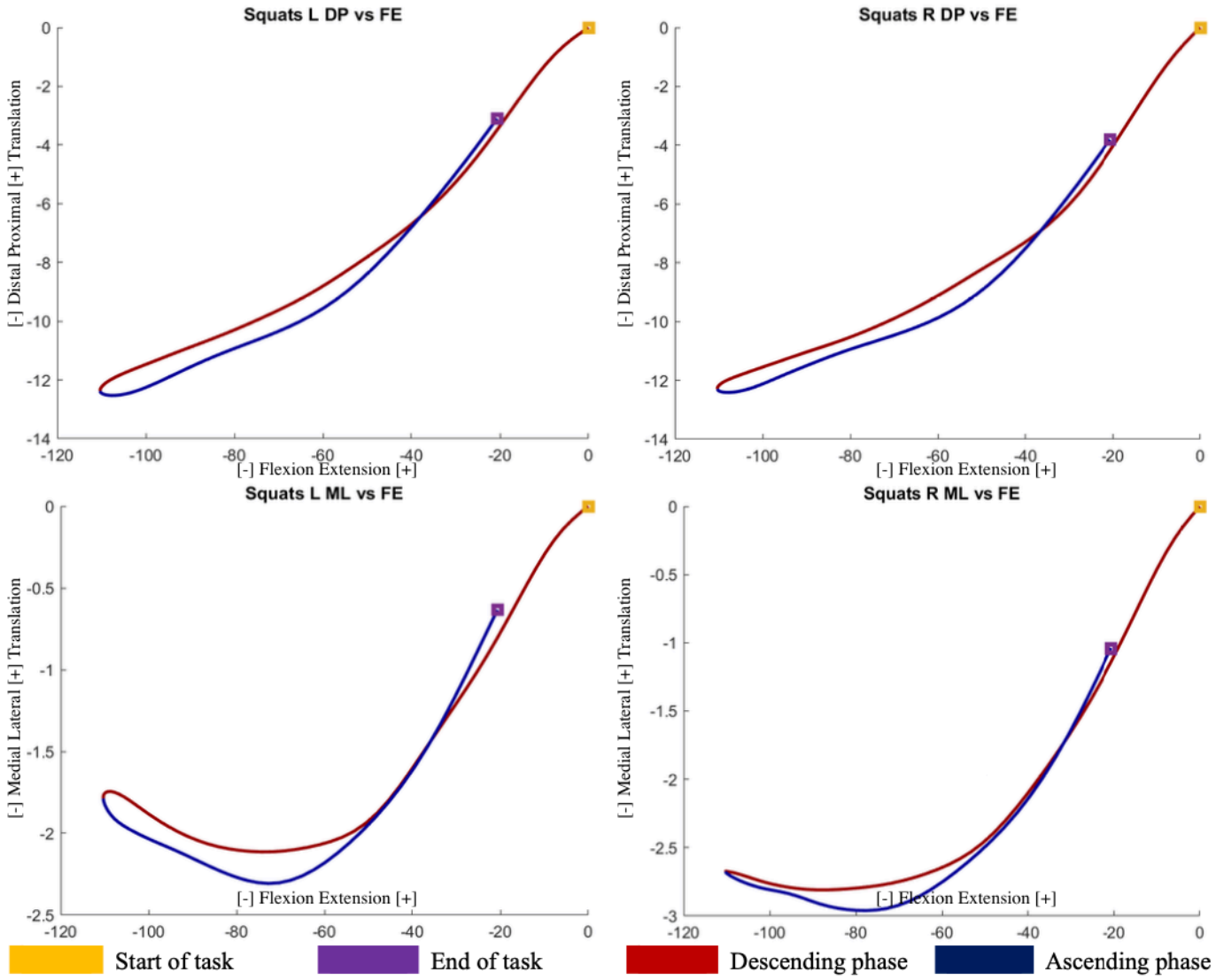

Figure A 5.7: Squatting curves representing the relationships between knee flexion-extension angle and the remaining 5 DoF of the knee, for both left and right legs. Abduction-adduction and internal-external rotation vs. flexion-extension plots are in degrees on the y-axis, while AP, DP, and ML translations vs. flexion-extension plots are in mm on the y-axis. The x-axis is in degrees for all plots. The squat task is broken up into two phases, which are represented by their corresponding colour.

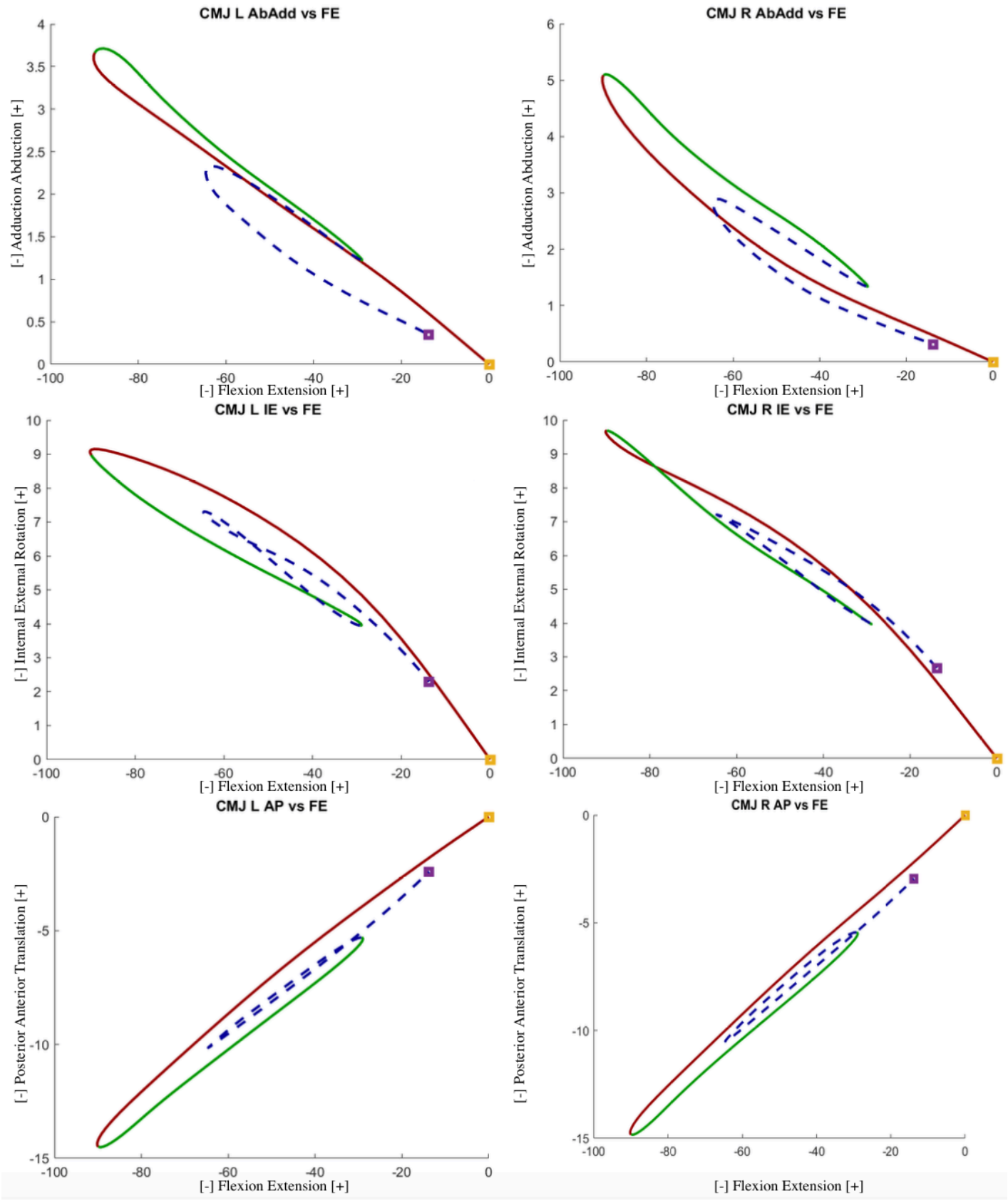
CMJ L AbAdd vs FE
[-] Adduction Abduction [+]
[-] Flexion Extension [+]
CMJ R AbAdd vs FE
[-] Adduction Abduction [+]
[-] Flexion Extension [+]
CMJ L IE vs FE
[-] Internal External Rotation [+]
[-] Flexion Extension [+]
CMJ R IE vs FE
[-] Internal External Rotation [+]
[-] Flexion Extension [+]
CMJ L AP vs FE
[-] Posterior Anterior Translation [+]
[-] Flexion Extension [+]
CMJ R AP vs FE
[-] Posterior Anterior Translation [+]
[-] Flexion Extension [+]

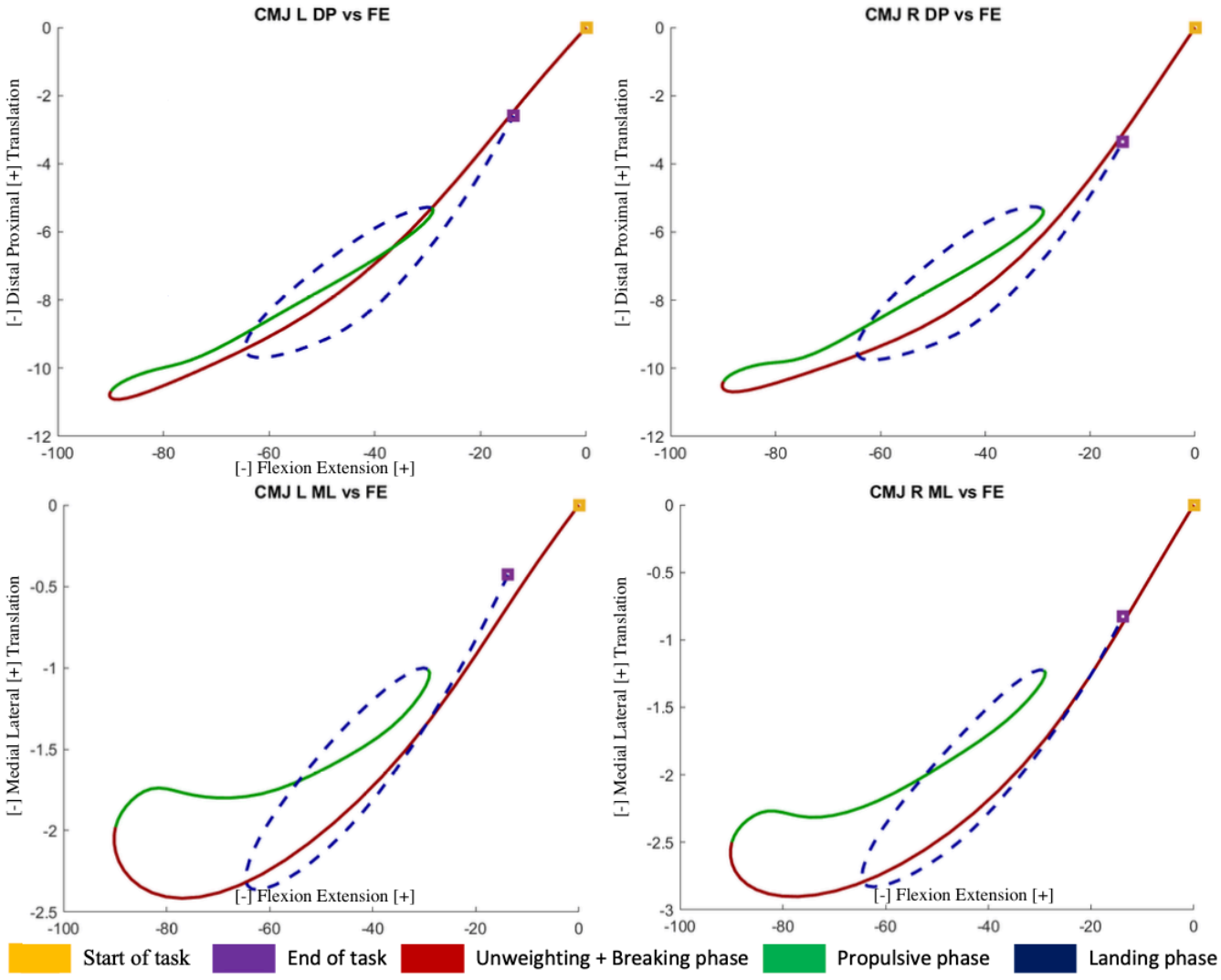

Figure A 5.8: CMJ curves representing the relationships between knee flexion-extension angle and the remaining 5 DoF of the knee, for both left and right legs. Abduction-adduction and internal-external rotation vs. flexion-extension plots are in degrees on the y-axis, while AP, DP, and ML translations vs. flexion-extension plots are in mm on the y-axis. The x-axis is in degrees for all plots. The CMJ task is broken up into three phases, which are represented by their corresponding colour.

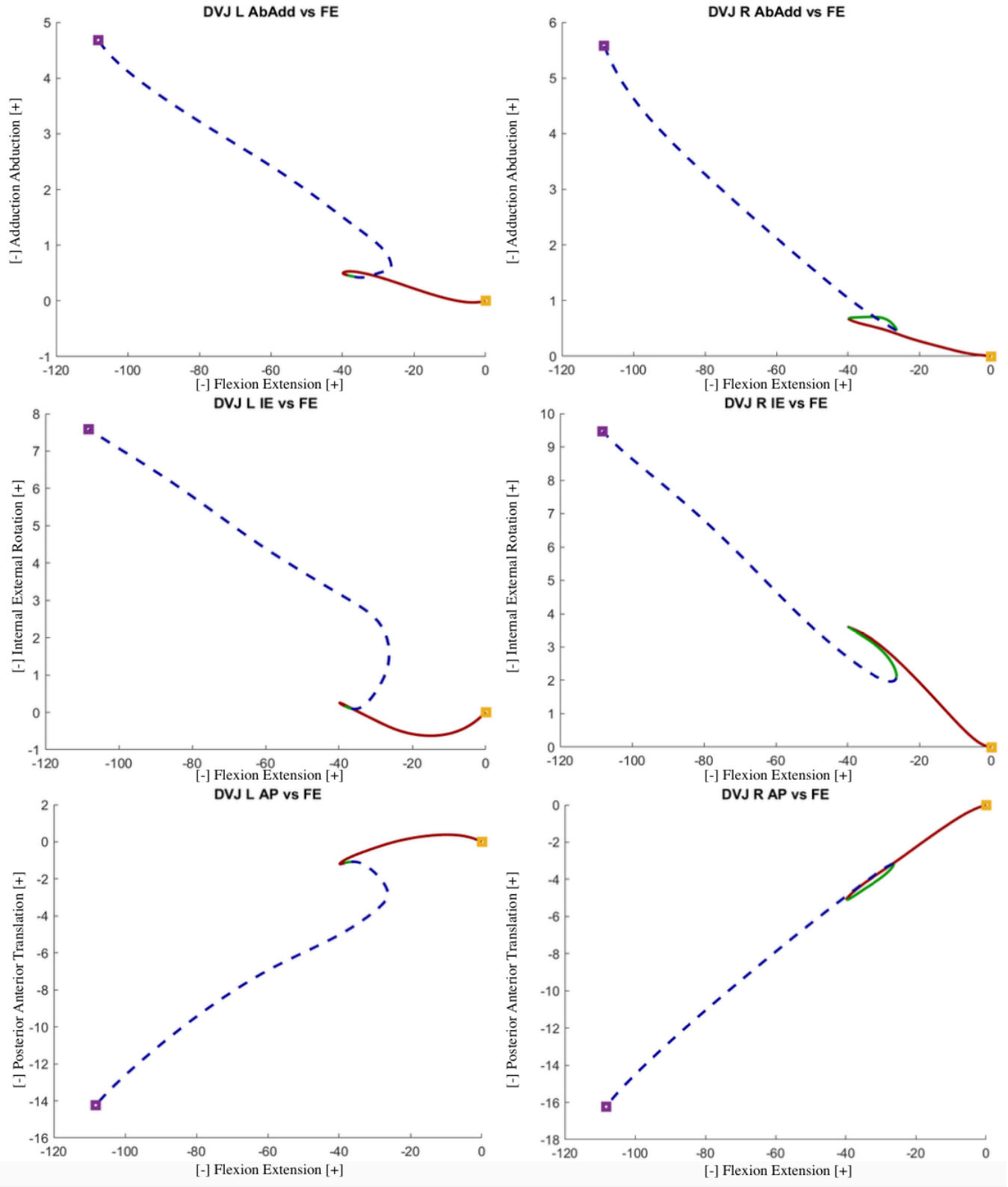
DVJ L AbAdd vs FE
[-] Adduction Abduction [+]
[-] Flexion Extension [+]
DVJ R AbAdd vs FE
[-] Adduction Abduction [+]
[-] Flexion Extension [+]
DVJ L IE vs FE
[-] Internal External Rotation [+]
[-] Flexion Extension [+]
DVJ R IE vs FE
[-] Internal External Rotation [+]
[-] Flexion Extension [+]
DVJ L AP vs FE
[-] Posterior Anterior Translation [+]
[-] Flexion Extension [+]
DVJ R AP vs FE
[-] Posterior Anterior Translation [+]
[-] Flexion Extension [+]

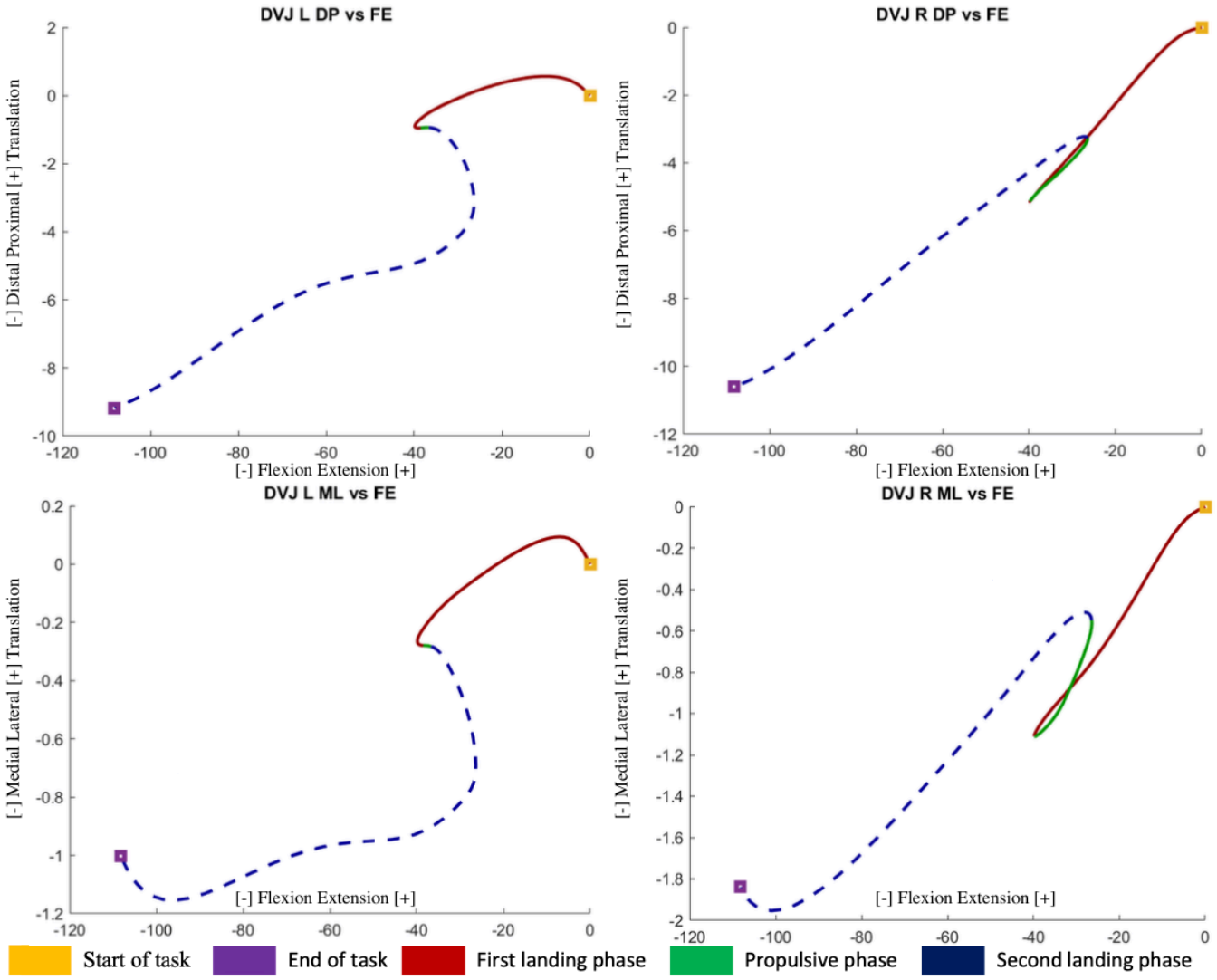

Figure A 5.9: DVJ curves representing the relationships between knee flexion-extension angle and the remaining 5 DoF of the knee, for both left and right legs. Abduction-adduction and internal-external rotation vs. flexion-extension plots are in degrees on the y-axis, while AP, DP, and ML translations vs. flexion-extension plots are in mm on the y-axis. The x-axis is in degrees for all plots. The DVJ task is broken up into three phases, which are represented by their corresponding colour.

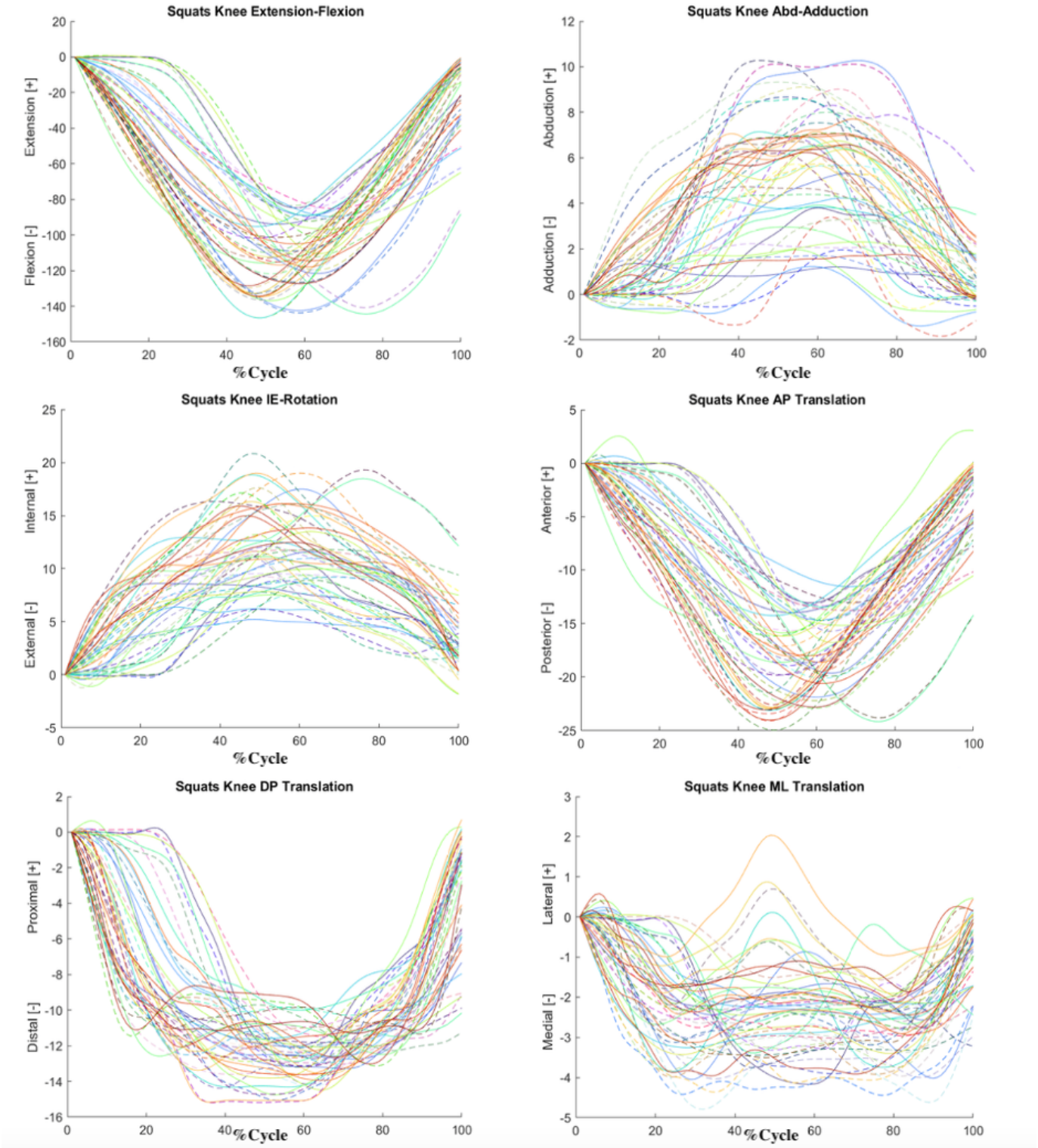

Figure A 5.10: Plots of all resultant curves for each participant, for all 6 DoF for the squatting task. Each participant is represented by a unique color, with both a solid line (right leg) and dashed line (left leg) for each of the 6 DoF.

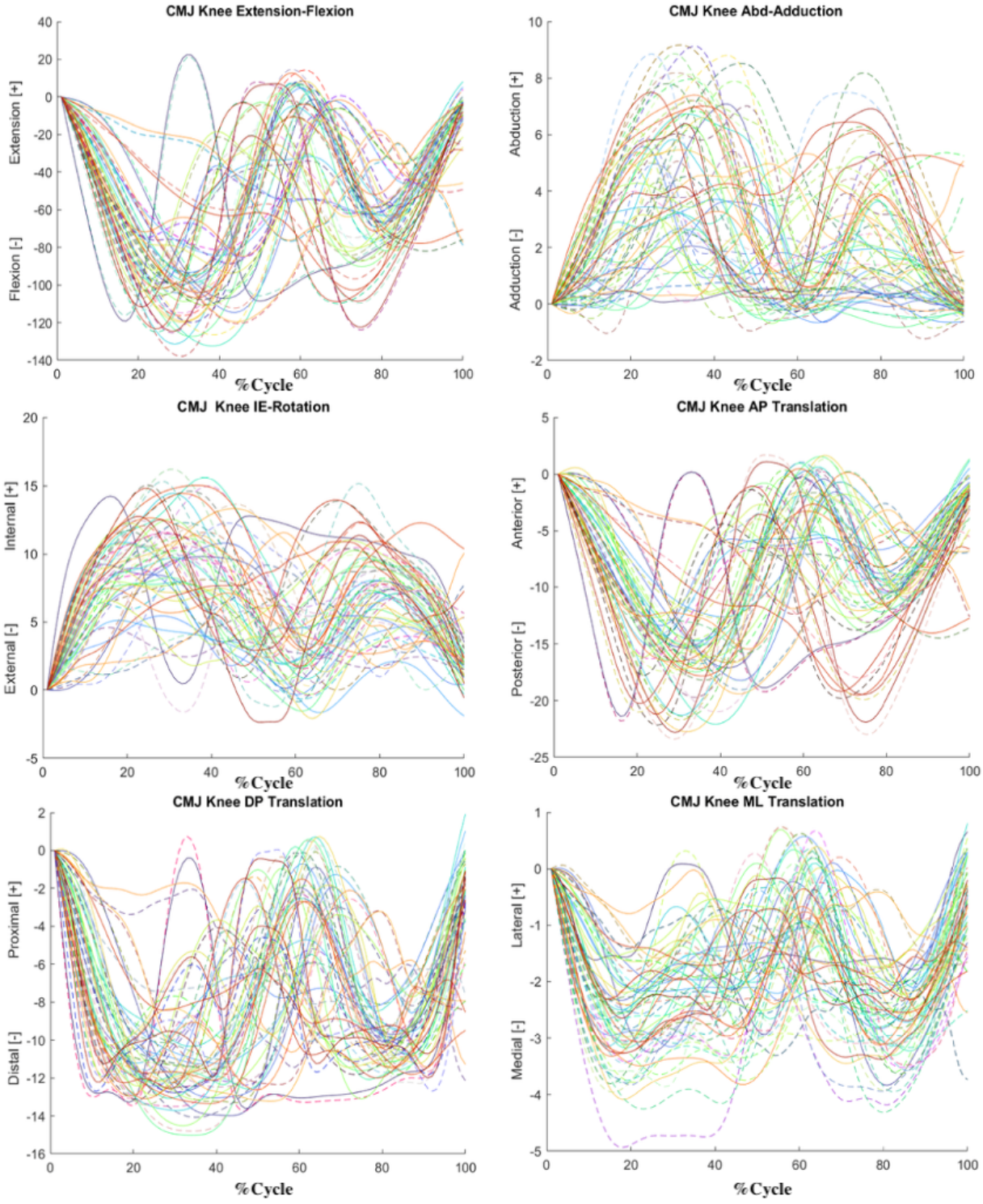

Figure A 5.11: Plots of all resultant curves for each participant, for all 6 DoF for the CMJ task. Each participant is represented by a unique color, with both a solid line (right leg) and dashed line (left leg) for each of the 6 DoF.

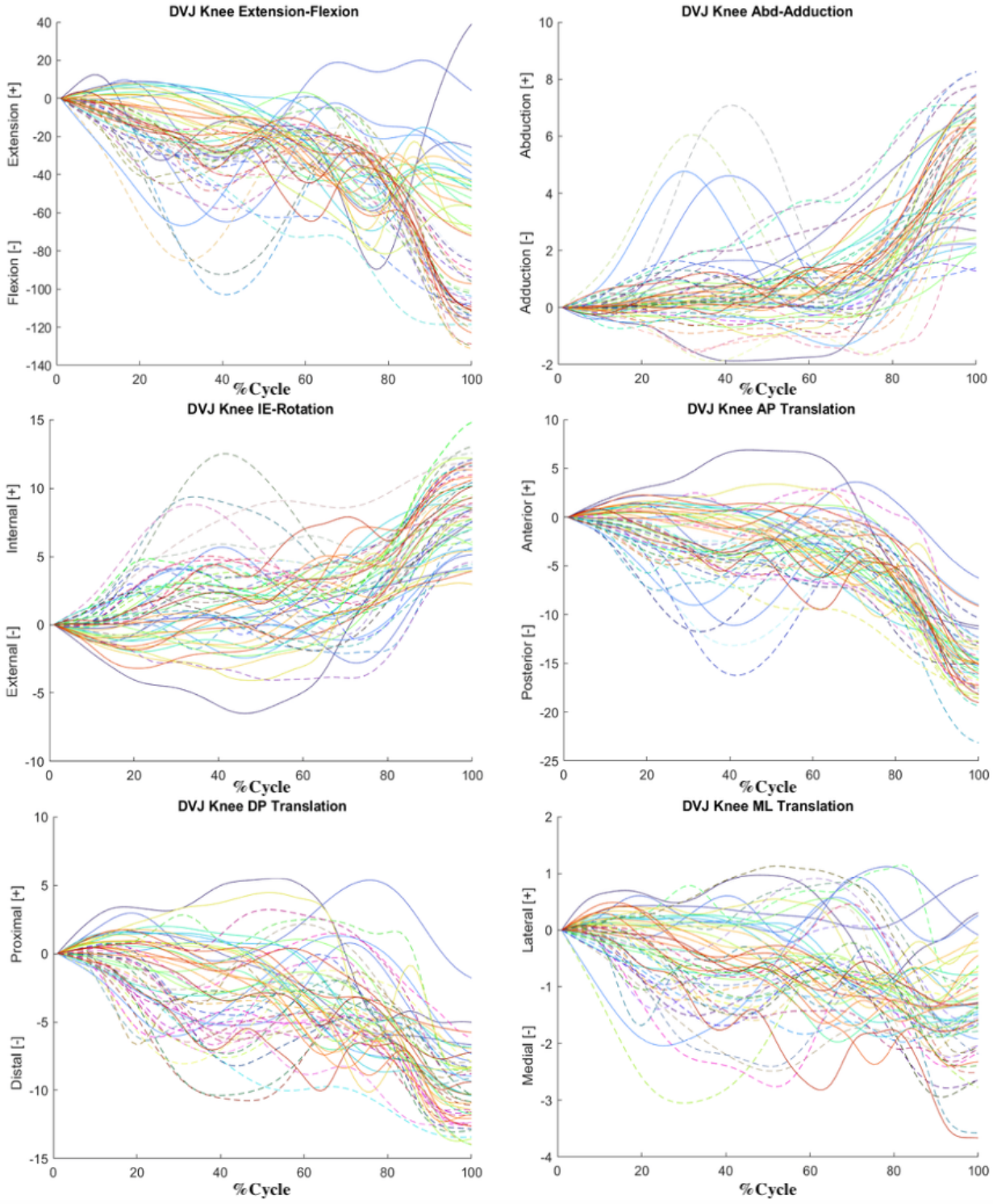

Figure A 5.12: Plots of all resultant curves for each participant, for all 6 DoF for the DVJ task. Each participant is represented by a unique color, with both a solid line (right leg) and dashed line (left leg) for each of the 6 DoF.

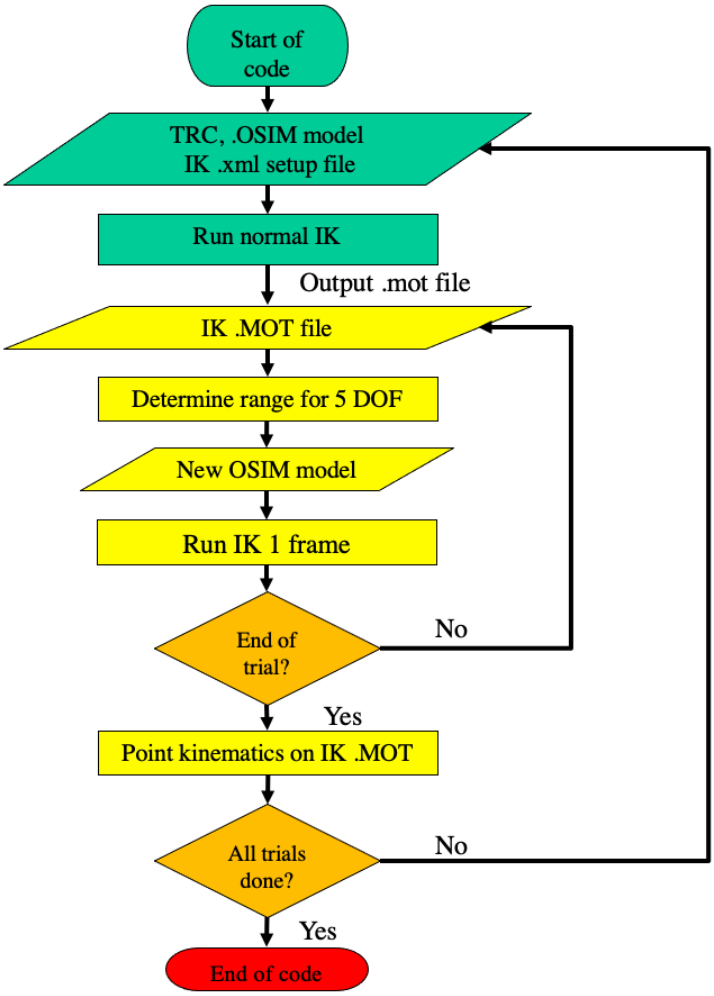

Figure A 5.13: Code process flow diagram used to create the partially unlocked knee model. All blocks in green represent the existing OpenSim workflow for inverse kinematics. All blocks in yellow represent the new pipeline created to determine knee DoF range of motion based on the knee flexion angle, as well as to run inverse kinematics for one frame, and then to run point kinematics once the trial is done. All orange blocks represent loop conditionals.

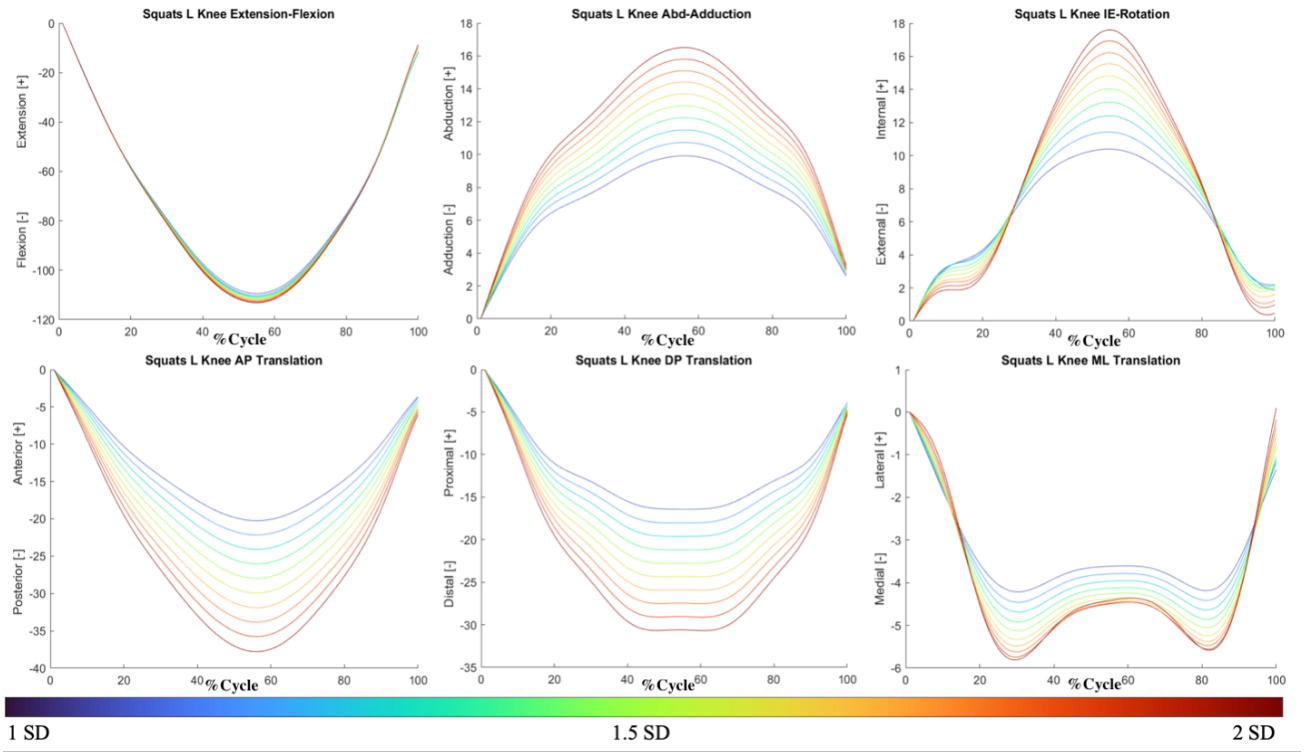

Figure A 5.14: Prescribed bounds sensitivity plots for all six knee kinematics of the left leg during the squat task, where bounds were incremented by 0.1 from 1 standard deviation to 2 standard deviations, using the existing knee kinematics data from literature. As the standard deviation doubled, knee abduction, AP, and DP translation doubled as well. Knee IE translation nearly doubled, and ML translation was reduced from 3.5 mm medial at full flexion to 1 mm medial. Therefore, for the squat task, apart from medial-lateral translation, as the bounds are increased, so too will the range of motion of the knee.

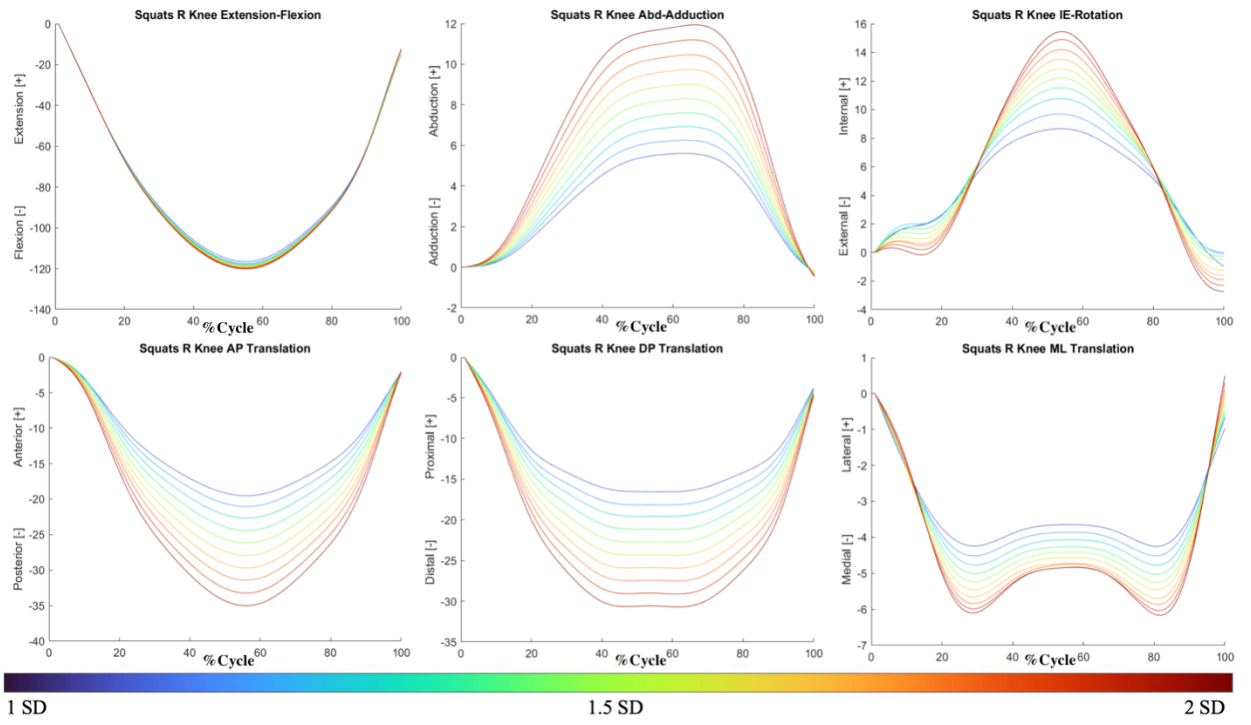

Figure A 5.15: Prescribed bounds sensitivity plots for all six knee kinematics of the right leg during the squat task, where bounds were incremented by 0.1 from 1 standard deviation to 2 standard deviations, using the existing knee kinematics data from literature. As the standard deviation doubled, AP and DP translation doubled. Knee abduction-adduction nearly doubled, IE rotation doubled at high flexion and was reduced at low flexion. ML rotation increased by 1 mm at high flexion and nearly 2 mm at lower flexion. As the bounds increased, all ROM of the knee increased as well.

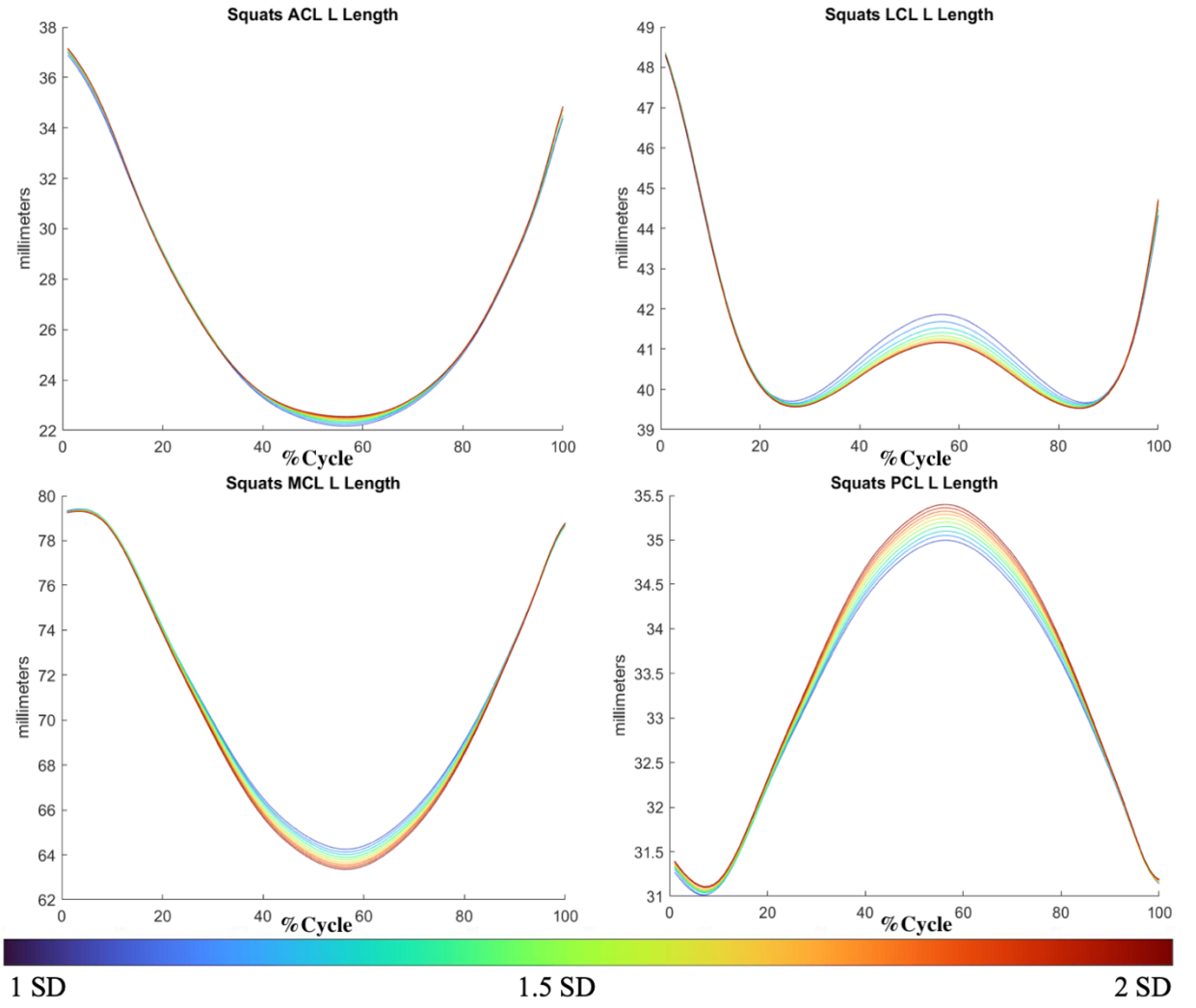

Figure A 5.16: Resultant ligament lengths for the left knee during the squat task, as the kinematic bounds were increased from 1 to 2 standard deviations. As the bounds increased, the length of the ACL underwent few changes, the LCL and MCL slightly shortened, and the PCL slightly lengthened. Ligament lengths were less sensitive to increases in bounds than knee kinematics.

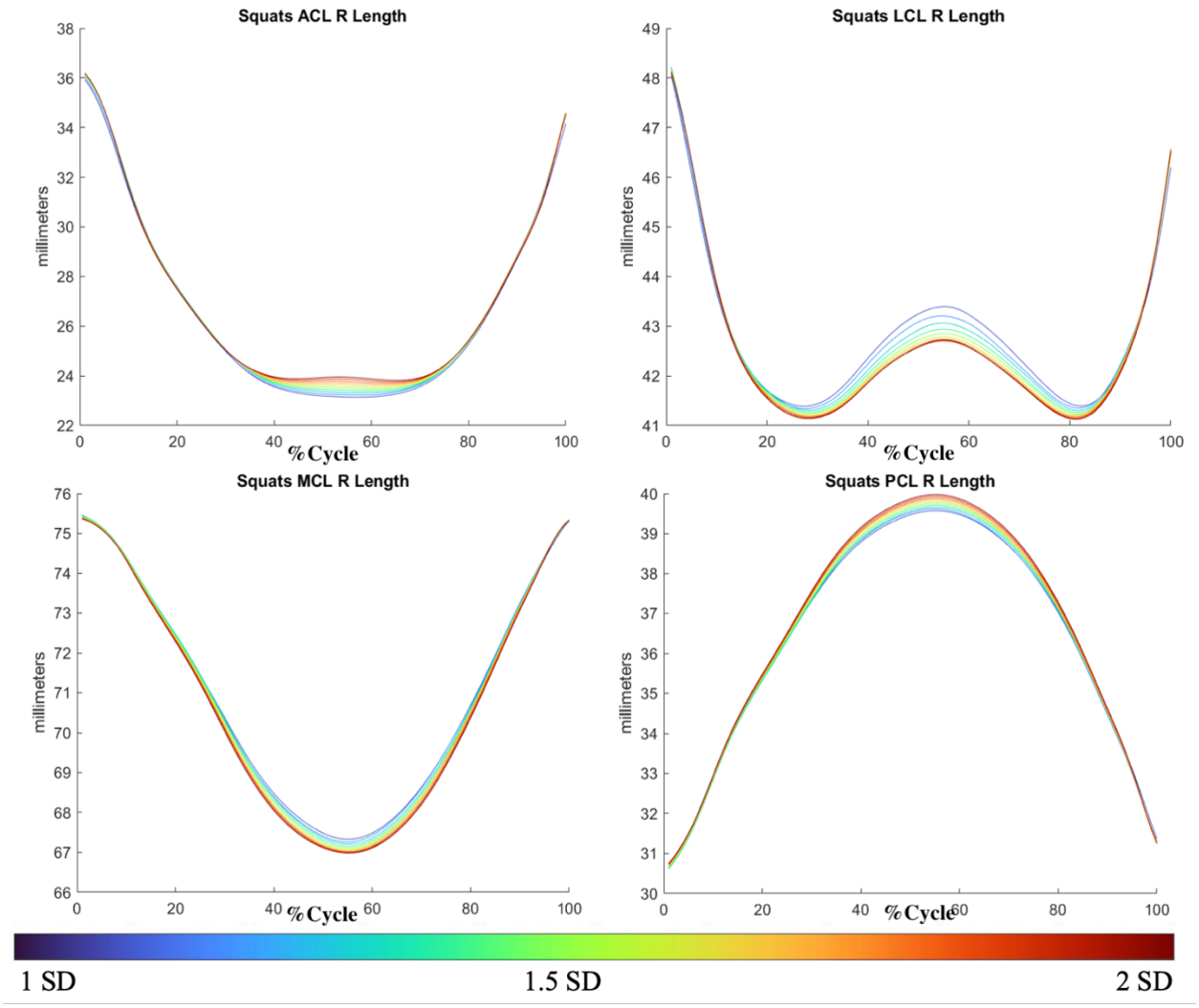

Figure A 5.17: Resultant ligament lengths for the right knee during the squat task, as the kinematic bounds were increased from 1 to 2 standard deviations. As the bounds increased, the length of the ACL underwent few changes, the LCL and MCL slightly shortened, and the PCL slightly lengthened. Ligament lengths in the right leg were less sensitive to increases in bounds than knee kinematics.

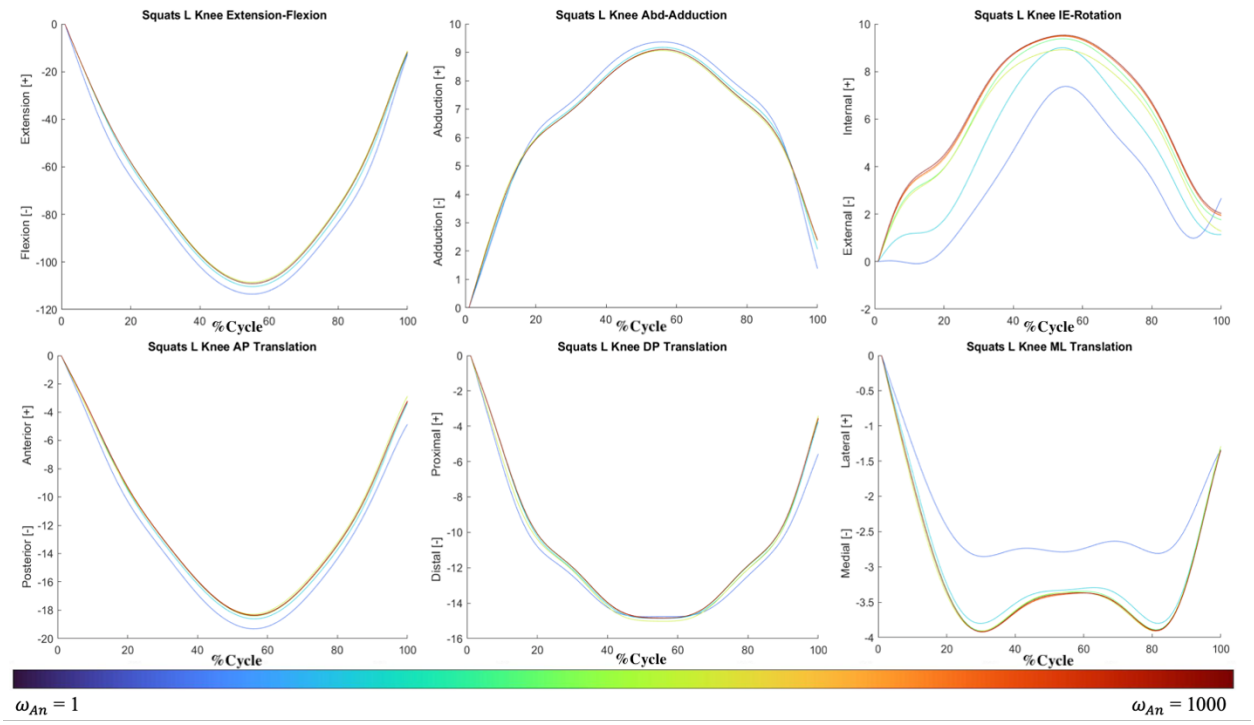

Figure A 5.18: Resultant kinematics of the left knee during the squat task, as anatomical marker weights were increased. Anatomical marker weights went from 1,10,100, to 1000. As marker weights increased, knee abduction, AP and DP translation decreased, IE rotation and ML translation increased Over all six-knee DOF, there were few changes between marker weights of 100, and 1000, the greatest change occurred from marker weights 1 to 10.

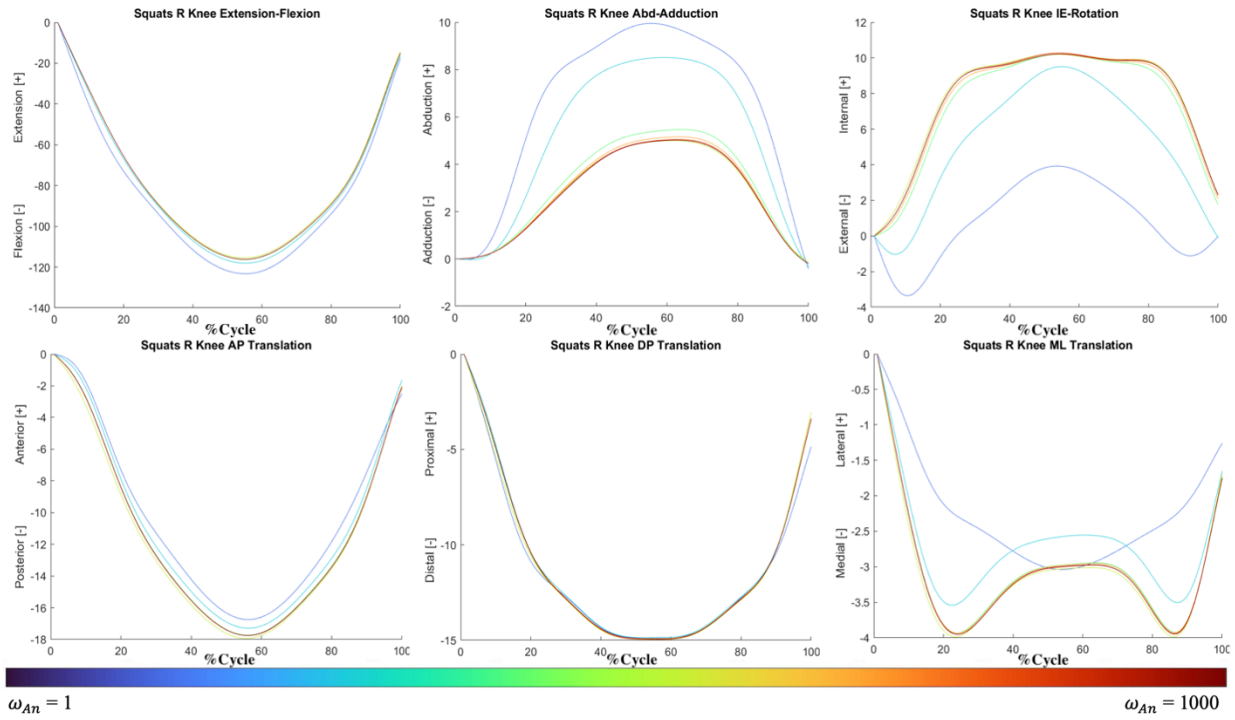

Figure A 19: Resultant kinematics of the right knee during the squat task, as anatomical marker weights were increased. Anatomical marker weights went from 1,10,100, to 1000. As marker weights increased, IE rotation and AP and ML translation increased, flexion-extension and abduction-adduction decreased, and DP translation were unaffected. Over all six-knee-DoF, there were few changes between marker weights of 10, 100, and 1000; the greatest change occurred from marker weights 1 to 10.

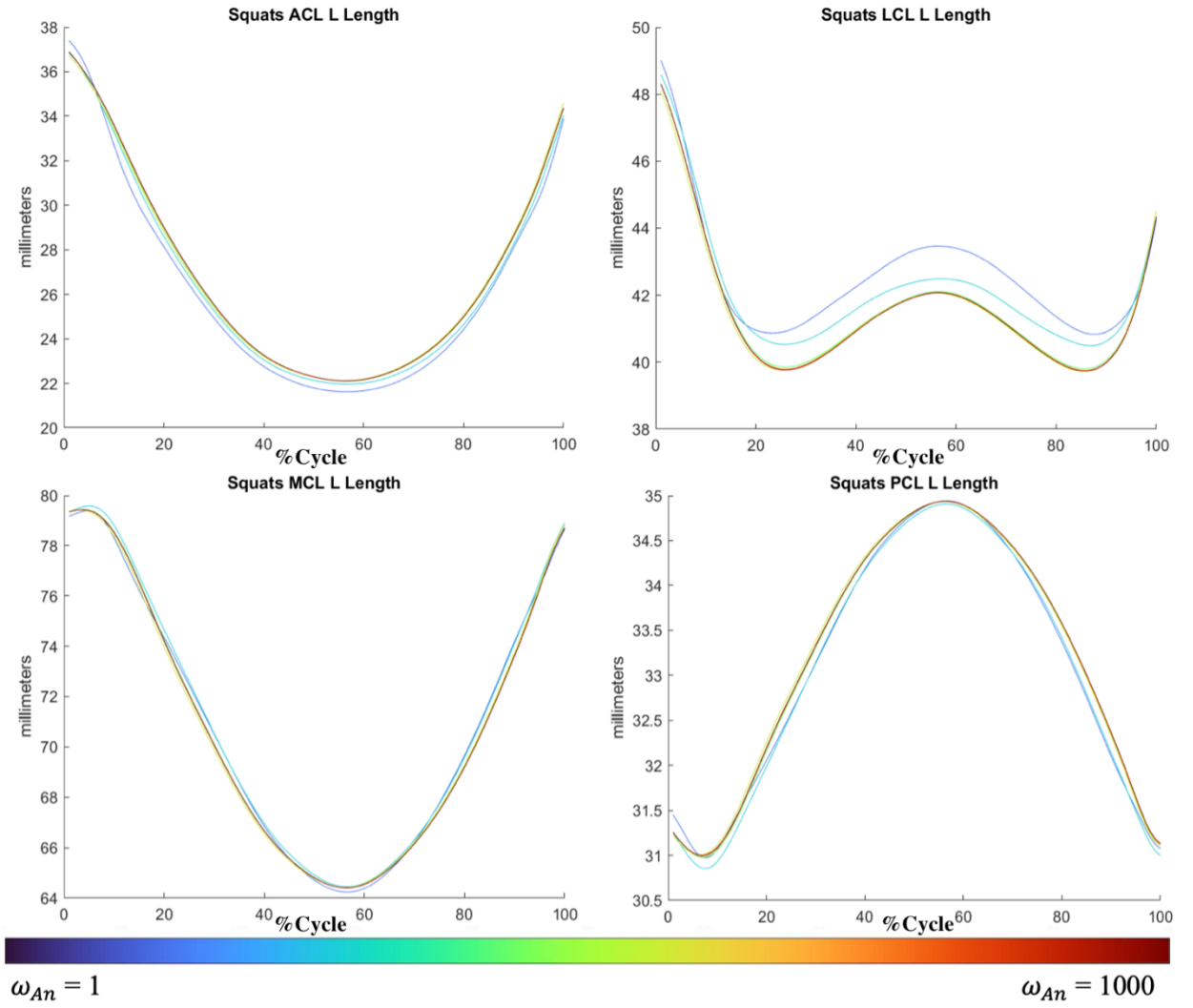

Figure A 5.20: Resultant ligament lengths of the left knee during the squat task, where anatomical marker weights were steadily increased. As marker weights increased, only the LCL presented any notable change in length. The LCL shortened as marker weights were increased, with the greatest change in length occurring between marker weights 1 and 10.

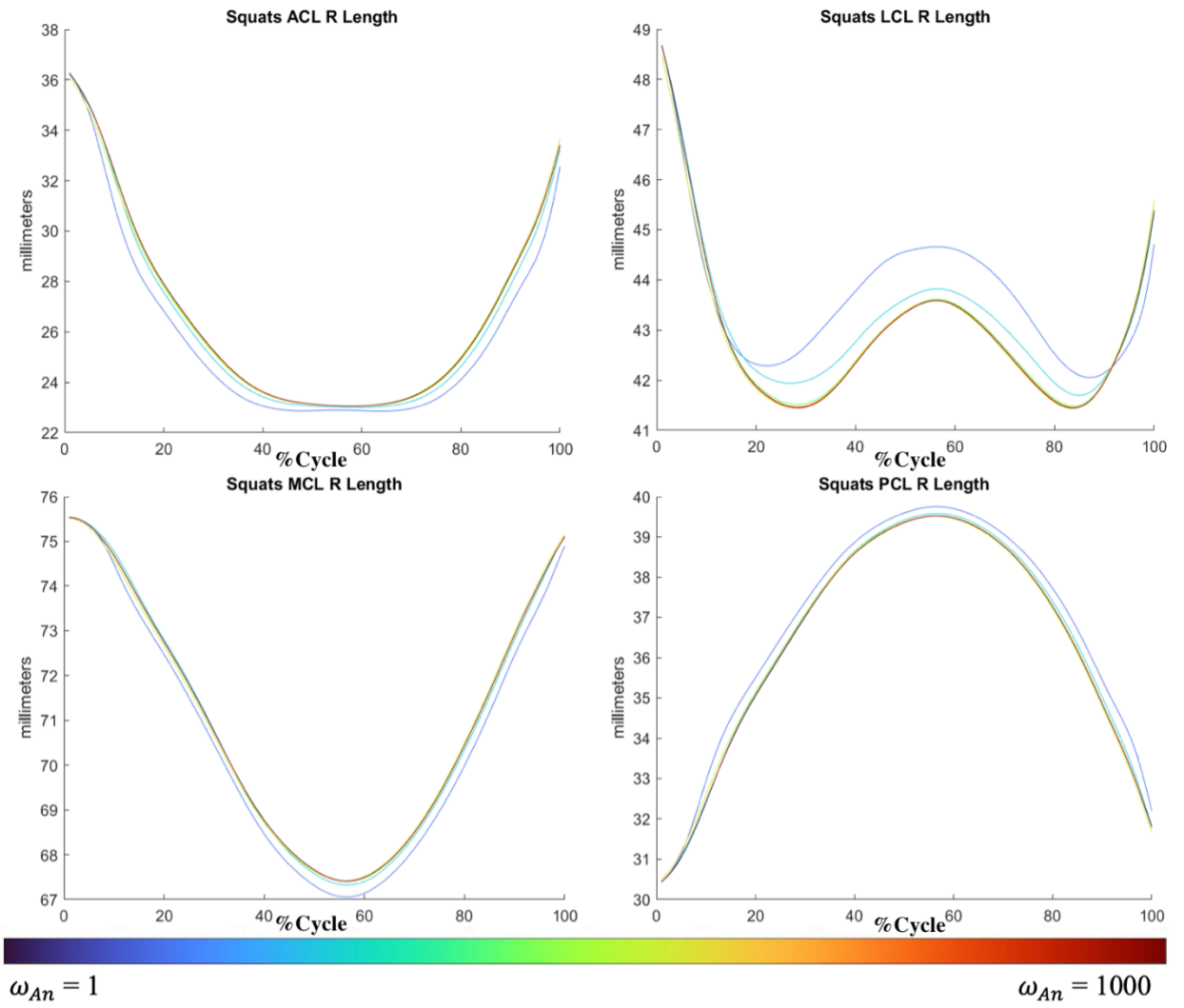

Figure A 5.21: Resultant ligament lengths of the right knee during the squat task, where anatomical marker weights were steadily increased. As marker weights increased, only the LCL presented any notable change in length. The LCL shortened as marker weights were increased, with the greatest change in length occurring between marker weights 1 and 10.

5.8 References

Arbes, S., Resinger, C., Vecsei, V., & Nau, T. (2007). The functional outcome of total tears of the anterior cruciate ligament (ACL) in the skeletally immature patient. *International Orthopaedics, 31*(4), 471-475.

Banks, J. J., Umberger, B. R., & Caldwell, G. E. (2022). EMG optimization in OpenSim: A model for estimating lower back kinetics in gait. *Medical Engineering & Physics, 103*, 103790.

Beck, N. A., Lawrence, J. T. R., Nordin, J. D., DeFor, T. A., & Tompkins, M. (2017). ACL tears in school-aged children and adolescents over 20 years. *Pediatrics, 139*(3), 1-9.

Benoit, D. L., Ramsey, D. K., Lamontagne, M., Xu, L., Wretenberg, P., & Renstrom, P. (2006). Effect of skin movement artifact on knee kinematics during gait and cutting motions measured in vivo. *Gait Posture, 24*(2), 152-164.

Carbone, V., Fluit, R., Pellikaan, P., van der Krogt, M. M., Janssen, D., Damsgaard, M., . . . Verdonschot, N. (2014). TLEM 2.0 – A comprehensive musculoskeletal geometry dataset for subject-specific modeling of lower extremity. *Journal of Biomechanics, 48*(5), 734-741.

Del Bel, M. J., Flaxman, T. E., Smale, K. B., Alkjaer, T., Simonsen, E. B., Krogsgaard, M. R., & Benoit, D. L. (2018). A hierarchy in functional muscle roles at the knee is influenced by sex and anterior cruciate ligament deficiency. *Clinical Biomechanics, 57*, 129-136.

Del Bel, M. J., Kemp, L. G., Girard, C. I., Rossignol, J., Goulet, S. F., Bourgon, J.-F., . . . Benoit, D. L. (2020). Translation and validation of the hospital for special surgery pediatric functional activity brief scale for french paediatric populations. *Physiotherapy Canada, 72*(4), 348-354.

Delp, S. L., Anderson, F. C., Arnold, A. S., Loan, P., Habib, A., John, C. T., . . . Thelen, D. G. (2007). OpenSim: open-source software to create and analyze dynamic simulations of movement. *IEEE Transactions in Biomedical Engineering, 54*(11), 1940-1950.

Donnelly, C. J., Jackson, C., Weir, G., Alderson, J., & Robinson, M. A. (2021). Prescribing joint co-ordinates during model preparation in OpenSim improves lower limb unplanned sidestepping kinematics. *Journal of Science and Medicine in Sport, 24*(2), 159-163.

Dunne, J. J., Uchida, T. K., Besier, T. F., Delp, S. L., & Seth, A. (2021). A marker registration method to improve joint angles computed by constrained inverse kinematics. *PloS One, 16*(5), 1-11.

Frank, J. S., & Gambacorta, P. L. (2013). Anterior cruciate ligament injuries in the skeletally immature athlete: diagnosis and management. *Journal of American Acadamy of Orthopaedic Surgeons, 21*(2), 78-87.

Fregly, B. J., Besier, T. F., Lloyd, D. G., Delp, S. L., Banks, S. A., Pandy, M. G., & D'Lima, D. D. (2012). Grand challenge competition to predict in vivo knee loads. *Journal of Orthopaedic Research, 30*(4), 503-513.

Gray, H. A., Guan, S., Thomeer, L. T., Schache, A. G., De Steiger, R., & Pandy, M. G. (2019). Three-dimensional motion of the knee-joint complex during normal walking revealed by mobile biplane x-ray imaging. *Journal of Orthopaedic Research, 37*(3), 615-630.

Herzog, M. M., Marshall, S. W., Lund, J. L., Pate, V., Mack, C. D., & Spang, J. T. (2017). Incidence of anterior cruciate ligament reconstruction among adolescent females in the United States, 2002 Through 2014. *JAMA Pediatrics, 171*(8), 808-810.

Hewett, T. E., Myer, G. D., & Ford, K. R. (2004). Decrease in neuromuscular control about the knee with maturation in female athletes. *Journal of Bone & Joint Surgery, 86*(8), 1601-1608.

Hewett, T. E., Myer, G. D., Ford, K. R., Heidt, R. S., Jr., Colosimo, A. J., McLean, S. G., . . . Succop, P. (2005). Biomechanical measures of neuromuscular control and valgus loading of the knee predict anterior cruciate ligament injury risk in female athletes: a prospective study. *American Journal of Sports Medicine, 33*(4), 492-501.

Hewett, T. E., Myer, G. D., Ford, K. R., Paterno, M. V., & Quatman, C. E. (2012). The 2012 ABJS Nicolas Andry Award: The sequence of prevention: a systematic approach to prevent anterior cruciate ligament injury. *Clinical Orthopaedics & Related Research, 470*(10), 2930-2940.

Hicks, J. L., Uchida, T. K., Seth, A., Rajagopal, A., & Delp, S. L. (2015). Is my model good enough? Best practices for verification and validation of musculoskeletal models and simulations of movement. *Journal of Biomechanical Engineering, 137*(2), 020905 1-24.

Iwahashi, T., Shino, K., Nakata, K., Nakamura, N., Yamada, Y., Yoshikawa, H., & Sugamoto, K. (2008). Assessment of the "functional length" of the three bundles of the anterior cruciate ligament. *Knee Surgery, Sports Traumatology, Arthroscopy, 16*(2), 167-174.

Larsson, S., B., & Karlsson, J. (1978). Histochemical and biochemical changes in human skeletal muscle with age in sedentary males, age 22-65 years. *Acta Physiologica Scandinavica, 103*, 31-39.

Li, G., Defrate, L. E., Sun, H., & Gill, T. J. (2004). In vivo elongation of the anterior cruciate ligament and posterior cruciate ligament during knee flexion. *The American Journal of Sports Medicine, 32*(6), 1415-1420.

Lund, M. E., De Zee, M., Andersen, M. S., & Rasmussen, J. (2012). On validation of multibody musculoskeletal models. *Proceedings of the Institution of Mechanical Engineers, Part H: Journal of Engineering in Medicine, 226*(2), 82-94.

Mantovani, G., & Lamontagne, M. (2017). How different marker sets affect joint angles in inverse kinematics framework. *Journal of Biomechanical Engineering, 139*(4), 1-7.

Marshall, W. A., & Tanner, J. M. (1969). Variations in pattern of pubertal changes in girls. *Archives of disease in childhood, 44*(235), 291.

Modenese, L., & Renault, J.-B. (2021). Automatic generation of personalised skeletal models of the lower limb from three-dimensional bone geometries. *Journal of Biomechanics, 116*, 110186 1-11.

Murakami, K., Hamai, S., Okazaki, K., Ikebe, S., Shimoto, T., Hara, D., . . . Iwamoto, Y. (2016). In vivo kinematics of healthy male knees during squat and golf swing using image-matching techniques. *Knee, 23*(2), 221-226.

Neumann, D, A., (2010). Kinesiology of the Musculoskeletal System: Foundations for Rehabilitation. *Mosby/Elsevier, 2nd ed.*

Otsuki, R., Del Bel, M. J., & Benoit, D. L. (2021). Sex differences in muscle activation patterns associated with anterior cruciate ligament injury during landing and cutting tasks: A systematic review. *Journal of Electromyography and Kinesiology, 60*, 102583 1-15.

Park, S. E., DeFrate, L. E., Suggs, J. F., Gill, T. J., Rubash, H. E., & Li, G. (2006). Erratum to "The change in length of the medial and lateral collateral ligaments during in vivo knee flexion". *The Knee, 13*(1), 77-82.

Pataky, T. C. (2010). Generalized n-dimensional biomechanical field analysis using statistical parametric mapping. *Journal of Biomechanics, 43*(10), 1976-1982.

Potvin, B. (2016). Predicting muscle activations in a forward-inverse dynamics framework using stabilityinspired optimization and an in vivo-based 6DoF knee joint. *MASc Thesis*, University of Ottawa.

Qi, W., Hosseini, A., Tsai, T.-Y., Li, J.-S., Rubash, H. E., & Li, G. (2013). In vivo kinematics of the knee during weight bearing high flexion. *Journal of Biomechanics, 46*(9), 1576-1582.

Rajagopal, A., Dembia, C. L., DeMers, M. S., Delp, D. D., Hicks, J. L., & Delp, S. L. (2016). Full-body musculoskeletal model for muscle-driven simulation of human gait. *IEEE Tranasactions on Biomedical Engineering, 63*(10), 2068-2079.

Reinbolt, J. A., Seth, A., & Delp, S. L. (2011). Simulation of human movement: applications using OpenSim. *Procedia IUTAM, 2*, 186-198.

Romanchuk, N. J., Del Bel, M. J., & Benoit, D. L. (2020). Sex-specific landing biomechanics and energy absorption during unanticipated single-leg drop-jumps in adolescents: implications for knee injury mechanics. *Journal of Biomechanics, 113*, 110064 1-7.

Romanchuk, N. J., Smale, K. B., Del Bel, M. J., & Benoit, D. L. (2020). Divergence analysis of failed and successful unanticipated single-leg landings reveals the importance of the flight phase and upper body biomechanics. *Journal of Biomechanics, 109*, 109879.

Shea, K. G., Pfeiffer, R., Wang, J. H., Curtin, M., & Apel, P. J. (2004). Anterior cruciate ligament injury in pediatric and adolescent soccer players: an analysis of insurance data. *Journal of Pediatric Orthopaedics, 24*(6), 623-628.

Smale, K. B., Conconi, M., Sancisi, N., Krogsgaard, M., Alkjaer, T., Parenti-Castelli, V., & Benoit, D. L. (2019). Effect of implementing magnetic resonance imaging for patient-specific OpenSim models on lower-body kinematics and knee ligament lengths. *Journal of Biomechanics, 83*, 9-15.

Uchida, T. K., & Seth, A. (2022). Conclusion or illusion: quantifying uncertainty in inverse analyses from marker-based motion capture due to errors in marker registration and model scaling. *Frontiers in Bioengineering and Biotechnology, 10*, 874725 1-11.

Yoo, Y.-S., Jeong, W.-S., Shetty, N. S., Ingham, S. J. M., Smolinski, P., & Fu, F. (2010). Changes in ACL length at different knee flexion angles: an in vivo biomechanical study. *Knee Surgery, Sports Traumatology, Arthroscopy, 18*(3), 292-297.

6.0 Manuscript 2

Title: Kinematic and ligament length differences between an ACL-injured and control pediatric population using a knee model bounded by in vivo constraints in OpenSim

Blake S. Miller[1], Céline I. Girard[2], Michael J. Del Bel[3], Daniel L. Benoit[3]

[1]School of Human Kinetics, University of Ottawa

[2]Department of Mechanical Engineering

[3]School of Rehabilitation Sciences, University of Ottawa

6.1 Abstract

Background: Despite its high prevalence in the pediatric population, there is limited knowledge if kinematics of the knee will alter following an anterior cruciate ligament (ACL) injury. To examine for differences in knee kinematics following an ACL injury, both ACL-injured and uninjured controls (CON) were asked to perform successful countermovement jumps (CMJ). Following completion of the CMJ tasks, the purpose of this study was to determine whether differences in kinematics and subsequent simulated ligament lengths existed between ACL injured and healthy control participants.

Methods: Forty ACL-injured participants (20 male [MACL], 20 female [FACL]) and 40 CON participants (20 male [MCON], 20 female [FCON]) performed a CMJ while being recorded using marker-based motion capture. Resultant marker positions were inputted into an OpenSim model where knee joint kinematics (3 rotations, 3 translations) and knee ligament lengths (ACL posterior cruciate ligament (PCL), medial and lateral collateral ligament (MCL & LCL)) were obtained using a custom pipeline. Following this, a 2x2 ANOVA was conducted with injury and sex as factors. Then, post-hoc independent samples t-tests were conducted using statistical parametric mapping (SPM) to determine timeseries differences in kinematics between ACL injured, and control participants.

Results: Female CON participants obtained deeper maximum knee flexion angles (p=0.001), and greater internal rotation (p<0.001) and distal translation (p=0.007) when compared to their ACL-injured counterparts. For males, MACL had greater distal-proximal translation (p=0.004) and MCON had greater anterior-posterior translation (p=0.012). For ligament lengths, FACL had shorter peak LCL (p= 0.007) and PCL lengths (p<0.001) when compared to FCON. Finally, MACL had shorter peak ACL (p<0.001), LCL (p<0.001), MCL (p<0.001) and PCL lengths (p<0.001) when compared to MCON.

Conclusion: Using the partially unlocked OpenSim knee model, we identified few differences in kinematics between ACL-injured and CON groups for both sexes. However, several ligament length differences between injury status were found indicating the sensitivity of ligament length to tibiofemoral motion., Based on these results, the movement strategies of the ACL- injured females and males led to smaller ligament lengths at the knee during the CMJ task.

6.2 Introduction

The human knee is a complex joint, consisting of both rotation and translation of the femoral condyles across the tibial plateau. Motion of the knee is driven by agonist muscle actuation while antagonist co-activation and passive structures (ligaments, menisci, etc.) help to constrain this motion to prevent damage to the knee (Neumann, 2010). As the antagonist muscles fatigue, passive knee structures must bear more of the load to stabilize the knee (Hirokawa et al., 1991). If these passive structures become overloaded, they will become injured and damaged and the anterior cruciate ligament (ACL) is the most injured structure in the knee (Majewski et al., 2006). The ACL is at the greatest risk for tearing during tasks that invoke high knee valgus, with external rotation of the tibia, such as landing from a jump (Hewett et al., 2005). Following an ACL injury, knee pain and perceived instability are common and can affect the psychosocial wellbeing of an athlete (Ardern et al., 2016). This type of injury is especially a concern in the adolescent population, a group where ACL reconstruction rates have drastically increased (Arbes et al., 2007; Beck et al., 2017; Herzog et al., 2017). Female adolescents are more likely to suffer an ACL injury, with estimates as high as 1 in 20 young female athletes suffering an ACL tear (Prodromos et al., 2007). Despite the high frequency of this injury in the pediatric population, there is a lack of literature on how the knee will change following an ACL tear. One such change may be the kinematics of the knee itself.

The change in knee kinematics following an ACL injury is poorly understood in adults and less so in adolescents. This may be in part due to the noise that comes with estimating knee kinematics using marker-based motion capture (Andersen, 2009; Benoit et al., 2006). The difference between ACL-injured participants and healthy control (CON) participants may only be a few degrees which is a similar magnitude to soft tissue artifact errors in joint angle calculations

with surface-based markers (Benoit et al., 2006). These small changes can nevertheless result in differences in ligament lengths at the knee (see Manuscript 1 above). Using OpenSim (Delp et al., 2007), a musculoskeletal modelling software, soft tissue artifact can be better controlled through properly constraining kinematics (Andersen, 2009; Potvin, 2016) to determine more valid estimates of 6-DoF knee kinematics between ACL-injured and CON participants.

Potvin. (2016) and Smale et al. (2019) have shown that a six-degree-of-freedom (6-DoF) knee model based on in vivo tibio-femoral motion data (Benoit et al., 2006) and implemented though OpenSim (Delp et al., 2007) can improve the validity of kinematic estimates at the knee. We have adapted this method of using kinematic ranges of motion linked to knee flexion angle (Miller et al., 2023) to include in vivo literature data for high knee flexion tasks (Gray et al., 2019; Murakami et al., 2016). However, this model has not been tested for its intended use: participants with a knee injury, specifically, an ACL injury. To establish a baseline, ACL-injured participants were compared to control (CON) participants as to determine whether differences in kinematics and ligament lengths occur. Both male and female pediatric participants were tested; however, sexes will not be compared against one another as it is well-established that there are kinematic differences between them (Ford et al., 2005; Lephart et al., 2002; Otsuki et al., 2021) and the objective of this work is not to determine whether kinematic differences occur between sexes. Therefore, female ACL-injured (FACL) will be tested against female control (FCON) and male ACL-injured (MACL) will be tested against male control (MCON). It is hypothesized that FACL and MACL participants will have significantly smaller knee translations and rotations to their control counterparts, due to perceived pain and instability (Yamazaki et al., 2010) (H1a). Due to the reduced range of motion, it is hypothesized that the lateral and medial collateral ligament (LCL and MCL) and posterior cruciate ligament (PCL) lengths will be shorter for the FACL and MACL

groups, in comparison to the CON groups (H1b). This hypothesis was made with knowledge that the LCL, MCL, and PCL reach their maximum length at high knee flexion (Li et al., 2004; Park et al., 2006).

6.3 Methods

6.3.1 Participants

Forty female (20 ACL injured, 20 Control, age = 14 ± 1.5 years, height = 162.2 ± 7.8 cm, mass = 58.4 ± 12.2 kg, Tanner stage = 4 ± 1) and forty male participants (20 ACL injured, 20 Control, age = 15 ± 1.6 years, height = 171.1 ± 10.8 cm, mass = 62.2 ± 16.2 kg, Tanner stage = 4 ± 1) were included in the study. ACL-injured (ACLi) participants were referred from the Children's Hospital of Eastern Ontario (CHEO) and had an MRI or arthroscopically confirmed ACL tear. Control participants were recruited through word of mouth from sports organisations. The inclusion criteria for control (CON) participants were that they actively participated in organized sport, had no history of any previous lower extremity injury or pain in the past six months, and had no prior traumatic knee injury (i.e., meniscal tear, ligament rupture/tear) including any diseases/illnesses that would impact the neuromuscular function. All participants read and signed a letter of informed consent approved by the local research ethics boards. Participants completed a series of self-assessment forms that reported their pubertal stage rated from 1-5, where 1 denotes the commencement of puberty and 5 denotes the end of puberty (Marshall & Tanner, 1969; Marshall & Tanner, 1970). Finally, each participant's participation in sport was measured using the HSS/FR Pedi-FABS, in English or French (Del Bel et al., 2020; Fabricant et al., 2013).

6.3.2 Protocol

Participants had their height, weight, hip, knee, and ankle width, leg lengths, and thigh and shank circumferences measured. Participants had 84 retroreflective markers (14 mm in diameter) placed according to a hybrid marker set (Mantovani & Lamontagne, 2017). Kinematic data was sampled at 200 Hz using infrared cameras (8 Vero and 2 Vantage, Vicon, Nexus, Oxford, UK). Kinetic data was sampled at 1000 Hz with 2 Bertec force plates (Model 4060, Bertec Corp., Columbus, USA). Participants completed a series of functional tasks including hop tests (Wright et al., 2015), running and cutting, squats, lunges, and jumps; however, only the CMJ tasks are described here. Five successful CMJ trials were required where a successful trial was defined by participants not losing balance upon landing. For the CMJ task, participants were instructed to squat with the goal of jumping as high as they could following the squat. The CMJ task was time normalized with the task starting when the participant first exceeded 5 degrees of knee flexion. The trial finished when the participant extended past 5 degrees of knee flexion for the final time following their landing.

6.3.3 The Partially Unlocked Knee Model

An OpenSim model with a new knee joint developed to improve physiological tibiofemoral kinematics during knee flexions beyond 60 degrees was used (Miller et al., 2023; Manuscript 1 above). Firstly, the OpenSim model (modified Rajagopal model, Rajagopal et al., 2016; 3-DoF hip, 6-DoF knee, 1-DoF ankle) had generic upper body bones (torso, spine, and head; no arms were present), and STAPLE pipeline lower body bones (pelvis, femur, tibia, and feet bones, for both legs) (Modenese & Renault, 2021). Additionally, the OpenSim model featured a partially unlocked 6-DoF knee joint. Knee flexion angle was used to define the range of motion for the five

remaining DoF. These relationships between knee flexion and the remaining 5 DoF were determined using an inverse kinematics function which assigned ranges of motion based on two in vivo studies which used biplanar fluoroscopy to assess tibio-femoral motion during deep knee flexion tasks (Gray et al., 2019; Murakami et al., 2016). This inverse kinematics function (MATLAB 2021a, The MathWorks Inc, Natick, USA) used the frame-by-frame knee flexion angle to identify the instantaneous range of the 5 remaining DoF. Depending on the knee flexion angle, corresponding upper and lower-bound range of motion were interpolated using the *interp1* function. Using the *point kinematics* function, ligament lengths were estimated by using the distance between ligament insertion points as per practice of previous studies (Li et al., 2004; Park et al., 2006). The movement trials were then time normalized based on the start of the squat (defined as the first-time knee flexion exceeded 5 degrees) to the end (the final time knee flexion was less than 5 degrees). Finally, we took the mean across all trials for each participant and then statistics were run across all participants. Group means and standard deviations were calculated as well.

6.3.4 Statistical Analysis

Participants descriptors (age, height, weight, and Tanner stage) were compared between groups using a two-samples two-tailed t-test ($p < 0.05$). Kinematic and ligament length differences between ACLi and CON participants for both males and females were assessed using statistical parametric mapping (SPM) (Pataky, 2010) and a 2x2 ANOVA was performed with sex and injury status as factors (Figures A15-16). Following this, post-hoc independent samples t-tests were performed (6 knee kinematics and 4 ligament lengths) using SPM (Figures A 6.1-6.4 for kinematics and Figures A 6.5-6.6 for ligament lengths). To control for type-1 error, the

significance threshold was adjusted using a Bonferroni *p*-value correction. All six knee DoF and all four knee ligament lengths were compared between the injured limb of the ACLi group and the non-dominant limb of the CON group (Myer et al., 2011). As well, the healthy limb of the ACLi group was compared against the dominant limb of the CON group for knee DoF and ligament lengths.

6.4 Results

Firstly, Table 6.2 shows age, height, mass, and Tanner stage data for all four groups: FACL, FCON, MACL, and MCON. For FACL and FCON, FACL participants weighed significantly more than FCON. For MACL vs. MCON, MACL participants were significantly older, taller, and had greater mass.

Table 6.2*:* Descriptive data for male and female participants with and without an ACL injury, including age, height, weight, and Tanner stage.

Group	Age [years]	*p-Age*	Height [cm]	*p-Height*	Mass [kg]	*p-* Mass	Tanner Stage (1-5)	*p-Tanner*
FACL	14±1.1	0.102	166.0±7.2	0.31	62.9±10.0	0.02*	4±1	0.75
FCON	14±1.7		163.3±8.4		54.1±11.8		3±1	
MACL	15±1.2	<0.001*	174.2±9.3	0.049*	70.3±16.0	<0.001*	4±1	0.58
MCON	14±1.4		166.7±11.4		52.3±9.7		3±1	

6.4.1 Kinematic data

The resultant kinematics are presented in the following order. First, Figure 6.1 shows the kinematic waveforms for female ACL injured limb (FACLi) and female control non-dominant limb (FCONnd). Next, Figure 6.2 shows the kinematic waveforms for female ACL healthy limb (FACL) and female control dominant limb (FCONd). Following this, Figure 6.3 and Figure 6.4 shows the kinematic waveforms for male ACL injured limb (MACLi) and control non-dominant

limb (MCONnd), and male ACL healthy limb (MACL) and male control dominant limb (MCONd).

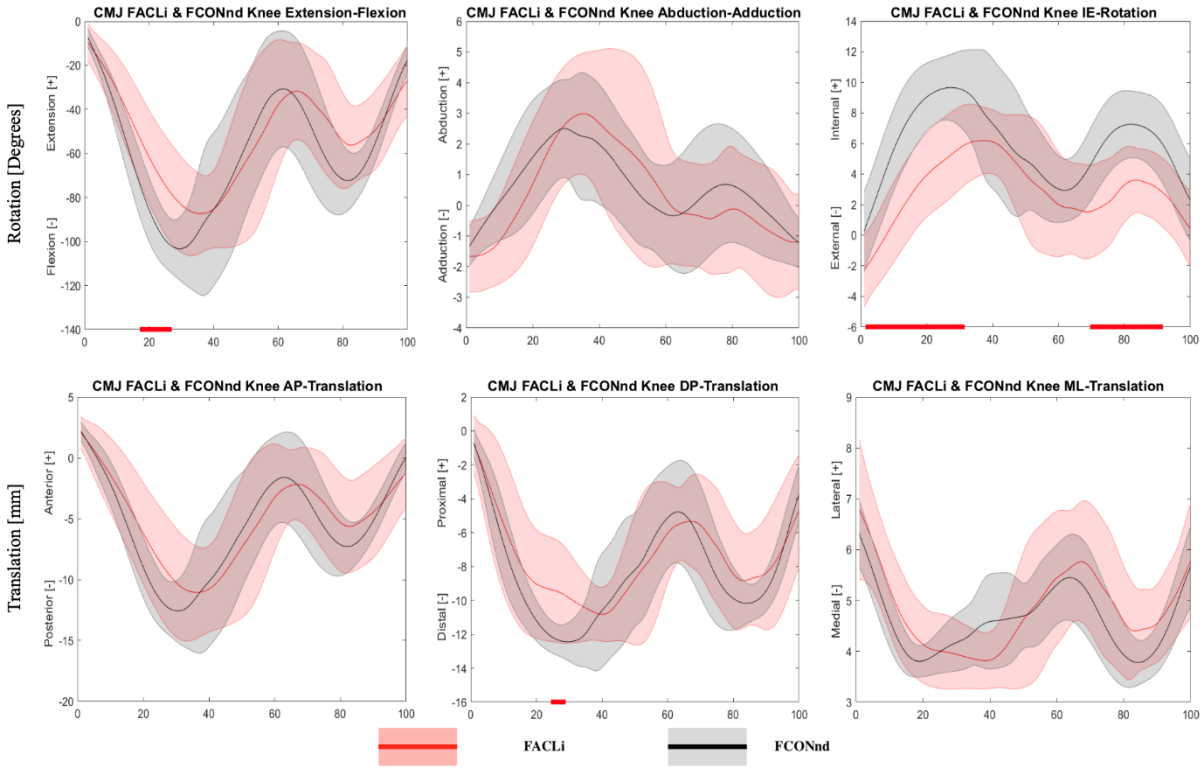

Figure 6.1: Rotation and translation waveforms of mean and ± 1 standard deviation for FACLi (red) and FCONnd limb (black), for the CMJ task. All waveforms were time normalized to 100%.

During the CMJ for FACLi vs. FCONnd, the following kinematics occurred: FCONnd participants flexed significantly more than FACLi from 18-23% of the task (p=0.001, d=1.353, Figure 6.1), and FCONnd internally rotated significantly more from 0-32% of the task (p<0.001, d= 1.915) and from 71-91% of the task (p<0.001, d=1.541). Finally, the FCONnd group translated significantly more distally from the FACLi group at 23-27% of the task (p=0.007, d=1.249) (Figure 6.1).

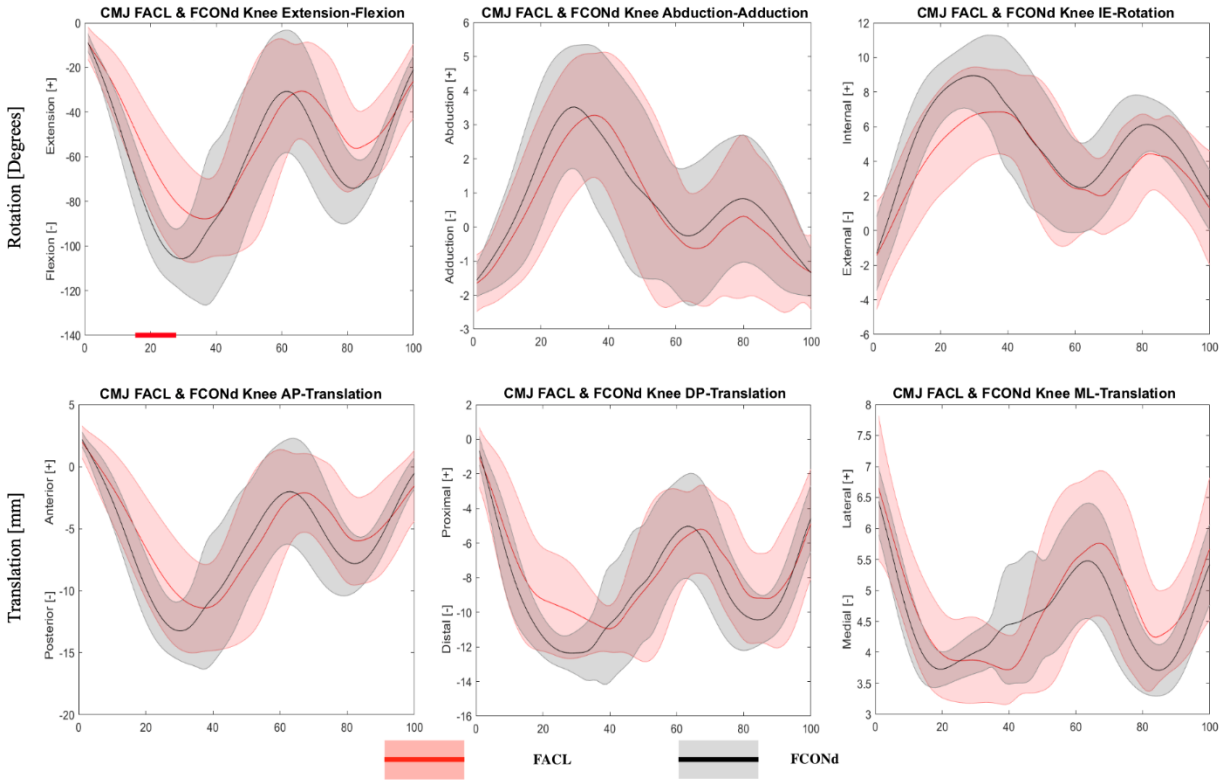

Figure 6.2: Rotation and translation waveforms of mean and ± 1 standard deviation for FACL limb and FCONd limb, for the CMJ task. All waveforms were time normalized to 100%.

During the CMJ for FACL vs. FCONd, the following kinematics occurred: the FCONd group obtained significantly greater knee flexion from 18-28% of the task (p<0.001, d=1.348; Figure 6.2).

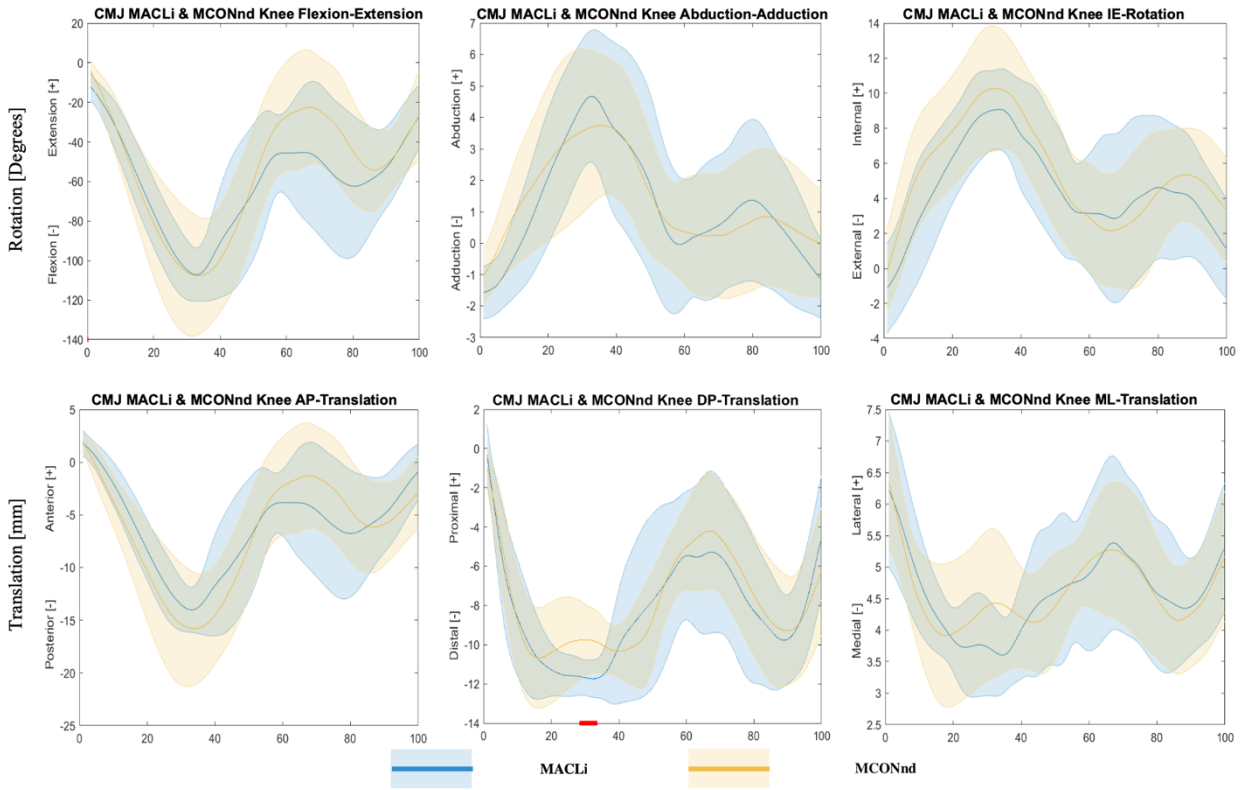

Figure 6.3: Rotation and translation waveforms of mean and ± 1 standard deviation for MACLi limb and MCONnd limb, for the CMJ task. All waveforms were time normalized to 100%.

During the CMJ for MACLi vs. MCONnd, the following kinematics occurred: the MACLi limb began in a more flexed position from 1-2% of the task (p=0.013, d=1.247; Figure 6.3) and MACLi translated significantly more distally from 29-33% of the task (p =0.004, *d*=1.332) (Figure 6.3).

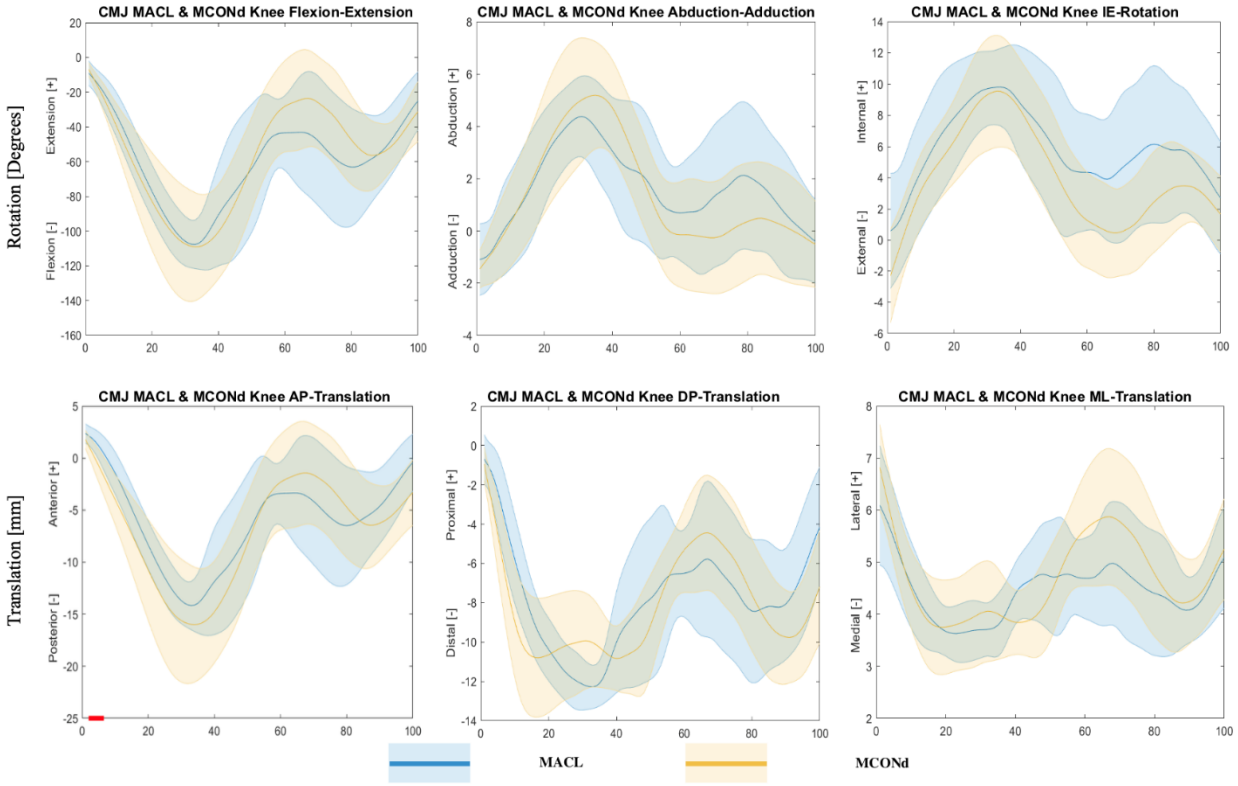

Figure 6.4: Rotation and translation waveforms of mean and ± 1 standard deviation for MACL limb and MCONd limb, for the CMJ task. All waveforms were time normalized to 100%.

During the CMJ for MACL vs. MCONd, the following kinematics occurred: the MCONd limb began in a more anteriorly translated position from 0-5% of the task (p=0.012, d=1.530; Figure 6.4).

6.4.2 Knee ligament lengths

The resultant kinematics are presented in the following order. First, Figure 6.5 shows the ligament length waveforms for FACLi and FCONnd. Figure 6.6 shows the ligament length waveforms for FACL and FCONd. Following this, Figure 6.7 shows the ligament length waveforms for MACLi and MCONnd, and Figure 6.8 shows the ligament length waveforms for MACL and MCONd.

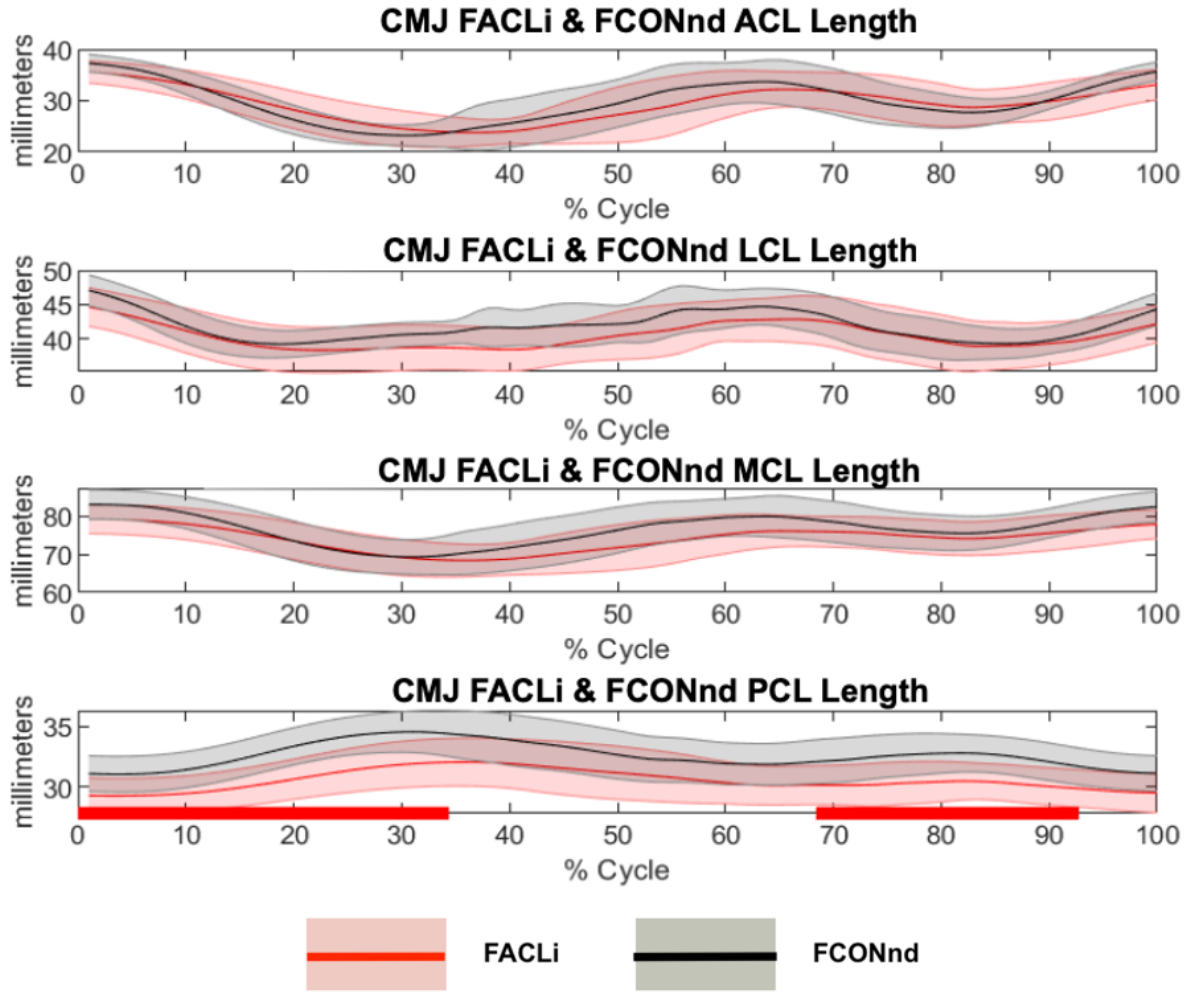

Figure 6.5: Ligament lengths for FACLi and FCONnd. Means and ± 1 standard deviation were plotted, and significant difference regions were highlighted with a bright red bar at the bottom of the plot.

Starting with FACLi vs. FCONnd (left column): FACLi had significantly shorter PCL lengths from 0-33% of the cycle (p<0.001, d=1.415) and from 68-93% of the cycle (p<0.001, d=1.288) (Figure 6.5).

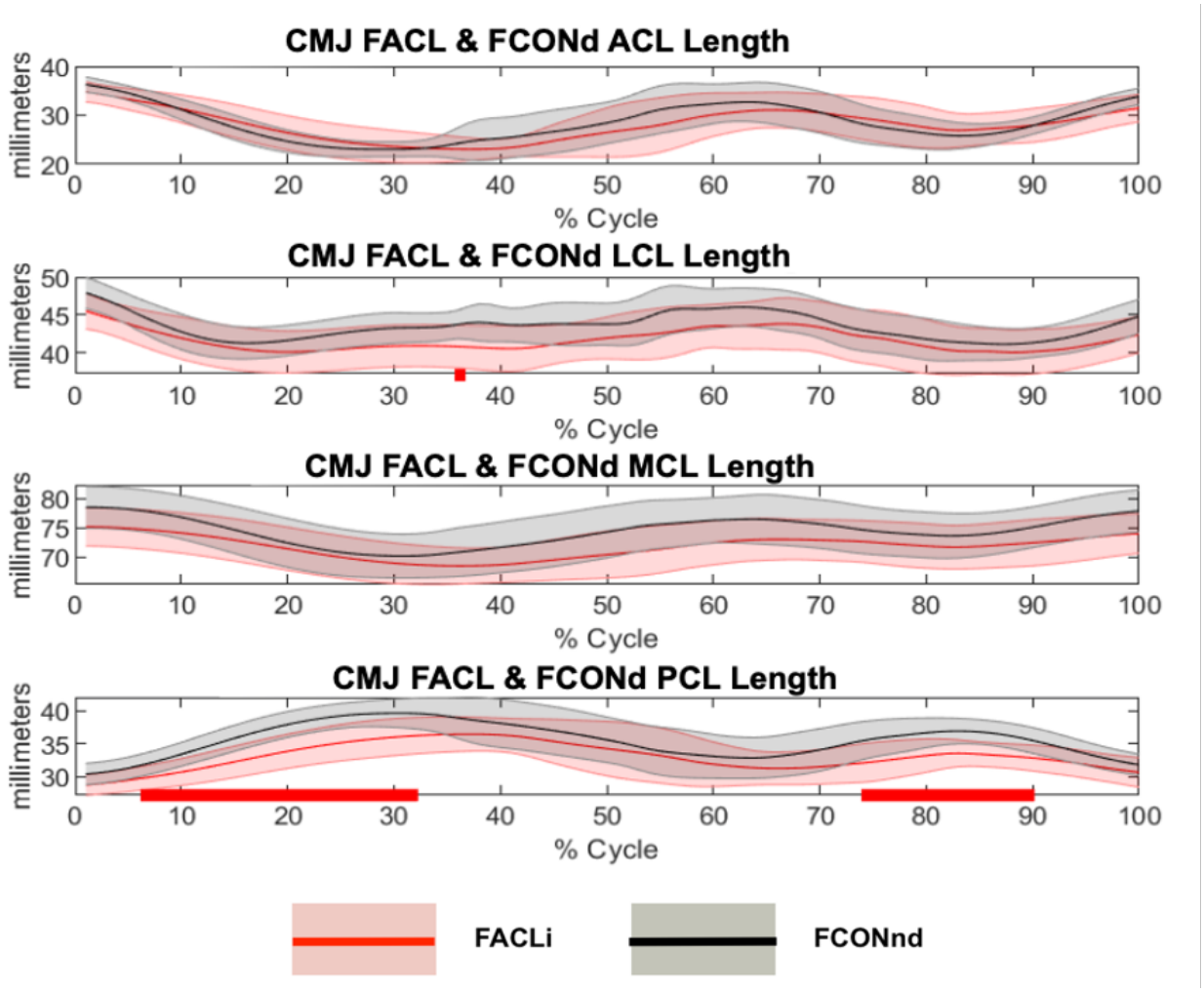

Figure 6.6: Ligament lengths for FACL and FCONd. Means and ± 1 standard deviation were plotted, and significant difference regions were highlighted with a bright red bar at the bottom of the plot.

For FACL vs. FCONd the FACL limb had significantly shorter LCL lengths from 35-37% of the cycle (p= 0.008, d=1.164), and FACL had significantly shorter PCL lengths from 7-32% cycle (p<0.001, d=1.549) and from 73-91% of the cycle (p<0.001, d=1.464) (Figure 6.6).

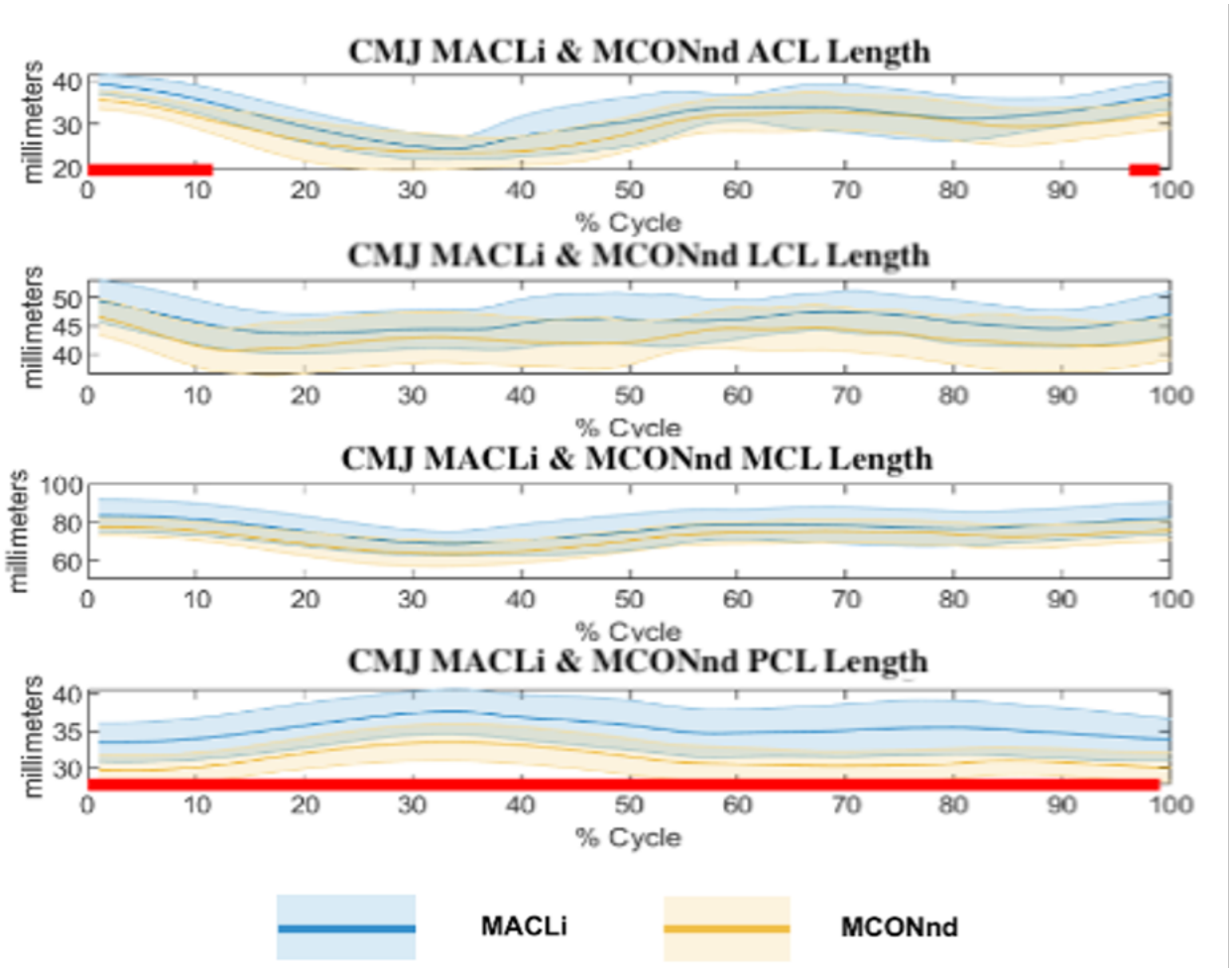

Figure 6.7: Ligament lengths for MACLi and MCONnd. Means and ± 1 standard deviation were plotted, and significant difference regions were highlighted with a bright red bar at the bottom of the plot.

MCONnd had significantly shorter ACL lengths from 0-11% cycle (p =0.038, d=1.495) and 96-99% cycle (p=0.028, d=1.228), and MCONnd had significantly shorter PCL lengths for the entire trial (p<0.001, d=1.523) (Figure 6.7).

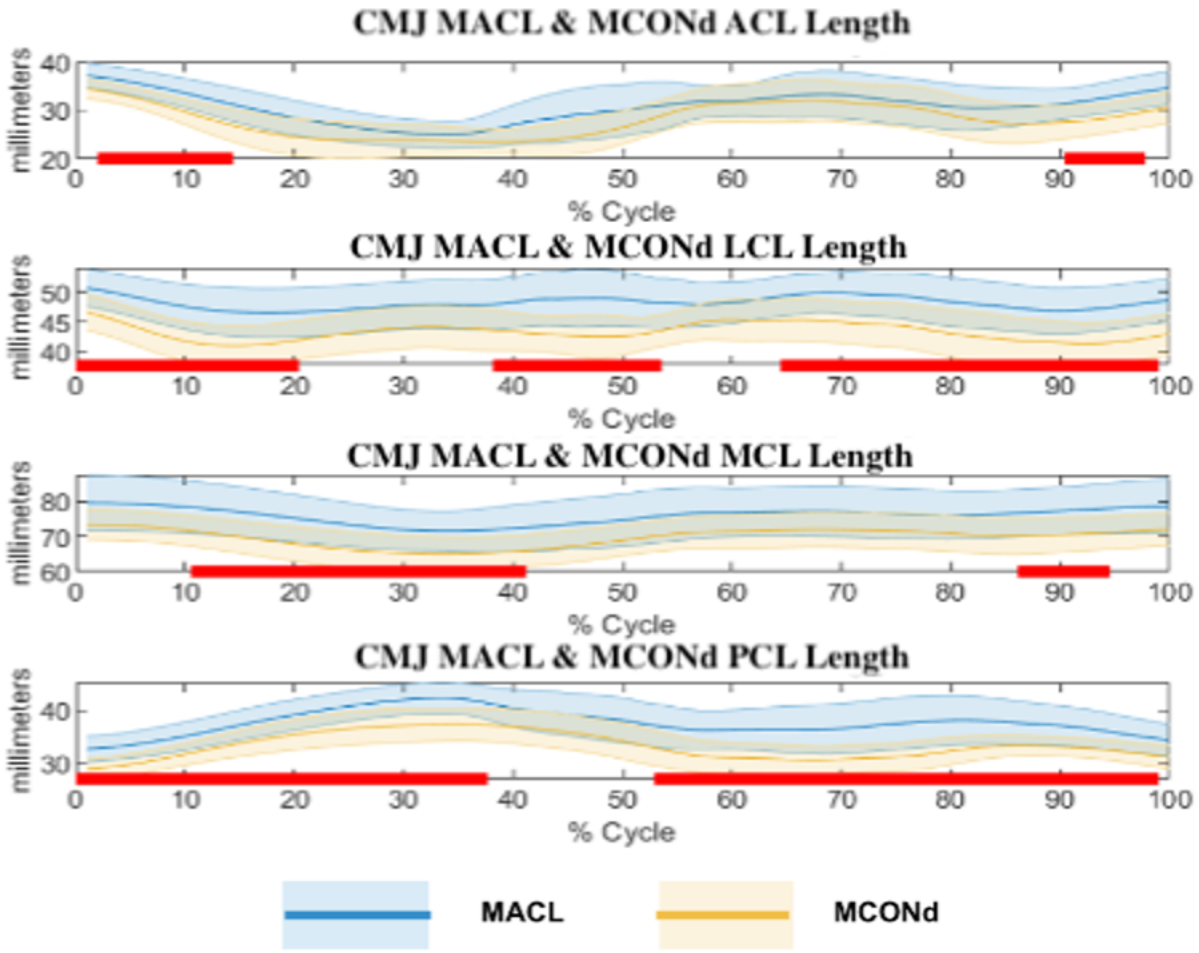

Figure 6.8: Ligament lengths for MACL and MCONd. Means and ± 1 standard deviation were plotted, and significant difference regions were highlighted with a bright red bar at the bottom of the plot.

For MACL vs. MCONd: MCONd had significantly shorter ACL lengths for 3-15% cycle (p<0.001, d=1.306) and 91-97% cycle (p=0.006, d=1.274), MCONd had significantly shorter LCL lengths for 0-20% cycle (p<0.001, d=1.490), 38-53% cycle (p=0.001, d=1.285), and from 65-98% cycle (p<0.001, d=1.407), MCONd had significantly shorter MCL lengths from 11-41% cycle (p<0.001, d=1.210) and from 87-93% cycle (p<0.001, d=1.131), and MCONd had significantly shorter PCL lengths from 0-38% cycle (p<0.001, d=1.471) and from 53-99% cycle (p<0.001, d=1.435) (Figure 6.8).

6.5 Discussion

The purpose of this study was to examine knee kinematics and ligament length differences between female ACLi and CON, and male ACLi and CON. All participants performed five successful CMJ trials and results were averaged. Several differences in kinematics between ACLi injured limb and CON non-dominant limb for both sexes were identified. Female participants displayed more differences between the healthy and injured population than male participants, especially for the ACLi limb during high knee flexion. Despite the often-increased ranges of motion in the healthy cohort, simulated ligament lengths were generally higher in the injured cohort, with the PCL having the greatest differences between groups.

6.5.1 FACL vs. FCON

For FACLi vs. FCONnd, significant differences were found for flexion-extension, IE rotation, and DP translation, all at high knee flexion. The FACLi group had 20 degrees less knee flexion and 5 degrees less internal-external rotation which is in line with hypotheses H1a that FACL participants will have significantly smaller knee translations and rotations than their control counterparts, due to perceived pain and instability. This reduction in knee flexion may be a strategy to reduce the amount of external rotation that the FACL injured limb must endure as due to the loss of structural support from the ACL, there is likely additional instability in the transverse plane of the knee (Neumann, 2010; Shin et al., 2011; Yu & Garrett, 2007).

For FACL vs. FCONd, the only significant differences in kinematics were observed in flexion-extension at maximum flexion with FACL participants obtaining approximately 20 degrees less flexion than their FCONd counterparts. This reduced knee flexion angle aligns with previous literature on the adult population suffering from an ACL injury (de Fontenay et al., 2015). Despite the increased flexion angles and as opposed to the ACLi limb, there were no significant differences for the remaining 5 DoF.

In addition to kinematic differences, ligament length differences were present for both FACLi vs. FCON and FACL vs. FCONd. The PCL was shorter by approximately 3 mm for FACL limbs in comparison to FCON limbs. This partially supports hypothesis H1b that the LCL, MCL, and PCL lengths would be shorter for the FACL group in comparison to the FCON group. This may be due to the reduction in knee flexion in the FACL group, in comparison to the FCON group for both limbs. From Figure 6.1 and Figure 6.2, the FACL group achieved approximately 10 degrees less peak knee flexion angle and went into the squat portion of the CMJ at a decreased slope. This reduction in knee flexion angle is directly related to PCL length which reached a maximum at the highest knee flexion (Defrate et al., 2004). In addition to the PCL length, there was also a difference in LCL length between FACL and FCONd during the highest portion of knee flexion. This could be related to the slight increase in knee abduction at high flexion in the FCON dominant limb, which would lengthen the LCL, as knee abduction will attempt to separate the lateral tibial plateau and femoral condyle (Xu et al., 2015).

6.5.2 MACL vs. MCON

In contrast to the FACL and FCON groups, knee flexion angles were more similar between MACL and MCON. These results contrasted with hypothesis H1a, that MACL participants would have significantly smaller knee translations and rotations than their control counterparts, due to perceived pain and instability. MACLi and MCONnd had a greater variance in flexion-extension angles, which can be seen in Figure 6.12. There were few significant differences in kinematics between the two groups. However, there were several small regions (<5%) where significant differences occurred. A small region was found in AP translation for MACL healthy and MCON non-dominant, and in DP translation for MACL injured and MCON non-dominant. No significant

differences in kinematics occurred in ML translation. Of all six knees DoF, ML translation had the highest standard deviation and was especially high for the MACLi group.

Despite the few changes in kinematics, there were numerous changes in ligament lengths between the MACL and MCON groups for both limbs. Most notably, the PCL was 3-4 mm shorter for the MCON group for the entire trial for the non-dominant limb and most of the trial for the dominant limb. This contrasted with hypothesis H1b, that the LCL, MCL, and PCL lengths would be shorter for the MACL group, in comparison to the MCON group. Due to the lack of kinematic differences between MACL and MCON, the difference in ligament length may be due to anthropometric factors. This was surmised as all MACL ligament lengths were longer than MCON. From Table 6.2 as the MACL group were significantly taller, it was expected that ligament lengths would be longer (Brown et al., 2007; Hosseinzadeh & Kiapour, 2021; Stijak et al., 2009).

6.5.3 Limitations

While marker registration error was minimized as much as possible by the authors (making small shifts to marker positions as to reduce RMSE during scaling), this error type will always be present during constrained inverse kinematics simulation (Dunne et al., 2021). As well, the depth of squat before performing the jump portion of the CMJ was not standardized as the instructions were to squat then jump as high as possible. This in turn resulted in various squatting depths, resulting in highly variable maximum knee flexion angles across groups (Figures A 7-8 & Figures A11-12). Finally, it is difficult to ensure that the scaling function performed the task ideally; a photo of the participant from a static trial overlaid on the scaled model may be an approach to verify this step.

6.6 Conclusion

The partially unlocked knee model was sensitive enough to identify differences in kinematics and ligament lengths between ACLi and CON participants within the physiologically defined ranges of motion. FACLi and FCONnd groups had the greatest differences while MACL and MCONd had the least number of differences between groups. Additionally, differences were present in both the LCL and PCL across groups with the PCL being significantly longer for the MACL group and shorter for the FACL group when compared to their respective CON counterparts.

6.7 References

Andersen, M., Benoit, D., Damsgaard, M., Ramsey, D., & Rasmussen, J. (2009). Do kinematic models reduce the effects of soft tissue artefacts in skin marker-based motion analysis? An in vivo study of knee kinematics. *Journal of Biomechanics, 43*(2), 268-273.

Arbes, S., Resinger, C., Vecsei, V., & Nau, T. (2007). The functional outcome of total tears of the anterior cruciate ligament (ACL) in the skeletally immature patient. *International Orthopeadics, 31*(4), 471-475.

Ardern, C. L., Kvist, J., & Webster, K. E. (2016). Psychological aspects of anterior cruciate ligament injuries. *Operative Techniques in Sports Medicine, 24*(1), 77-83.

Beck, N. A., Lawrence, J. T. R., Nordin, J. D., DeFor, T. A., & Tompkins, M. (2017). ACL tears in school-aged children and adolescents over 20 years. *Pediatrics, 139*(3), 1-9.

Benoit, D. L., Ramsey, D. K., Lamontagne, M., Xu, L., Wretenberg, P., & Renstrom, P. (2006). Effect of skin movement artifact on knee kinematics during gait and cutting motions measured in vivo. *Gait Posture, 24*(2), 152-164.

Del Bel, M. J., Kemp, L. G., Girard, C. I., Rossignol, J., Goulet, S. F., Bourgon, J.-F., . . . Benoit, D. L. (2020). Translation and validation of the hospital for special surgery pediatric functional activity brief scale for french paediatric populations. *Physiotherapy Canada, 72*(4), 348-354.

Delp, S. L., Anderson, F. C., Arnold, A. S., Loan, P., Habib, A., John, C. T., . . . Thelen, D. G. (2007). OpenSim: open-source software to create and analyze dynamic simulations of movement. *IEEE Transactions in Biomedical Engineering, 54*(11), 1940-1950.

Dunne, J. J., Uchida, T. K., Besier, T. F., Delp, S. L., & Seth, A. (2021). A marker registration method to improve joint angles computed by constrained inverse kinematics. *PloS One, 16*(5), e0252425 1-11.

Fabricant, P. D., Robles, A., Downey-Zayas, T., Do, H. T., Marx, R. G., Widmann, R. F., & Green, D. W. (2013). Development and validation of a pediatric sports activity rating scale: The hospital for special surgery pediatric functional activity brief scale (HSS Pedi-FABS). *The American Journal of Sports Medicine, 41*(10), 2421-2429.

Gray, H. A., Guan, S., Thomeer, L. T., Schache, A. G., De Steiger, R., & Pandy, M. G. (2019). Three-dimensional motion of the knee-joint complex during normal walking revealed by mobile biplane x-ray imaging. *Journal of Orthopaedic Research, 37*(3), 615-630.

Herzog, M. M., Marshall, S. W., Lund, J. L., Pate, V., Mack, C. D., & Spang, J. T. (2017). Incidence of anterior cruciate ligament reconstruction among adolescent females in the United States, 2002 Through 2014. *JAMA Pediatrics, 171*(8), 808-810.

Hewett, T. E., Myer, G. D., & Ford, K. R. (2004). Decrease in neuromuscular control about the knee with maturation in female athletes. *Journal of Bone & Joint Surgery, 86*(8), 1601-1608.

Hewett, T. E., Myer, G. D., Ford, K. R., Heidt, R. S., Jr., Colosimo, A. J., McLean, S. G., . . . Succop, P. (2005). Biomechanical measures of neuromuscular control and valgus loading of the knee predict anterior cruciate ligament injury risk in female athletes: a prospective study. *American Journal of Sports Medicine, 33*(4), 492-501.

Hirokawa, S., Solomonow, M., Luo, Z., Lu, Y., & D'Ambrosia, R. (1991). Muscular co-contraction and control of knee stability. *Journal of Electromyography and Kinesiology, 1*(3), 199-208.

Li, G., Defrate, L. E., Sun, H., & Gill, T. J. (2004). In vivo elongation of the anterior cruciate ligament and posterior cruciate ligament during knee flexion. *The American Journal of Sports Medicine, 32*(6), 1415-1420.

Majewski, M., Susanne, H., & Klaus, S. (2006). Epidemiology of athletic knee injuries: A 10-year study. *Knee, 13*(3), 184-188.

Mantovani, G., & Lamontagne, M. (2017). How different marker sets affect joint angles in inverse kinematics framework. *Journal of Biomechanical Engineering, 139*(4), 1-7.

Marshall, W. A., & Tanner, J. M. (1969). Variations in pattern of pubertal changes in girls. *Archives of Disease in Childhood, 44*(235), 291.

Marshall, W. A., & Tanner, J. M. (1970). Variations in the pattern of pubertal changes in boys. *Archives of Disease in Childhood, 45*(239), 13-23.

Murakami, K., Hamai, S., Okazaki, K., Ikebe, S., Shimoto, T., Hara, D., . . . Iwamoto, Y. (2016). In vivo kinematics of healthy male knees during squat and golf swing using image-matching techniques. *Knee, 23*(2), 221-226.

Myer, G. D., Schmitt, L. C., Brent, J. L., Ford, K. R., Barber Foss, K. D., Scherer, B. J., . . . Hewett, T. E. (2011). Utilization of modified NFL combine testing to identify functional deficits in athletes following ACL reconstruction. *Journal of Orthopaedic & Sports Physical Therapy, 41*(6), 377-387.

Neumann, D. A., (2010). Kinesiology of the Musculoskeletal System : Foundations for Rehabilitation. *Mosby/Elsevier, 2nd ed.*

Otsuki, R., Del Bel, M. J., & Benoit, D. L. (2021). Sex differences in muscle activation patterns associated with anterior cruciate ligament injury during landing and cutting tasks: A systematic review. *Journal of Electromyography and Kinesiology, 60*, 102583 1-15.

Park, S. E., DeFrate, L. E., Suggs, J. F., Gill, T. J., Rubash, H. E., & Li, G. (2006). Erratum to "The change in length of the medial and lateral collateral ligaments during in vivo knee flexion". *The Knee, 13*(1), 77-82.

Pataky, T. C. (2010). Generalized n-dimensional biomechanical field analysis using statistical parametric mapping. *Journal of Biomechanics, 43*(10), 1976-1982.

Potvin, B. (2016). Predicting muscle activations in a forward-inverse dynamics framework using stability-inspired optimization and an in vivo-based 6DoF knee joint. *MASc Thesis, University of Ottawa.*

Prodromos, C. C., Han, Y., Rogowski, J., Joyce, B., & Shi, K. (2007). A meta-analysis of the incidence of anterior cruciate ligament tears as a function of gender, sport, and a knee injury–reduction regimen. *Arthroscopy: The Journal of Arthroscopic & Related Surgery, 23*(12), 1320-1325.

Smale, K. B., Conconi, M., Sancisi, N., Krogsgaard, M., Alkjaer, T., Parenti-Castelli, V., & Benoit, D. L. (2019). Effect of implementing magnetic resonance imaging for patient-specific OpenSim models on lower-body kinematics and knee ligament lengths. *Journal of Biomechanics, 83*, 9-15.

Xu, H., Bloswick, D., & Merryweather, A. (2015). An improved OpenSim gait model with multiple degrees of freedom knee joint and knee ligaments. *Computer Methods in Biomechanics and Biomedical Engineering, 18*(11), 1217-1224.

Yamazaki, J., Muneta, T., Ju, Y. J., & Sekiya, I. (2010). Differences in kinematics of single leg squatting between anterior cruciate ligament-injured patients and healthy controls. *Knee Surgery, Sports Traumatology, Arthroscopy, 18*(1), 56-63.

Yu, B., & Garrett, W. E. (2007). Mechanisms of non-contact ACL injuries. *British Journal of Sports Medicine, 41*(1), 47-51.

6.8 Appendix

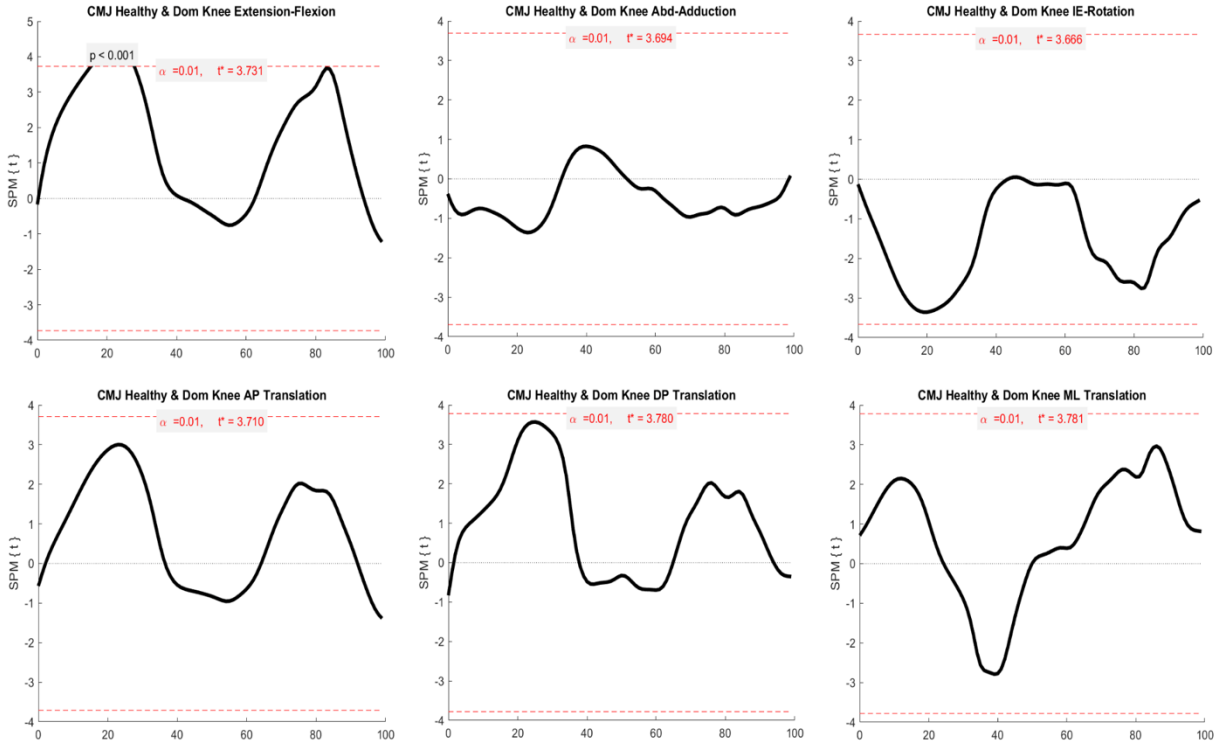

Figure A 6.1: SPM plots for rotations and translations for FACL healthy vs. FCON dominant. Regions of significant differences are shaded in grey. The achieved level of significance is overlayed on top of the grey area.

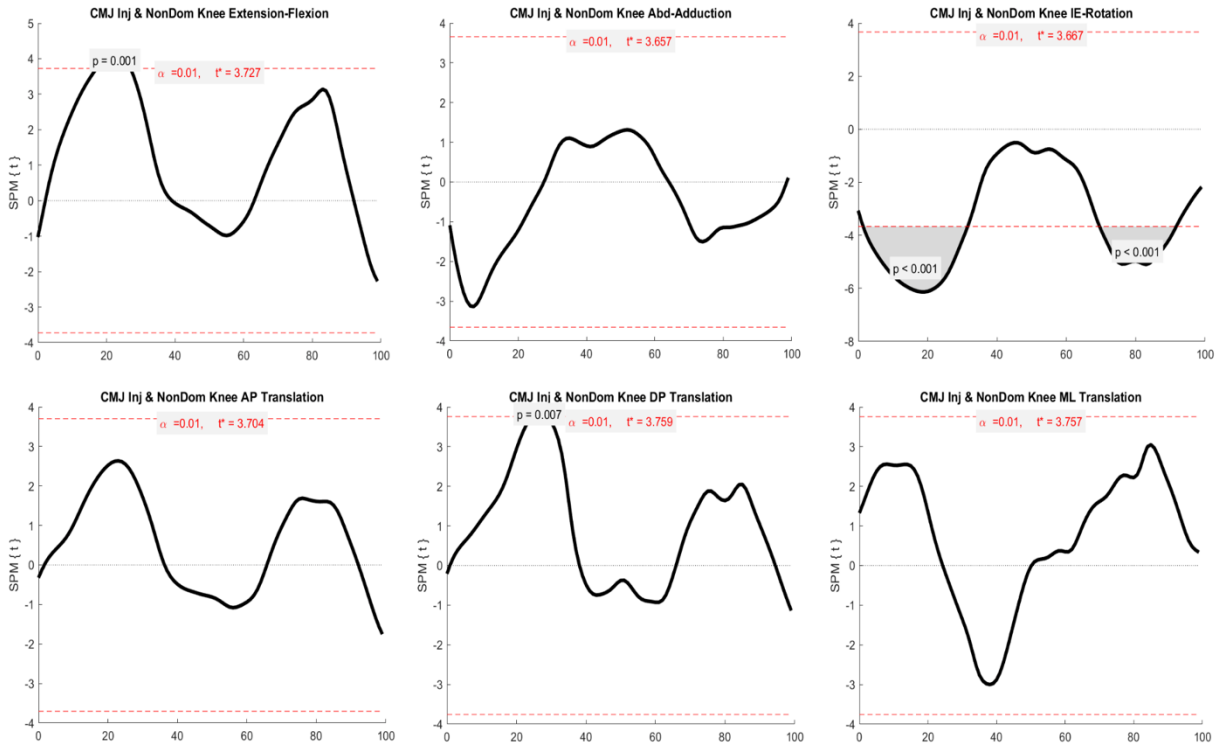

Figure A 6.2: SPM plots for rotations and translations for FACL injured vs. FCON non-dominant. Regions of significant differences are shaded in grey. The achieved level of significance is overlayed on top of the grey area.

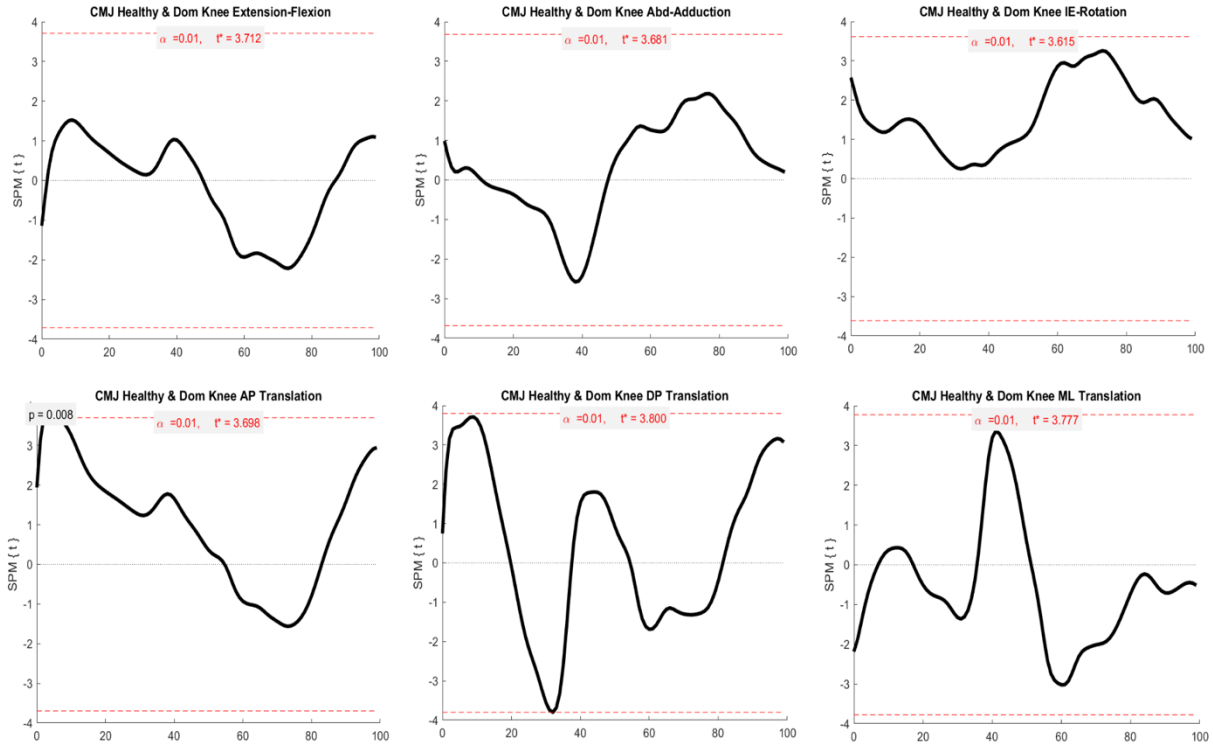

Figure A 6.3: SPM plots for rotations and translations for MACL healthy vs. MCON dominant. Regions of significant differences are shaded in grey. The achieved level of significance is overlayed on top of the grey area.

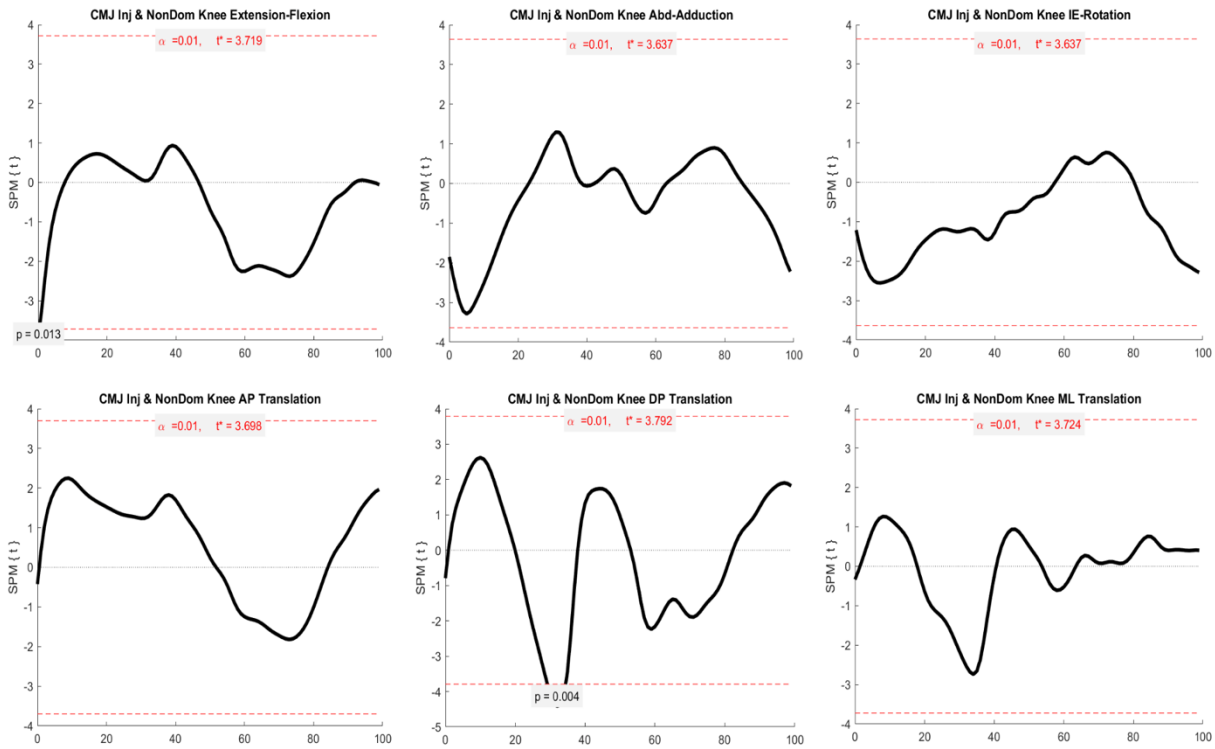

Figure A 6.4: SPM plots for rotations and translations for MACL injured vs. MCON non-dominant. Regions of significant differences are shaded in grey. The achieved level of significance is overlayed on top of the grey area.

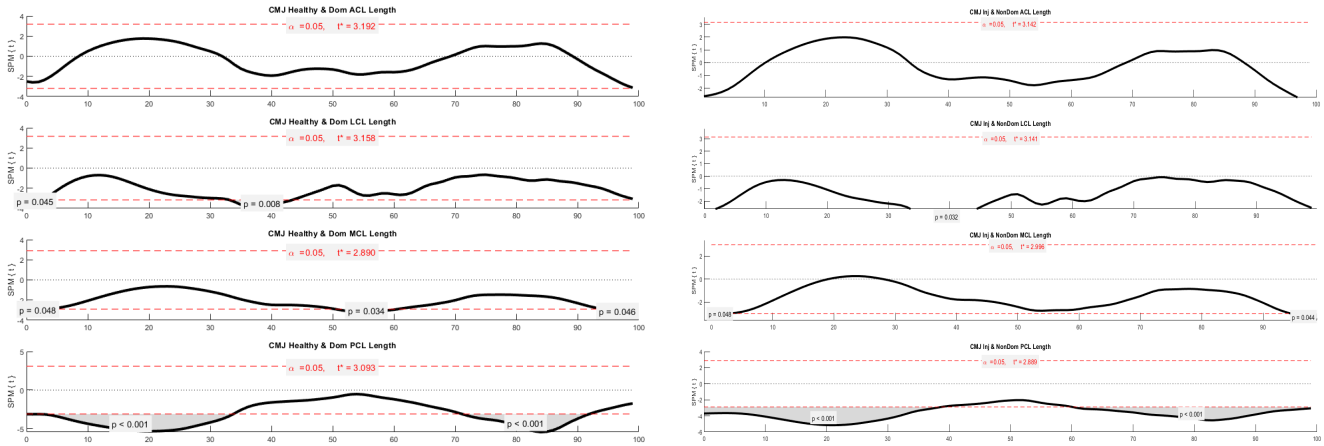

Figure A 6.5: SPM plots for ligament lengths for FACL healthy vs. FCON dominant (left column), and FACL injured vs. FCON non-dominant (right column). Regions of significant differences are shaded in grey. The achieved level of significance is overlayed on top of the grey area.

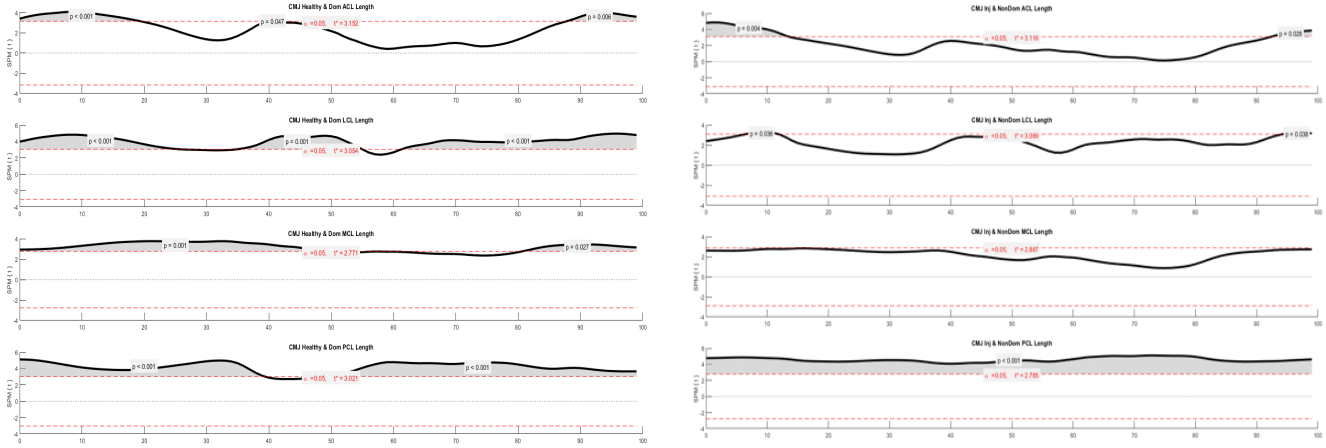

Figure A 6.6: SPM plots for ligament lengths for MACL healthy vs. MCON dominant (left column), and MACL injured vs. MCON non-dominant (right column). Regions of significant differences are shaded in grey. The achieved level of significance is overlayed on top of the grey area.

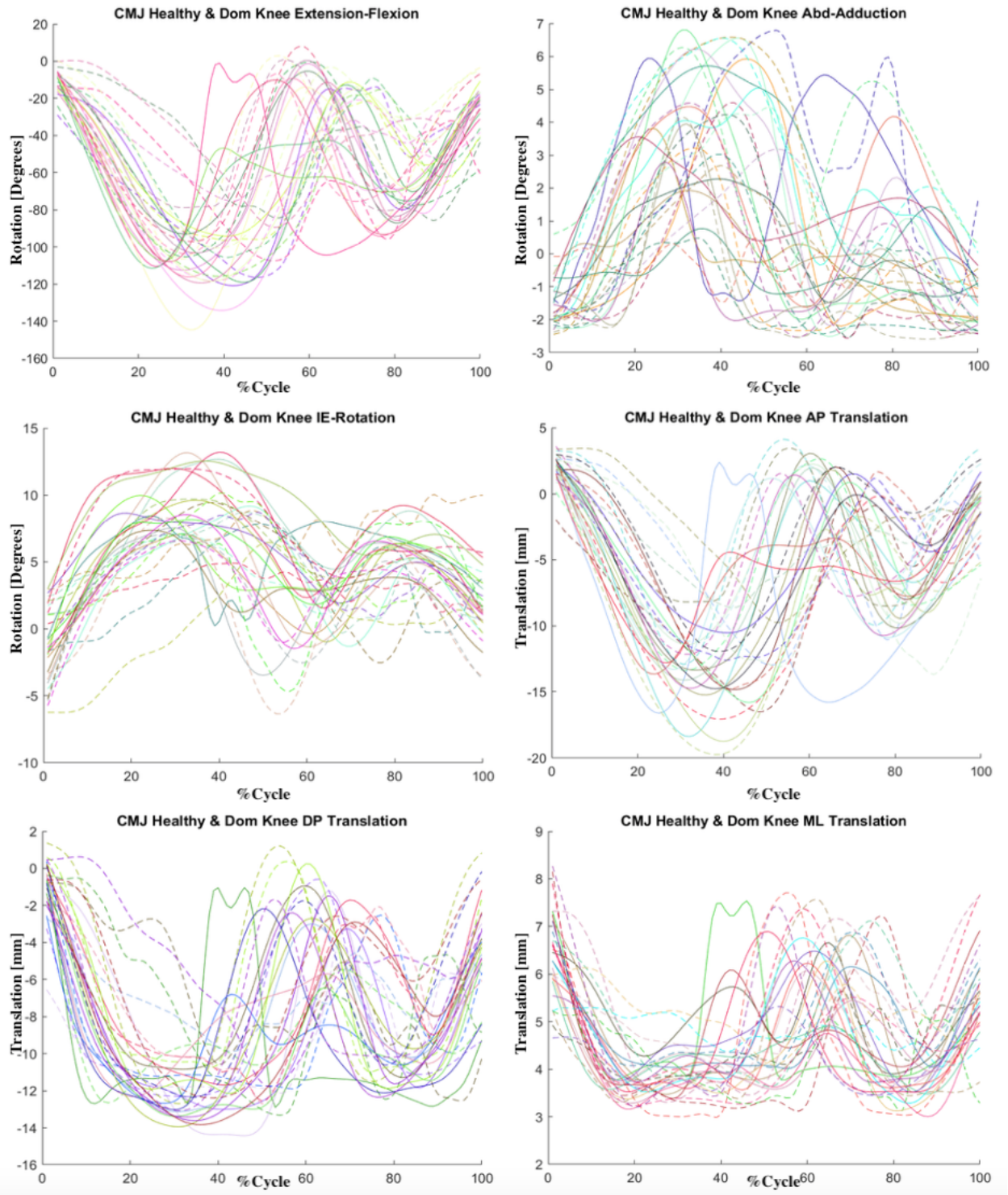

Figure A 6.7: Plots of all translations and rotations for FACL healthy (dashed lines), and FCON dominant (solid lines), for the CMJ task.

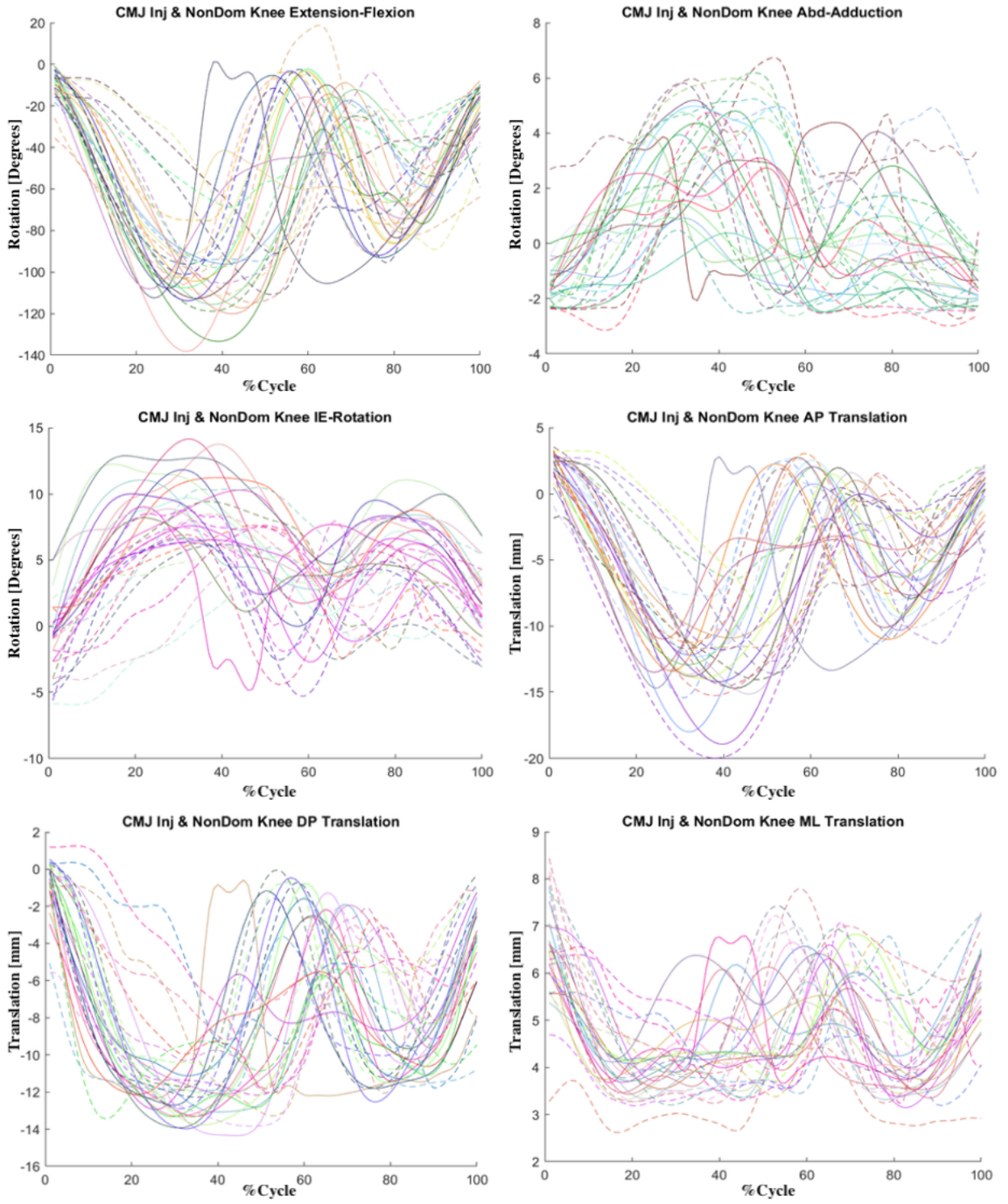

Figure A 6.8: Plots of all translations and rotations for FACL injured (dashed lines) and FCON non-dominant (solid lines), for the CMJ task.

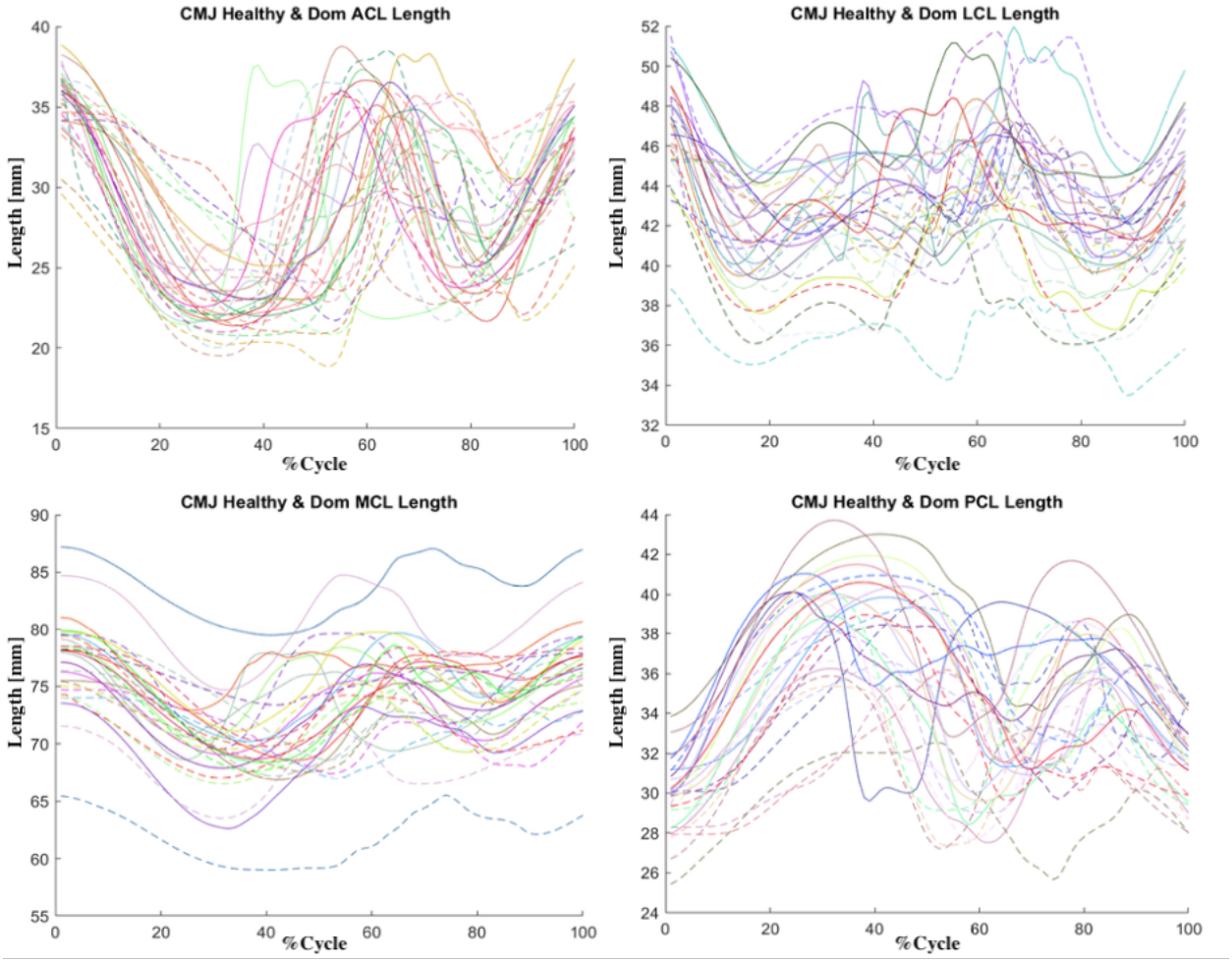

Figure A 6.9: Plots of all four knee ligament lengths for FACL healthy (dashed lines) and FCON dominant (solid lines), for the CMJ task.

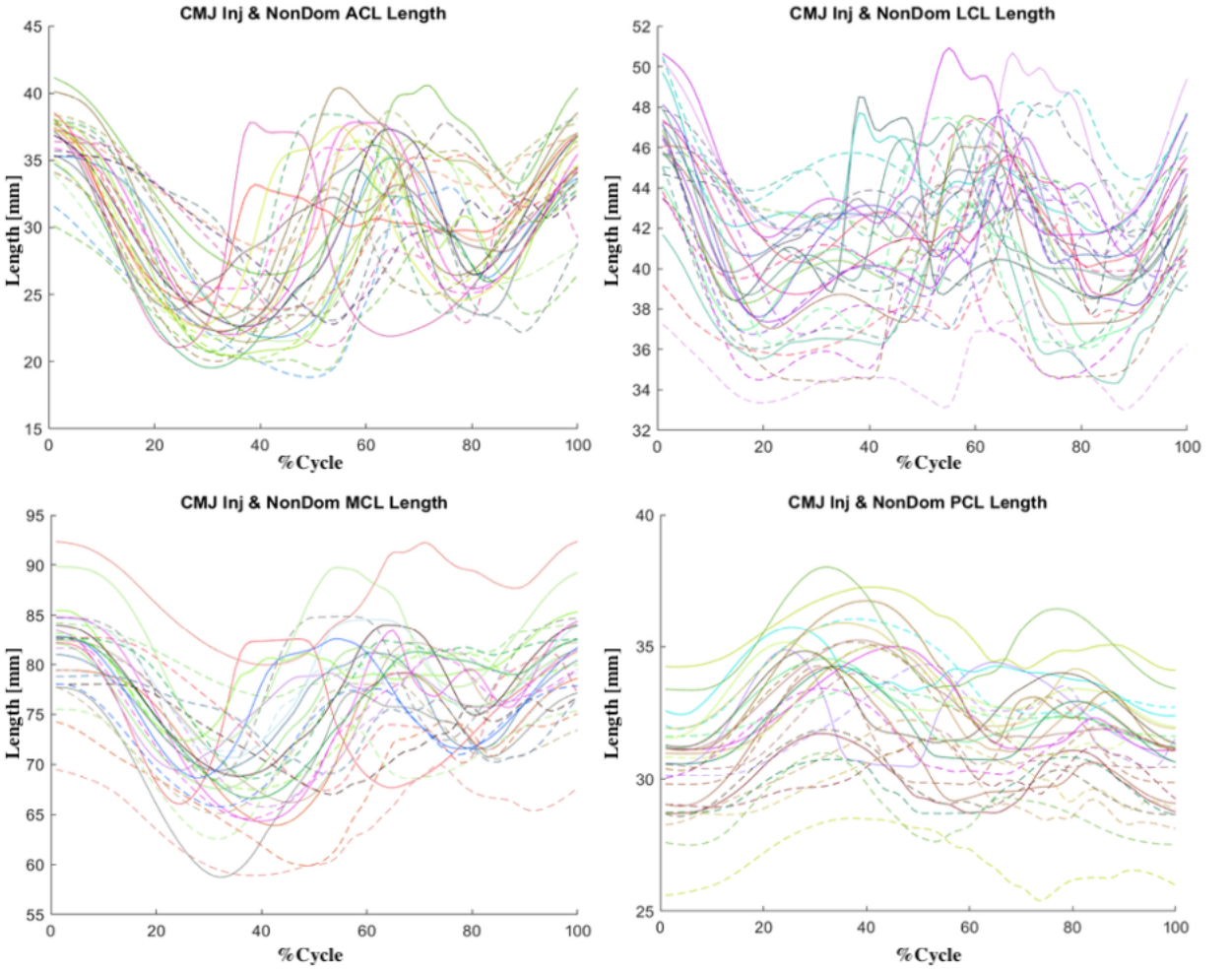

Figure A 6.10: Plots of all four knee ligament lengths for FACL injured (dashed lines) and FCON non-dominant (solid lines), for the CMJ task.

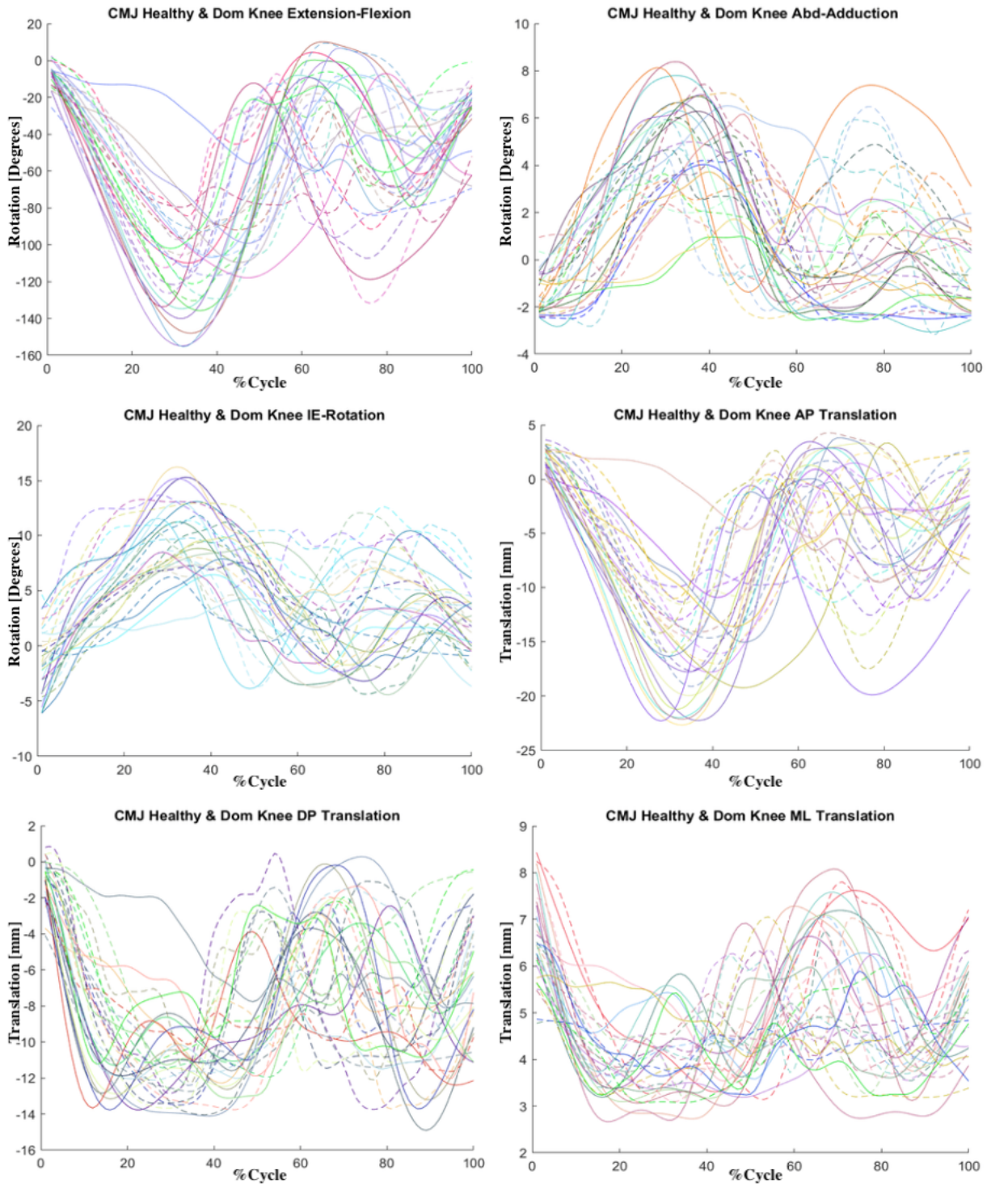

Figure A 6.11: Plots of all translations and rotations for MACL healthy (dashed lines) and MCON dominant (solid lines), for the CMJ task.

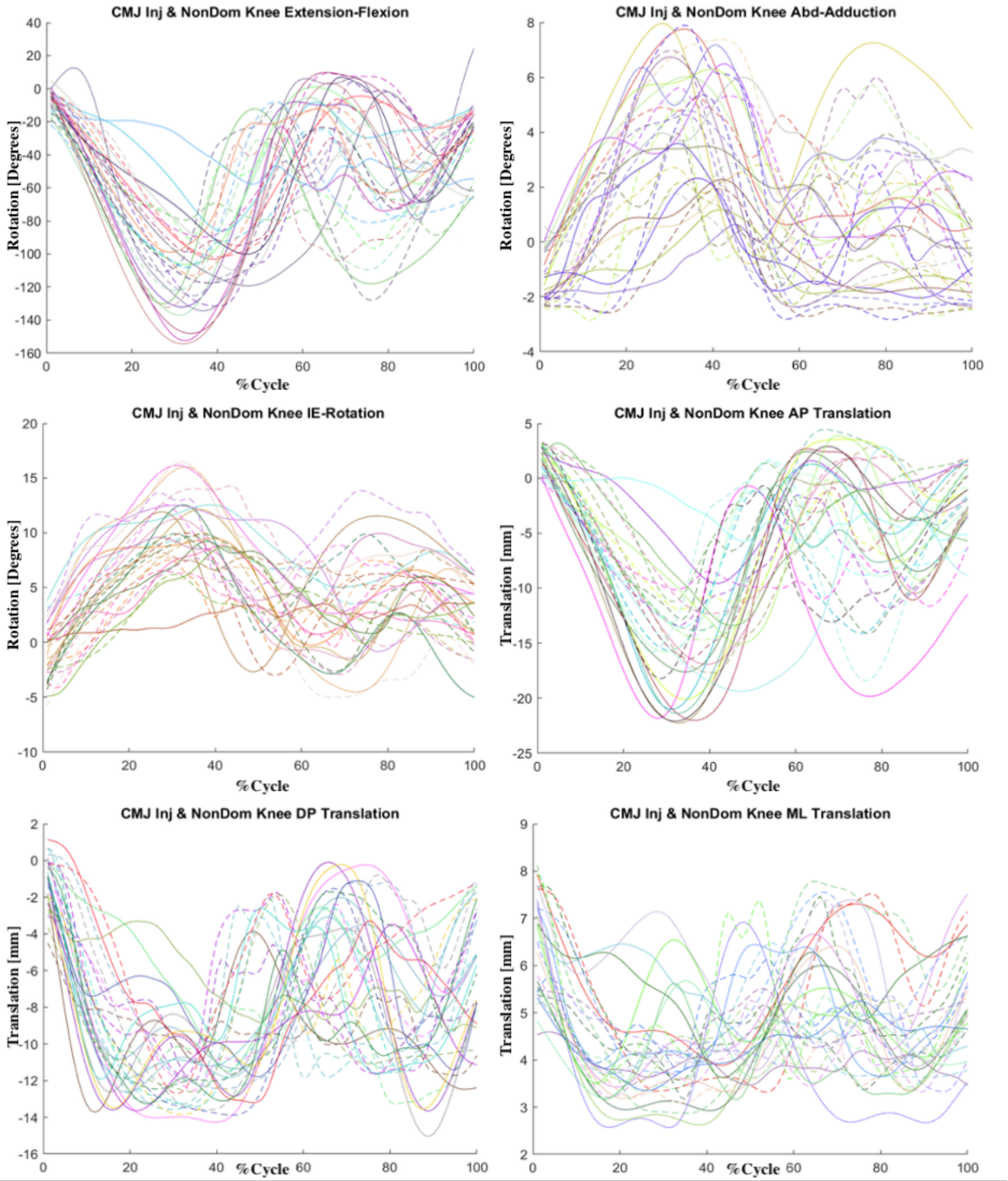

Figure A 6.12: Plots of all translations and rotations for MACL injured (dashed lines) and MCON non-dominant (solid lines), for the CMJ task.

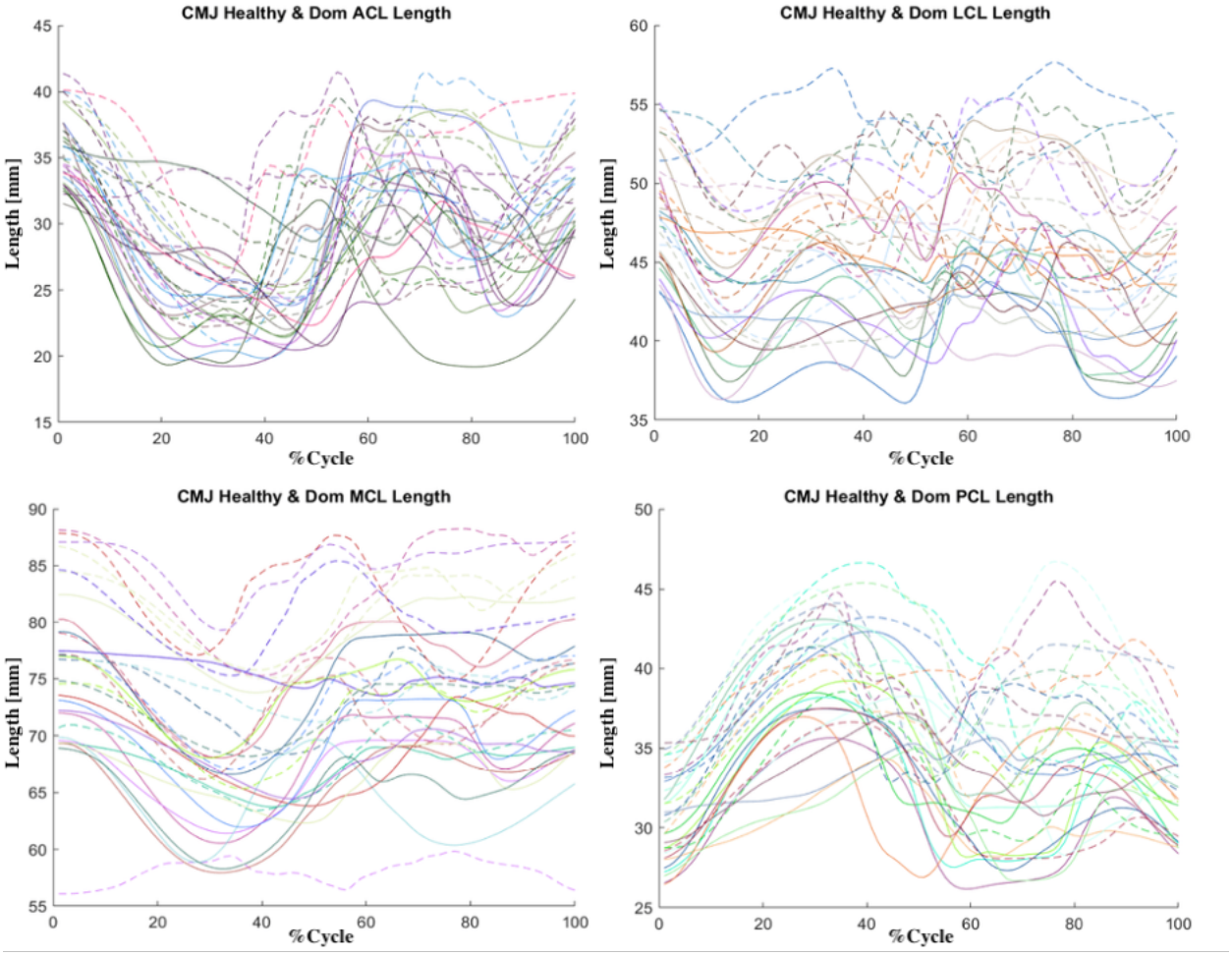

Figure A 6.13: Plots of all four knee ligament lengths for MACL healthy (dashed lines) and MCON dominant (solid lines), for the CMJ task.

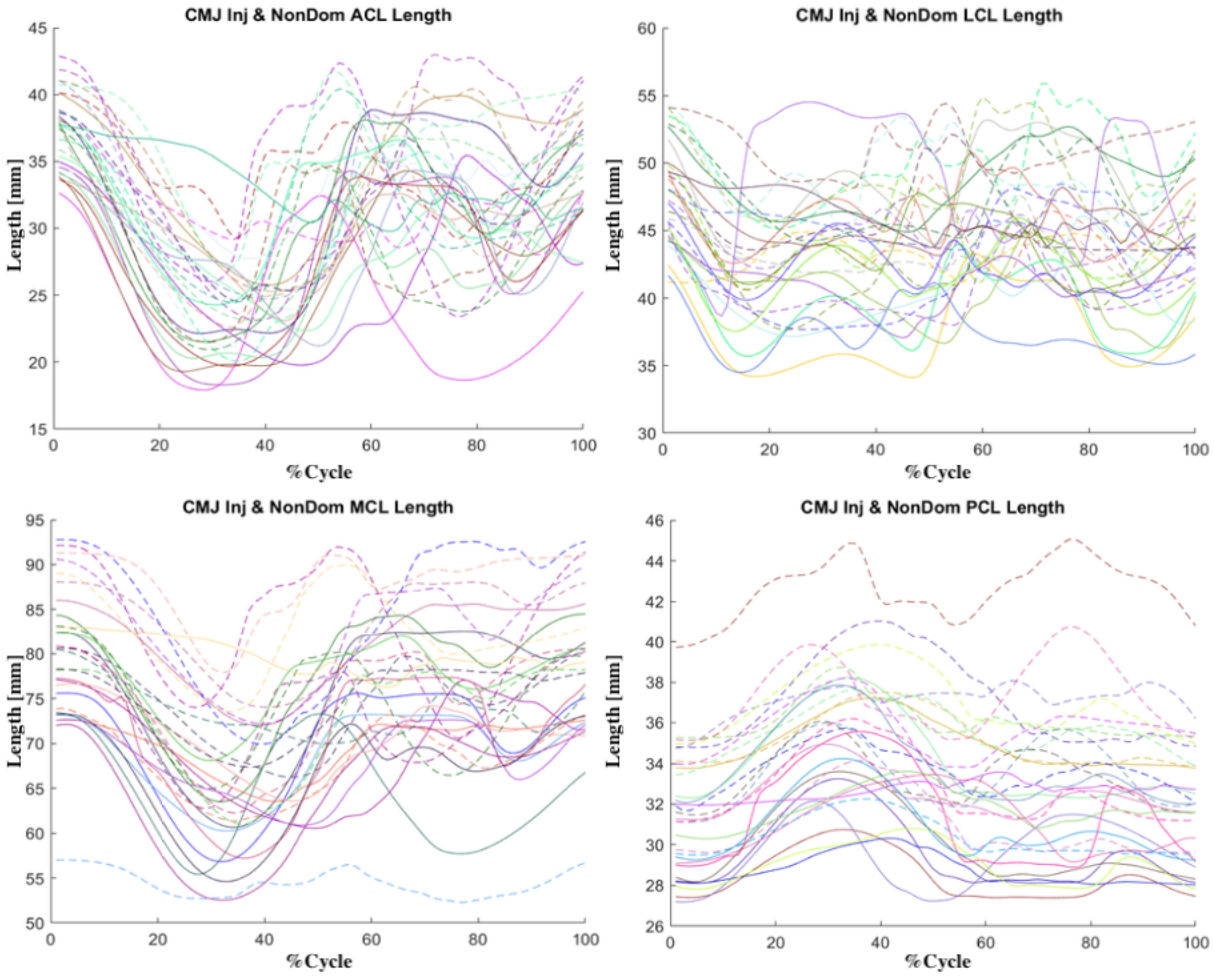

Figure A 6.14: Plots of all four knee ligament lengths for MACL injured (dashed lines) and MCON non-dominant (solid lines), for the CMJ task.

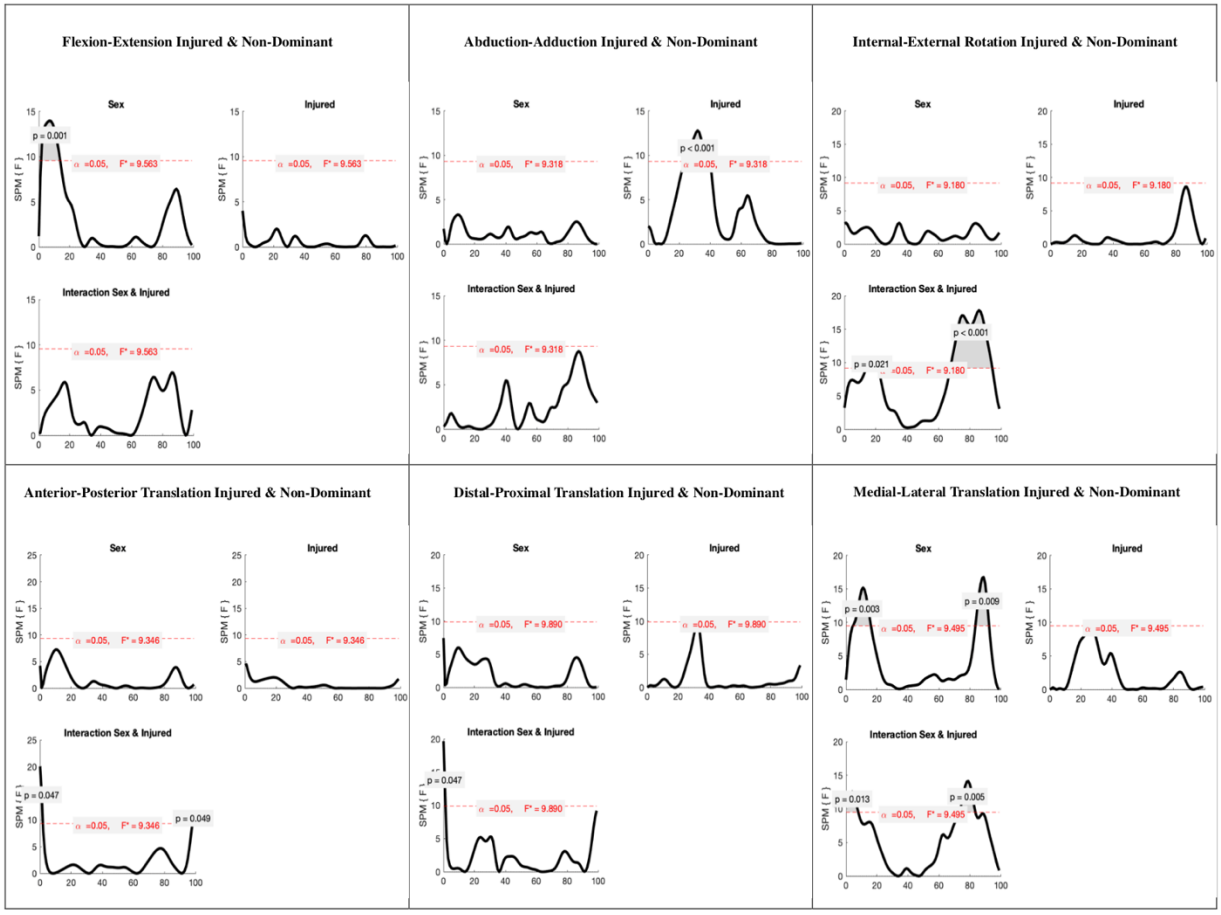

Figure A 6.15: Plots of injured/ non-dominant SPM 2x2 ANOVA results for all six degrees of freedom, for factors sex, injury status, and the interaction of sex and injury status. Significance is denoted by regions with grey area, in which they exceed the critical F-score.

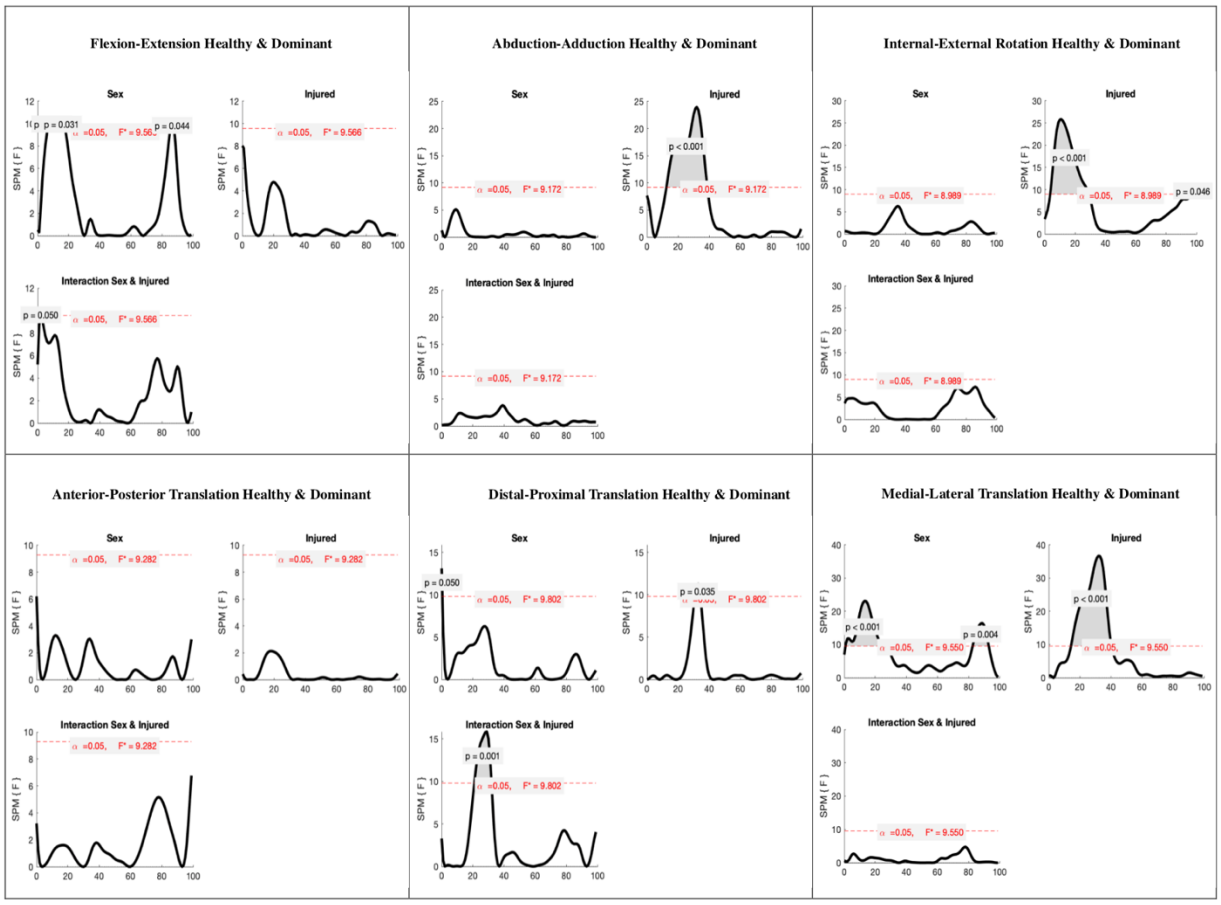

Figure A 6.16*:* Plots of healthy/ dominant SPM 2x2 ANOVA results for all six degrees of freedom, for factors sex, injury status, and the interaction of sex and injury status. Significance is denoted by regions with grey area, in which they exceed the critical F-score.

7.0 General Discussion

The objective of this thesis was twofold. The first objective was to explore the possibility of creating a model that used simple kinematic constraints to output physiological knee ligament lengths for high knee flexion (greater than 60 degrees knee flexion) tasks. The second objective was to determine whether differences in knee kinematics and ligament lengths could be detected between ACLi and CON groups using the partially unlocked knee model in OpenSim. The first manuscript of this thesis focused on creating a new OpenSim model which used a similar methodology to that which was previously proposed by our lab (Potvin, 2016). This methodology was to determine the physiological range of motion for the remaining 5 DoF of the knee, based on the knee flexion angle. To minimize soft tissue artifact, in vivo biplanar fluoroscopy studies were used as the reference data to determine the range of this motion for the knee (Gray et al., 2019; Murakami et al., 2016; Qi et al., 2013). Based on the resultant femur and tibia positions, ligament lengths were calculated using the distance between ligament insertion points. Finally, using other biplanar fluoroscopy studies, knee kinematics were then obtained, and knee ligament lengths were compared to results from Li et al. (2004), and Park et al. (2005). Despite the simplicity of the constraints, resultant kinematics and ligament lengths remained between physiological bounds which like more complex OpenSim models from literature (Schmitz & Piovesan, 2016; Smale et al., 2019; Xu et al., 2015). This concluded the first study, in which the partially unlocked knee model was validated so it could be used to compare between ACL injured and CON participants.

The second manuscript of this thesis examined potential differences in knee kinematics and corresponding knee ligament lengths between ACL injured and CON participants. Both males and females were included in the sample. Both limbs were compared where the ACL injured limb was compared to the CON non-dominant limb while the ACL healthy limb was compared to the CON

dominant limb. For both males and females there were few significant kinematic differences between groups. Despite this, there were multiple differences in ligament lengths throughout the trial. Interpretation and applicability of these kinematics and ligament lengths will be discussed in the following two sections.

7.1 Knee Kinematics

Using marker data from several adolescent females, the first study sought to obtain the knee flexion angle for both limbs with two sets of knee constraints: biplanar fluoroscopy, and bone pin. Based on this, the five-remaining knee DoF were calculated. The result was a 6-DoF partially unlocked knee, which was capable of outputting physiological knee motion. Unlike popular OpenSim models, such as the Rajagopal model (Rajagopal et al., 2016), this method allowed for non-flexion knee DoF variation between participants. This approach was previously performed in our lab but only for tasks involving low knee flexion (Potvin, 2016). However, this thesis work extended the kinematics of this model by using constraints from literature involving high knee flexion tasks (Gray et al., 2019; Murakami et al., 2016; Qi et al., 2013). Each of these papers contained plots of various knee DoF vs. knee flexion with ranges from full extension to 140 degrees knee flexion. In theory, this should allow the knee model to function for a wide variety of tasks, such as squats, CMJs, and DVJs.

The resultant kinematics from the first study yielded several interesting results. Firstly, over all three tasks, the biplanar fluoroscopy knee had greater external rotation and posterior translation at deep flexion. In contrast, the bone pin knee had greater abduction at higher knee flexion. This was due to the range of motion defined in the constraints which helped to highlight that if this approach is to be taken, constraints must be based on the correct motion. Trying to constrain the knee with the range of motion during gait may be too conservative to predict a side cut or drop-

vertical jump task. Therefore, with careful consideration, various in vivo data sets can be used as constraints for OpenSim models. Doing so will allow for variability across participants rather than simply assigning one value based on knee flexion.

With regards to the individual tasks, the squat had the least variation and the smallest effect size between constrained knees. The squat task was the easiest task to simulate, followed by the CMJ, which presented greater variation and effect size. The CMJ task presented a greater challenge for the model as it contained a squat phase and a jump and landing phase. Finally, the DVJ task had the highest variability of all three tasks which aligns with previous literature on this task (Malfait et al., 2014; Wren et al., 2020). Of all kinematics, ML translation presented the most variation across participants followed by abduction-adduction. This may suggest that the frontal plane may be the most susceptible to marker placement error (Osis et al., 2016).

Therefore, when simulating tasks of high inter- and intra-participant variability using OpenSim, extra time should be placed on marker registration, constraint choice, and participant scaling, as error in this step can increase later (Uchida & Seth, 2022). A model will perform well in the task it was designed for; however, to truly validate a model, it must also be tested in difficult situations (Lund et al., 2012). This was the objective of the first study, to test the partially unlocked knee model for various tasks of increasing complexity. The next step was to see whether the model could detect differences between CON and ACLi participants, as is the objective with a case-control study (Rothman et al., 2008).

The second study of this thesis attempted to find any significant difference in kinematics between ACLi and CON participants during a CMJ task. It is well-documented that following an ACL injury, kinematic and kinetic changes will occur at the knee (Chaudhari et al., 2008; Scarvell et al., 2005; Yamazaki et al., 2010); therefore, it was expected that kinematic differences should

be present between CON and ACLi groups. Results from the second study partially confirmed this hypothesis as significant differences were found for FACLi and FCON participants. FACLi participants achieved reduced peak knee flexion and internal rotation during the CMJ task which aligned with previous work from our lab (Kemp, 2020). In contrast, MACLi participants presented small kinematic differences from their MCON counterparts. This may suggest that FACLi present with a more unstable knee following an ACL injury in comparison to males which may be due to a reduction in neuromuscular control (Fagenbaum & Darling, 2003; Hewett et al., 2005). However, this is only a claim and could be tested further by increasing participant size and the tasks which are being tested while also evaluating neuromuscular control. Certain tasks such as the one-legged hop, may be a better indicator of kinematic difference between ACLi and CON participants (Barrance et al., 2007; Deneweth et al., 2010; Nagano et al., 2006). Overall, the resultant kinematics from the partially unlocked knee model yielded intriguing results when comparing between ACLi and CON. These results aligned with previous work from our lab (Kemp, 2020), and suggest that greater deficits may exist between FACLi and FCON in comparison to MACLi and MCON. Before any conclusion can be drawn, it is important to discuss the resultant ligament lengths (see Section 7.2).

While results such as these could be calculated using unconstrained inverse kinematics, such as those calculated using dynamic pipelines on Vicon Nexus, could have soft tissue artifact errors as high as 13 degrees for knee rotations and 13-16 mm for knee translations (Benoit et al., 2006). As well, the constrained inverse kinematics approach of OpenSim offers complete control over the entire process. In the context of a wearable constraint, such as a knee brace, specific constraints could be input into the partially unlocked knee model to ensure the knee will not move past a

certain point. This work could also be used to further the design of robotic limbs, to allow for physiological knee motion simply based on the knee flexion angle.

7.2 Ligament Lengths

While knee kinematics were allowed to solve within the range of previous literature (Gray et al., 2019; Murakami et al., 2016; Qi et al., 2013), resultant ligament lengths were not constrained. For the first study, the resultant ligament lengths mostly remained in agreement with existing literature (Li et al., 2004; Park et al., 2006) except for the ACL during high knee flexion (greater than 90 degrees flexion). For the squat and DVJ, the ACL length diverged at high knee flexion. This is not as important since the ACL is under less stress at this point and is at a relatively low risk of tearing (Hewett et al., 2012). At low knee flexion, for all three tasks, the ACL remained within 1 SD of literature data for the CON participants for *study 1*.

Next, the experimental LCL length was on the lower bound of literature data for a normal LCL length. This underestimate of LCL length was likely due to error in insertion point placement which is difficult to identify by default (Shin et al., 2014; Tschauner et al., 2016). Despite this, the experimental LCL length remained within 1 SD of literature data (Park et al., 2006) with the maximum error being less than 10 mm. Meanwhile, the MCL appeared to vary substantially for all three tasks as the knee approached higher flexion which aligns with results found with in vivo literature (Kono et al., 2020). However, much like the LCL, the MCL is a difficult ligament for which to identify exact insertion points through the usage of MRI (Tschauner et al., 2016). Caution should be used during placement of insertion points when utilizing any OpenSim model. A potential solution would be to analyze the engineering strain of the MCL, and to compare the results to established literature on MCL stress-strain curves (Quapp & Weiss, 1998).

Of all four ligaments, the PCL had the best agreement with experimental data suggesting that the PCL insertion point placement was correctly done. This may be due to the PCL being relatively easy to identify with an MRI (Servant et al., 2004). Despite the PCL being the "best" fit for *study 1*, it also had the greatest amount of significant difference between groups for *study 2*.

For *study 2*, FACLi had significantly shorter PCL lengths when compared to FCON while MACLi had significantly longer PCL lengths when compared to MCON. This was especially true for males, where MACLi had longer PCL lengths for almost the entire CMJ trial. As previously stated, this might be due to the significant height increase in the MACLi group (see Table 6.1) which would result in a greater distance between origin and insertion points. In contrast, females did not have a significant height difference between ACLi and CON groups which could explain why there were less-significant differences in ligament lengths between the female groups. To remedy this, ligament lengths could be normalized; however, this poses the problem of what values to use for normalization. As per Kono et al. (2020), the PCL is longest at full flexion (130 degrees +) and shortest near full extension (20 degrees flexion. Therefore, this approach could be used in future work to better compare between groups with significant anthropometric differences.

In addition to differences in PCL lengths, MACLi also had significantly longer ACL lengths at low flexion when the ACL is at its longest and at the highest risk of injury (Hewett et al., 2012). However, from *Study 1*, the partially unlocked knee model was able to produce physiological ACL lengths at low flexion. This significant difference was likely due to significant height differences between MACLi and MCON. The same region of significances was found for LCL and MCL lengths. This is further supported by the observation that the female groups did not have any significant differences in height or ACL, LCL, or MCL lengths. Overall, *study 2* demonstrated how sensitive the partially unlocked knee model is to ligament insertion point

identification. Future work should focus on either normalizing ligament lengths or consulting an imaging specialist such as a radiologist to ensure insertion points have been correctly identified.

7.3 Limitations

This project had several limitations that should be addressed. Firstly, while freely available, the musculoskeletal modelling software OpenSim (Delp et al., 2007) has yet to be widely utilized outside of an academic setting. The software itself is still being developed and being brought to a point where it can be used to inform clinical decisions. For this thesis, scaling and inverse kinematics were used through OpenSim and both applications have their limitations. Starting with scaling, only the participant's height was used to ensure the goodness of fit of the scaled model. However, participant anthropometrics were taken prior to the data collection based on anatomical landmark separation distance. These anatomical landmarks (ASIS, medial and lateral epicondyles, and so on) had markers placed on them and with more time, an optimization algorithm could be created as to ensure the scaled OpenSim model's segment lengths agreed with the measured lengths.

Next, when using the inverse kinematics function, there were two main limitations: marker weightings and marker registration error. Anatomical marker weightings set to 100 as per sensitivity testing, while the remaining marker weightings were set to 1. This created a heavy dependence on the correct placement of surface-based markers which may have led to some form of marker registration error. During scaling, when markers were slightly shifted, such as pelvis markers, additional pelvis tilt would occur for certain participants, signaling revision of marker placement. This could likely be remedied by using an approach recently proposed by Uchida & Seth. (2022) in which marker positions were slightly shifted several times, to determine the downstream error of various OpenSim functions. By using this approach, marker positions could

be slightly altered through iteratively until marker registration RMSE was minimized and thus improved registration. This would likely be a computationally expensive process as there are several markers for each segment of the model.

Another computationally expensive limitation was running inverse kinematics one frame at a time. This was done because the range of motion for the remaining 5 knee DoF were updated for the OpenSim body while the start and finish times had to be updated for the Inverse Kinematics Object. Future work will likely include the re-working of the default inverse kinematics equation to allow for the work of this thesis to be included as a plugin. As well, different optimization algorithms could be explored as the default least-squares optimization may be minimizing the knee motion of the model which could result in a stiffer knee. However, before a plugin can be created, the computational demand of this process will need to be addressed so that this procedure can be widely adopted by the OpenSim community.

Next, when considering the *point kinematics* function, simple linear distance was used to track the ligament lengths. While the point kinematics method is simple, it calculates the straight-line distance from one point to the other. Point kinematics does not consider any sort of bone surface such as the tibial spine or the femoral condyles. Also, while the distance between more than two points could be tracked, minimal documentation exists on this function limiting its accessibility.

With regards to the participants themselves, there were also several limitations for both studies. For *Study 1*, we did not have access to in vivo participant data for high knee flexion tasks. Therefore, a literature search was performed to find in vivo data for high knee flexion tasks which yielded a handful of studies. Of these studies, only two studies used younger healthy participants (Murakami et al., 2016; Qi et al., 2013). The remaining studies focused on participants with total knee arthroplasty. Because literature data was used, only the reported mean and standard deviation

could be used for statistical purposes. This limited the usage of SPM, which requires all participant data for both groups. As per previous studies which compared OpenSim data to literature data, RMSE was used (Barrett et al., 2021; Green et al., 2022). While RMSE provides a metric of total waveform error, it cannot account for significant differences at a specific time. Future studies that focus on validating this model should include the data capture of the same participants with and without in vivo motion capture methods, such as biplanar fluoroscopy.

Continuing the limitations of the participants for *study 2*, only twenty participants were used for each group. Using G* Power, with a large effect size of 0.8, an alpha value of 0.05, and a Power value of 0.95, 42 participants would be required for each group to achieve the specified significance. However, due to the pandemic, data collection with participants ceased, as elective surgeries such as ACL surgeries were cancelled. This resulted in the smallest of all four groups (FACL, FCON, MACL, MCON) being only twenty for MACL. Therefore, to maintain equal sample sizes, only twenty participants were used from each of the four groups.

The final limitation which was previously highlighted in *study 2* of this thesis was the usage of the CMJ task as to differentiate groups. This task may not have been physically demanding enough to elicit a difference between ACLi and CON groups. Future work should seek to try this approach on more complicated tasks, such as a drop-vertical jump or a side cut, as these tasks have been shown to be high risk for ACL injury (Bencke et al., 2013; Ford et al., 2010).

7.4 General Conclusions

This thesis showed that simple kinematic constraints could produce knee kinematics and ligament lengths which were comparable to existing literature. No complex optimization methods were used to drive the knee; instead, the existing OpenSim constrained inverse kinematics function was

slightly expanded. This was done by setting the range of motion of the tibia in reference to the femur based on published literature (Benoit et al., 2006; Gray et al., 2019; Murakami et al., 2016). For *study 1*, frontal plane knee produced the largest errors. However, these errors were well within error associated with soft tissue artifact from marker-based motion capture (Benoit et al., 2006). *Study 1* of this thesis demonstrated that the partially unlocked knee model produced errors on the order of a few degrees for rotation and a few millimeters for translations. Therefore, the model was likely capable of detecting kinematic differences that existed between groups. For *study 2*, the partially unlocked knee model was used to determine whether kinematic differences existed between ACLi and CON participants, for both sexes. The model detected a few differences in kinematics and ligament lengths between injured and control participants. However, for even a simple task like a CMJ, the model determined that ACL injured females had reduced peak knee flexion angle and externally rotated less during high knee flexion. Finally, it should be noted that this work is one step and that work shall continue to improve the limitations that were addressed in the two studies. I am very excited to apply this method to not only an ACL-injured setting, but to other movement disorders as well as healthy knee motion to improve predictions of knee kinematics and ligament lengths in OpenSim.

8.0 References

Alentorn-Geli, E., Myer, G., Silvers, H., Samitier, G., Romero, D., Lázaro-Haro, C., & Cugat, R. (2009). Prevention of non-contact anterior cruciate ligament injuries in soccer players. Part 1: Mechanisms of injury and underlying risk factors. *Knee Surgery, Sports Traumatology, Arthroscopy, 17*(7), 705-729.

Amis, A. (2017). Anterolateral knee biomechanics. *Knee Surgery, Sports Traumatology, Arthroscopy, 25*(4), 1015-1023.

Andersen, M., Benoit, D., Damsgaard, M., Ramsey, D., & Rasmussen, J. (2009). Do kinematic models reduce the effects of soft tissue artefacts in skin marker-based motion analysis? An in vivo study of knee kinematics. *Journal of Biomechanics, 43*(2), 268-273.

Anderson, F. C., & Pandy, M. G. (2001). Dynamic optimization of human walking. *Journal of Biomechanical Engineering, 123*(5), 381-390.

Andriacchi, T. P., & Dyrby, C. O. (2005). Interactions between kinematics and loading during walking for the normal and ACL deficient knee. *Journal of Biomechanics, 38*(2), 293-298.

Angerame, M. R., Holst, D. C., Jennings, J. M., Komistek, R. D., & Dennis, D. A. (2019). Total knee arthroplasty kinematics. *The Journal of Arthroplasty, 34*(10), 2502-2510.

Arbes, S., Resinger, C., Vecsei, V., & Nau, T. (2007). The functional outcome of total tears of the anterior cruciate ligament (ACL) in the skeletally immature patient. *International Orthopaedics, 31*(4), 471-475.

Ardern, C. L., Kvist, J., & Webster, K. E. (2016). Psychological aspects of anterior cruciate ligament injuries. *Operative Techniques in Sports Medicine, 24*(1), 77-83.

Azus, A., Teng, H., Tufts, L., Wu, D., Ma, C. B., Souza, R., & Li, X. (2017). Biomechanical factors associated with pain and symptoms following anterior cruciate ligament injury and reconstruction. *PM & R, 10*(1), 56-63.

Barrance, P. J., Williams, G. N., Snyder-Mackler, L., & Buchanan, T. S. (2007). Do ACL-injured copers exhibit differences in knee kinematics?: An MRI study. *Clinical orthopaedics and related research, 454*, 74-80.

Barre, A., Thiran, J., Jolles, B. M., Theumann, N., & Aminian, K. (2013). Soft tissue artifact assessment during treadmill walking in subjects with total knee arthroplasty. *IEEE Transactions on Biomedical Engineering, 60*(11), 3131-3140.

Barrett, J. M., McKinnon, C. D., Dickerson, C. R., & Callaghan, J. P. (2021). An electromyographically driven cervical spine model in OpenSim. *Journal of Applied Biomechanics, 37*(5), 481-493.

Beck, N. A., Lawrence, J. T. R., Nordin, J. D., DeFor, T. A., & Tompkins, M. (2017). ACL Tears in school-aged children and adolescents over 20 years. *Pediatrics, 139*(3).

Bencke, J., Curtis, D., Krogshede, C., Jensen, L. K., Bandholm, T., & Zebis, M. K. (2013). Biomechanical evaluation of the side-cutting manoeuvre associated with ACL injury in young female handball players. *Knee Surgery, Sports Traumatology, Arthroscopy, 21*(8), 1876-1881.

Benoit, D. L., Ramsey, D. K., Lamontagne, M., Xu, L., Wretenberg, P., & Renstrom, P. (2006). Effect of skin movement artifact on knee kinematics during gait and cutting motions measured in vivo. *Gait & Posture, 24*(2), 152-164.

Benoit, D. L., Ramsey, D. K., Lamontagne, M., Xu, L., Wretenberg, P., & Renstrom, P. (2007). In vivo knee kinematics during gait reveals new rotation profiles and smaller translations. *Clinical Orthopaeics and Related Research, 454*, 81-88.

Blaha, J., Mancinelli, C. A., Simons, W. H., Kish, V. L., & Thyagarajan, G. (2003). Kinematics of the human knee using an open chain cadaver model: Knee kinematics and total knee replacement design. *Clinical Orthopaedics and Related Research*(410), 25-34.

Brodie, M. A., Walmsley, A., & Page, W. (2008). Dynamic accuracy of inertial measurement units during simple pendulum motion. *Computer Methods in Biomechanics and Biomedical Engineering, 11*(3), 235-242.

Brown, J. A., Brophy, R. H., Franco, J., Marquand, A., Solomon, T. C., Watanabe, D., & Mandelbaum, B. R. (2007). Avoiding allograft length mismatch during anterior cruciate ligament reconstruction: patient height as an indicator of appropriate graft length. *The American Journal of Sports Medicine, 35*(6), 986-989.

Bynum, B. E., Barrack, R. L., & Alexander, A. H. (1995). Open versus closed chain kinetic exercises after anterior cruciate ligament reconstruction. *The American Journal of Sports Medicine, 23*(4), 401-406.

Carbone, V., Fluit, R., Pellikaan, P., van der Krogt, M. M., Janssen, D., Damsgaard, M., . . . Verdonschot, N. (2014). TLEM 2.0 – A comprehensive musculoskeletal geometry dataset

for subject-specific modeling of lower extremity. *Journal of Biomechanics, 48*(5), 734-741.

Carsen, S., Grammatopoulos, G., Zaltz, I., Ward, L., Smit, K., & Beaule, P. E. (2021). The effects of physical activity on physeal and skeletal development. *Journal of Bone and Joint Surgery, 9*(10), 1-11.

Cerulli, G., Benoit, D. L., Lamontagne, M., Caraffa, A., & Liti, A. (2003). In vivo anterior cruciate ligament strain behaviour during a rapid deceleration movement: case report. *Knee Surgery, Sports Traumatology, Arthroscopy, 11*(5), 307-311.

Chaudhari, A. M., Briant, P. L., Bevill, S. L., Koo, S., & Andriacchi, T. P. (2008). Knee kinematics, cartilage morphology, and osteoarthritis after ACL injury. *Medicne and Science in Sports & Exercise, 40*(2), 215-222.

Chavda, S., Bromley, T., Jarvis, P., Williams, S., Bishop, C., Turner, A. N., . . . Mundy, P. D. (2018). Force-time characteristics of the countermovement jump: analyzing the curve in excel. *Strength & Conditioning Journal, 40*(2), 67-77.

Cohen, J. (1992). A power primer. *Psychological Bulletin, 112*, 155–159.

Costa E S, L., Fragoso, M., & Teles, J. (2017). Physical activity–related injury profile in children and adolescents according to their age, maturation, and level of sports participation. *Sports Health: A Multidisciplinary Approach, 9*(2), 118-125.

Costley, J. A. E., Miles, J. J., King, E., & Daniels, K. A. J. (2021). Vertical jump impulse deficits persist from six to nine months after ACL reconstruction. *Sports Biomechanics*, 1-19.

Dai, B., Layer, J. S., Bordelon, N. M., Critchley, M. L., Lacroix, S. E., George, A. C., . . . Jensen, M. A. (2021). Longitudinal assessments of balance and jump-landing performance before and after anterior cruciate ligament injuries in collegiate athletes. *Research in Sports Medicine, 29*(2), 129-140.

de Fontenay, B., Argaud, S., Blache, Y., & Monteil, K. (2015). Contralateral limb deficit seven months after ACL-reconstruction: an analysis of single-leg hop tests. *The Knee, 22*(4), 309-312.

Dekker, T. J., Godin, J. A., Dale, K. M., Garrett, W. E., Taylor, D. C., & Riboh, J. C. (2017). Return to sport after pediatric anterior cruciate ligament reconstruction and Its effect on subsequent anterior cruciate ligament injury. *Journal of Bone and Joint Surgery. American Volume, 99*(11), 897-904.

Del Bel, M. J., Flaxman, T. E., Smale, K. B., Alkjaer, T., Simonsen, E. B., Krogsgaard, M. R., & Benoit, D. L. (2018). A hierarchy in functional muscle roles at the knee is influenced by sex and anterior cruciate ligament deficiency. *Clinical Biomechanics, 57*, 129-136.

Del Bel, M. J., Kemp, L. G., Girard, C. I., Rossignol, J., Goulet, S. F., Bourgon, J., . . . Benoit, D. L. (2020). Translation and validation of the hospital for special surgery pediatric functional activity brief scale for french paediatric populations. *Physiotherapy Canada, 72*(4), 348-354.

Delp, S. L., Anderson, F. C., Arnold, A. S., Loan, P., Habib, A., John, C. T., . . . Thelen, D. G. (2007). OpenSim: open-source software to create and analyze dynamic simulations of movement. *IEEE Transactions on Biomedical Engineering, 54*(11), 1940-1950.

Deneweth, J. M., Bey, M. J., McLean, S. G., Lock, T. R., Kolowich, P. A., & Tashman, S. (2010). Tibiofemoral joint kinematics of the anterior cruciate ligament-reconstructed knee during a single-legged hop landing. *The American Journal of Sports Medicine, 38*(9), 1820-1828.

Dunne, J. J., Uchida, T. K., Besier, T. F., Delp, S. L., & Seth, A. (2021). A marker registration method to improve joint angles computed by constrained inverse kinematics. *PloS One, 16*(5), e0252425 1-11.

Fabricant, P. D., Robles, A., Downey-Zayas, T., Do, H. T., Marx, R. G., Widmann, R. F., & Green, D. W. (2013). Development and validation of a pediatric sports activity rating scale: the hospital for special surgery pediatric functional activity brief scale (HSS Pedi-FABS). *The American Journal of Sports Medicine, 41*(10), 2421-2429.

Fagenbaum, R., & Darling, W. G. (2003). Jump landing strategies in male and female college athletes and the implications of such strategies for anterior cruciate ligament injury. *The American Journal of Sports Medicine, 31*(2), 233-240.

Faul, F., Erdfelder, E., Lang, A.-G., & Buchner, A. (2007). G*Power 3: A flexible statistical power analysis program for the social, behavioral, and biomedical sciences. *Behavior Research Methods, 39*, 175-191.

Ford, K. R., Myer, G. D., Toms, H. E., & Hewett, T. E. (2005). Gender differences in the kinematics of unanticipated cutting in young athletes. *Medicine & Science in Sports & Exercise, 37*(1), 124-129.

Ford, K. R., Shapiro, R., Myer, G. D., Van Den Bogert, A. J., & Hewett, T. E. (2010). Longitudinal sex differences during landing in knee abduction in young athletes. *Medicine and Science in Sports and Exercise, 42*(10), 1923-1931.

Frank, J. S., & Gambacorta, P. L. (2013). Anterior cruciate ligament injuries in the skeletally immature athlete: diagnosis and management. *Journal of the American Academy of Orthopaedic Surgeons, 21*(2), 78-87.

Fregly, B. J., Besier, T. F., Lloyd, D. G., Delp, S. L., Banks, S. A., Pandy, M. G., & D'Lima, D. D. (2012). Grand challenge competition to predict in vivo knee loads. *Journal of Orthopaedic Research, 30*(4), 503-513.

Gasparutto, X., Moissenet, F., Lafon, Y., Chèze, L., & Dumas, R. (2017). Kinematics of the normal knee during dynamic activities: A synthesis of data from intracortical pins and biplane imaging. *Applied Bionics and Biomechanics, 2017*, 1-9.

Georgoulis, A. D., Papadonikolakis, A., Papageorgiou, C. D., Mitsou, A., & Stergiou, N. (2003). Three-dimensional tibiofemoral kinematics of the anterior cruciate ligament-deficient and reconstructed knee during walking. *American Journal of Sports Medicine, 31*(1), 75-79.

Ghezelbash, F., Shirazi-Adl, A., Plamondon, A., & Arjmand, N. (2020). Comparison of different lifting analysis tools in estimating lower spinal loads - Evaluation of NIOSH criterion. *Journal of Biomechanics, 112*, 110024 1-6.

Gray, A. D., Willis, B. W., Skubic, M., Huo, Z., Razu, S., Sherman, S. L., . . . Siesener, N. J. (2017). Development and validation of a portable and inexpensive tool to measure the drop vertical jump using the microsoft kinect v2. *Sports Health: A Multidisciplinary Approach, 9*(6), 537-544.

Gray, H. A., Guan, S., Thomeer, L. T., Schache, A. G., De Steiger, R., & Pandy, M. G. (2019). Three-dimensional motion of the knee-joint complex during normal walking revealed by mobile biplane x-ray imaging. *Journal of Orthopaedic Research, 37*(3), 615-630.

Green, M., Hong, Y., Roh, J., & Fregly, B. J. (2022). Computational modeling and simulation of closed chain arm-robot multibody dynamic systems in OpenSim. *Multibody System Dynamics*. *56*(4), 313-334.

Hamner, S. R., Seth, A., & Delp, S. L. (2010). Muscle contributions to propulsion and support during running. *Journal of Biomechanics, 43*(14), 2709-2716.

Herzog, M. M., Marshall, S. W., Lund, J. L., Pate, V., Mack, C. D., & Spang, J. T. (2017). Incidence of anterior cruciate ligament reconstruction among adolescent females in the united states, 2002 Through 2014. *JAMA Pediatrics, 171*(8), 808-810.

Herzog, M. M., Marshall, S. W., Lund, J. L., Pate, V., Mack, C. D., & Spang, J. T. (2018). Trends in incidence of ACL reconstruction and concomitant procedures among commercially insured individuals in the united states, 2002-2014. *Sports Health, 10*(6), 523-531.

Hewett, T. E., Myer, G. D., & Ford, K. R. (2004). Decrease in neuromuscular control about the knee with maturation in female athletes. *Journal of Bone and Joint Surgery. American Volume, 86*(8), 1601-1608.

Hewett, T. E., Myer, G. D., Ford, K. R., Heidt, R. S., Jr., Colosimo, A. J., McLean, S. G., . . . Succop, P. (2005). Biomechanical measures of neuromuscular control and valgus loading of the knee predict anterior cruciate ligament injury risk in female athletes: a prospective study. *American Journal of Sports Medicine, 33*(4), 492-501.

Hewett, T. E., Myer, G. D., Ford, K. R., Paterno, M. V., & Quatman, C. E. (2012). The 2012 ABJS Nicolas Andry Award: The sequence of prevention: a systematic approach to prevent anterior cruciate ligament injury. *Clinical Orthopaedics & Related Research, 470*(10), 2930-2940.

Hewett, T. E., Torg, J. S., & Boden, B. P. (2009). Video analysis of trunk and knee motion during non-contact anterior cruciate ligament injury in female athletes: lateral trunk and knee abduction motion are combined components of the injury mechanism. *British Journal of Sports Medicine, 43*(6), 417-422. Retrieved from

Hicks, J. L., Uchida, T. K., Seth, A., Rajagopal, A., & Delp, S. L. (2015). Is my model good enough? Best practices for verification and validation of musculoskeletal models and simulations of movement. *Journal of Biomechanical Engineering, 137*(2), 1-24.

Hill, A. V. (1938). The heat of shortening and the dynamic constants of muscle. *Proceedings of the Royal Society of London. Series B - Biological Sciences, 126*(843), 136-195.

Hirokawa, S., Solomonow, M., Luo, Z., Lu, Y., & D'Ambrosia, R. (1991). Muscular co-contraction and control of knee stability. *Journal of Electromyography and Kinesiology, 1*(3), 199-208.

Hosseinzadeh, S., & Kiapour, A. M. (2021). Age-related changes in ACL morphology during skeletal growth and maturation are different between females and males. *Journal of Orthopaedic Research, 39*(4), 841-849.

Iwahashi, T., Shino, K., Nakata, K., Nakamura, N., Yamada, Y., Yoshikawa, H., & Sugamoto, K. (2008). Assessment of the "functional length" of the three bundles of the anterior cruciate ligament. *Knee Surgery, Sports Traumatology, Arthroscopy, 16*(2), 167-174.

Johnson, D., Coley, S. J., Kyrion, J., & Taylor, W. J. (2001). Comparing the performance of mono- and biplane fluoroscopy systems in diagnostic and interventional neuroangiography using the dose-area product. *Neuroradiology, 43*(9), 728-734.

Karrholm, J., Selvik, G., Elmqvist, L. G., Hansson, L. I., & Jonsson, H. (1988). Three-dimensional instability of the anterior cruciate deficient knee. *Journal of Bone and Joint Surgery. American Volume, 70*(5), 777-783.

Kemp, L., & Benoit, D. L. (2020). *Evaluation of Lower Limb Muscle Synergies in Paediatric Females with and without ACL Injuries. MASc Thesis.*

Khuu, A., Foch, E., & Lewis, C. (2016). Not all single leg squats are equal: a biomechanical comparison of three variations. *International Journal of Sports Physical Therapy, 11*(2), 201.

Kim, Y., Jung, Y., Choi, W., Lee, K., & Koo, S. (2018). Similarities and differences between musculoskeletal simulations of OpenSim and AnyBody modeling system. *Journal of Mechanical Science and Technology, 32*(12), 6037-6044.

Kocher, M. S., Smith, J. T., Iversen, M. D., Brustowicz, K., Ogunwole, O., Andersen, J., . . . Zurakowski, D. (2011). Reliability, validity, and responsiveness of a modified International Knee Documentation Committee Subjective Knee Form (Pedi-IKDC) in children with knee disorders. *The American Journal of Sports Medicine, 39*(5), 933-939.

Kono, K., Konda, S., Yamazaki, T., Tanaka, S., Sugamoto, K., & Tomita, T. (2020). In vivo length change of ligaments of normal knees during dynamic high flexion. *BMC Musculoskeletal Disorders, 21*(1).

Krosshaug, T. (2005). Research approaches to describe the mechanisms of injuries in sport: limitations and possibilities. *British Journal of Sports Medicine, 39*(6), 330-339.

Ladenhauf, H. N., Graziano, J., & Marx, R. G. (2013). Anterior cruciate ligament prevention strategies: are they effective in young athletes - current concepts and review of literature. *Current Opinion in Pediatrics, 25*(1), 64-71.

Lafortune, M. A., Cavanagh, P. R., Sommer, H. J., & Kalenak, A. (1992). Three-dimensional kinematics of the human knee during walking. *Journal of Biomechanics, 25*(4), 347-357.

Larsson, S., B., & Karlsson, J. (1978). Histochemical and biochemical changes in human skeletal muscle with age in sedentary males, age 22-65 years. *Acta Physiologica Scandinavica, 103*, 31-39.

Leardini, A., Chiari, L., Della Croce, U., & Cappozzo, A. (2005). Human movement analysis using stereophotogrammetry. Part 3. Soft tissue artifact assessment and compensation. *Gait & Posture, 21*, 212–225.

Lenhart, R. L., Kaiser, J., Smith, C. R., & Thelen, D. G. (2015). Prediction and Validation of Load-Dependent behavior of the tibiofemoral and patellofemoral joints during movement. *Annals of Biomedical Engineering, 43*(11), 2675-2685.

Lephart, S. M., Ferris, C. M., Riemann, B. L., Myers, J. B., & Fu, F. H. (2002). Gender differences in strength and lower extremity kinematics during landing. *Clinical Orthopaedics and Related Research, 401*, 162-169.

Levine, J. W., Kiapour, A. M., Quatman, C. E., Wordeman, S. C., Goel, V. K., Hewett, T. E., & Demetropoulos, C. K. (2013). Clinically relevant injury patterns after an anterior cruciate ligament injury provide insight into injury mechanisms. *The American Journal of Sports Medicine, 41*(2), 385-395.

Li, G., Defrate, L. E., Sun, H., & Gill, T. J. (2004). In vivo elongation of the anterior cruciate ligament and posterior cruciate ligament during knee flexion. *The American Journal of Sports Medicine, 32*(6), 1415-1420.

Li, G., Moses, J. M., Papannagari, R., Pathare, N. P., DeFrate, L. E., & Gill, T. J. (2006). Anterior cruciate ligament deficiency alters the in vivo motion of the tibiofemoral cartilage contact points in both the anteroposterior and mediolateral directions. *Journal of bone and Joint Surgery, 88*(8), 1826-1834.

Lund, M. E., De Zee, M., Andersen, M. S., & Rasmussen, J. (2012). On validation of multibody musculoskeletal models. *Proceedings of the Institution of Mechanical Engineers, Part H: Journal of Engineering in Medicine, 226*(2), 82-94.

Lysholm, J., & Tegner, Y. (2007). Knee injury rating scales. *Acta orthopaedica, 78*(4), 445-453.

Majewski, M., Susanne, H., & Klaus, S. (2006). Epidemiology of athletic knee injuries: A 10-year study. *The Knee, 13*(3), 184-188.

Mansouri, M., & Reinbolt, J. (2012). A platform for dynamic simulation and control of movement based on OpenSim and MATLAB. *Journal of Biomechanics, 45*(8), 1517–1521.

Mantovani, G., & Lamontagne, M. (2017). How different marker sets affect joint angles in inverse kinematics framework. *Journal of Biomechanical Engineering, 139*(4), 044503.

Markolf, K. L., O'Neill, G., Jackson, S. R., & McAllister, D. R. (2004). Effects of applied quadriceps and hamstrings muscle loads on forces in the anterior and posterior cruciate ligaments. *The American Journal of Sports Medicine, 32*(5), 1144-1149.

Marra, M. A., Vanheule, V., Fluit, R., Koopman, B., Rasmussen, J., Verdonschot, N., & Andersen, M. S. (2015). A subject-specific musculoskeletal modeling framework to predict in vivo mechanics of total knee arthroplasty. *Journal of Biomechanical Engineering, 137*(2).

Marshall, W. A., & Tanner, J. M. (1969). Variations in pattern of pubertal changes in girls. *Archives of Disease in Childhood, 44*(235), 291.

Marshall, W. A., & Tanner, J. M. (1970). Variations in the pattern of pubertal changes in boys. *Archives of Disease in Childhood, 45*(239), 13-23.

Miranda, D. L., Rainbow, M. J., Crisco, J. J., & Fleming, B. C. (2013). Kinematic differences between optical motion capture and biplanar videoradiography during a jump–cut maneuver. *Journal of Biomechanics, 46*(3), 567-573.

Miyaji, G., K., Kidera, K., Ikuta, F., Yoneta, K., Shindo, H., Osaki, M., & Yonekura, A. (2012). In vivo kinematics of the anterior cruciate ligament deficient knee during wide-based squat using a 2D/3D registrationtechnique. *Journal of Sports Science & Medicine, 11*, 695-702.

Modenese, L., & Renault, J. (2021). Automatic generation of personalised skeletal models of the lower limb from three-dimensional bone geometries. *Journal of Biomechanics, 116*, 110186 1-11.

Murakami, K., Hamai, S., Okazaki, K., Ikebe, S., Shimoto, T., Hara, D., . . . Iwamoto, Y. (2016). In vivo kinematics of healthy male knees during squat and golf swing using image-matching techniques. *The Knee, 23*(2), 221-226.

Myer, G. D., Schmitt, L. C., Brent, J. L., Ford, K. R., Barber Foss, K. D., Scherer, B. J., . . . Hewett, T. E. (2011). Utilization of modified NFL combine testing to identify functional deficits in athletes following ACL reconstruction. *Journal of Orthopaedic & Sports Physical Therapy, 41*(6), 377-387.

Nagano, Y., Ida, H., Akai, M., & Fukubayashi, T. (2006). Gender differences in knee kinematics and muscle activity during single limb drop landing. *The Knee, 14*(3), 218-223.

Neumann. (2010). Kinesiology of the Musculoskeletal System: Foundations forRehabilitation. *Mosby/Elsevier, 2nd ed.*

Otsuki, R., Del Bel, M. J., & Benoit, D. L. (2021). Sex differences in muscle activation patterns associated with anterior cruciate ligament injury during landing and cutting tasks: A systematic review. *Journal of Electromyography and Kinesiology, 60*, 102583 1-14.

Park, S. E., DeFrate, L. E., Suggs, J. F., Gill, T. J., Rubash, H. E., & Li, G. (2006). Erratum to "The change in length of the medial and lateral collateral ligaments during in vivo knee flexion". *The Knee, 13*(1), 77-82.

Pataky, T. C. (2010). Generalized n-dimensional biomechanical field analysis using statistical parametric mapping. *Journal of Biomechanics, 43*(10), 1976-1982.

Paterno, M. V., Rauh, M. J., Schmitt, L. C., Ford, K. R., & Hewett, T. E. (2014). Incidence of second ACL injuries 2 years after primary ACL reconstruction and return to sport. *The American Journal of Sports Medicine, 42*(7), 1567-1573.

Paterno, M. V., Schmitt, L. C., Ford, K. R., Rauh, M. J., Myer, G. D., Huang, B., & Hewett, T. E. (2010). Biomechanical measures during landing and postural stability predict second anterior cruciateligament injury after anterior cruciate ligament reconstruction and return to sport. *The American Journal of Sports Medicine, 38*(10), 1968-1978.

Potvin, B. (2016). Predicting Muscle Activations in a Forward-Inverse Dynamics Framework Using Stability-Inspired Optimization and an In Vivo-Based 6DoF Knee Joint. *University of Ottawa*. *MASc Thesis*.

Prodromos, C. C., Han, Y., Rogowski, J., Joyce, B., & Shi, K. (2007). A meta-analysis of the incidence of anterior cruciate ligament tears as a function of gender, sport, and a knee injury–reduction regimen. *Arthroscopy: The Journal of Arthroscopic & Related Surgery, 23*(12), 1320-1325.

Qi, W., Hosseini, A., Tsai, T., Li, J., Rubash, H., & Li, G. (2013). In vivo kinematics of the knee during weight bearing high flexion. *Journal of Biomechanics, 46*(9), 1576-1582.

Quapp, K. M., & Weiss, J. A. (1998). Material characterization of human medial collateral ligament. *Journal of Biomechanical Engineering, 120*(6), 757-763.

Rajagopal, A., Dembia, C. L., DeMers, M. S., Delp, D. D., Hicks, J. L., & Delp, S. L. (2016). Full-body musculoskeletal model for muscle-driven simulation of human gait. *IEEE Trans Biomed Eng, 63*(10), 2068-2079.

Renstrom, P., Ljungqvist, A., Arendt, E., Beynnon, B., Fukubayashi, T., Garrett, W., . . . Engebretsen, L. (2008). Non-contact ACL injuries in female athletes: an International Olympic Committee current concepts statement. *British Journal of Sports Medicine, 42*(6), 394-412.

Robertson, D. G. E., Caldwell, G. E., Hamill, J., Kamen, G., & Whittlesey, S. (2013). *Research Methods in Biomechanics*. Human kinetics.

Romanchuk, N. J., & Benoit, D. L. (2019). Sex-Specific Neuromuscular and Kinematic Analysis Of Unanticipated Single-leg Landings in Young Althetes. *University of Ottawa*. *MASc Thesis*.

Romanchuk, N. J., Del Bel, M. J., & Benoit, D. L. (2020). Sex-specific landing biomechanics and energy absorption during unanticipated single-leg drop-jumps in adolescents: implications for knee injury mechanics. *Journal of Biomechanics, 113*, 110064 1-7.

Rudolph, K. S., Axe, M. J., & Snyder-Mackler, L. (2000). Dynamic stability after ACL injury: who can hop? *Knee Surgery, Sports Traumatology, Arthroscopy, 8*(5), 262-269.

Salem, G. J., Salinas, R., & Harding, F. V. (2003). Bilateral kinematic and kinetic analysis of the squat exercise after anterior cruciate ligament reconstruction. *Archives of Physical Medicine and Rehabilitation, 84*(8), 1211-1216.

Scarvell, J. M., Smith, P. N., Refshauge, K. M., Galloway, H., & Woods, K. (2005). Comparison of kinematics in the healthy and ACL injured knee using MRI. *Journal of Biomechics, 38*(2), 255-262.

Schmitz, A., & Piovesan, D. (2016). Development of an Open-Source, Discrete element knee model. *IEEE Transactions on Biomedical Engineering, 63*(10), 2056-2067.

Selvik, G. (1989). Roentgen stereophotogrammetry. *Acta Orthopaedica Scandinavica, 60*(sup232), 1-51.

Servant, C. T., Ramos, J. P., & Thomas, N. P. (2004). The accuracy of magnetic resonance imaging in diagnosing chronic posterior cruciate ligament injury. *The Knee, 11*(4), 265-270.

Shea, K. G., Pfeiffer, R., Wang, J. H., Curtin, M., & Apel, P. J. (2004). Anterior cruciate ligament injury in pediatric and adolescent soccer players: an analysis of insurance data. *Journal of Pediatric Orthopaedics, 24*(6), 623-628.

Shin, C. S., Chaudhari, A. M., & Andriacchi, T. P. (2011). Valgus plus internal rotation moments increase anterior cruciate ligament strain more than either alone. *Medicine & Science in Sports & Exercise, 43*(8), 1484-1491.

Shin, Y. K., Ryu, K. K., Park, J. S., Lee, J. E., Jin, W., Park, S. Y., . . . Lee, K. R. (2014). Biceps femoris tendon and lateral collateral ligament: analysis of insertion pattern using MRI. *Journal of the Korean Society of Magnetic Resonance in Medicine, 18*(3), 225.

Smale, K. B., Conconi, M., Sancisi, N., Krogsgaard, M., Alkjaer, T., Parenti-Castelli, V., & Benoit, D. L. (2019). Effect of implementing magnetic resonance imaging for patient-specific OpenSim models on lower-body kinematics and knee ligament lengths. *Journal of Biomechanics, 83*, 9-15.

Solomonow, M., Baratta, R., Zhou, B. H., Shoji, H., Bose, W., Beck, C., & D'Ambrosia, R. (1987). The synergistic action of the anterior cruciate ligament and thigh muscles in maintaining joint stability. *The American Journal of Sports Medicine, 15*(3), 207-213.

Stijak, L., Radonjić, V., Nikolić, V., Blagojević, Z., Aksić, M., & Filipović, B. (2009). Correlation between the morphometric parameters of the anterior cruciate ligament and the intercondylar width: gender and age differences. *Knee Surgery, Sports Traumatology, Arthroscopy, 17*, 812-817.

Tashman, S., & Anderst, W. (2003). In-Vivo Measurement of Dynamic Joint Motion Using High Speed Biplane Radiography and CT: Application to Canine ACL Deficiency. *Journal of Biomechanical Engineering, 125*(2), 238-245.

Tashman, S., Collon, D., Anderson, K., Kolowich, P. A., & Anderst, W. (2004). Abnormal rotational knee motion during running after anterior cruciate ligament reconstruction. *The American Journal of Sports Medicine, 32*(4), 975-983.

Trinler, U., Schwameder, H., Baker, R., & Alexander, N. (2019). Muscle force estimation in clinical gait analysis using AnyBody and OpenSim. *Journal of Biomechanics, 86*, 55-63.

Tschauner, S., Sorantin, E., Singer, G., Eberl, R., Weinberg, A., Schmidt, P., & Kraus, T. (2016). The origin points of the knee collateral ligaments: an MRI study on paediatric patients during growth. *Knee Surgery, Sports Traumatology, Arthroscopy, 24*(1), 18-25.

Uchida, T. K., & Seth, A. (2022). Conclusion or Illusion: Quantifying uncertainty in inverse analyses from marker-based motion capture due to errors in marker registration and model scaling. *Frontiers in Bioengineering and Biotechnology, 10*, 874725 1-11.

Walker, P. S., Rovick, J. S., & Robertson, D. D. (1988). The effects of knee brace hinge design and placement on joint mechanics. *Journal of Biomechanics, 21*(11), 965-974.

Withrow, T. J., Huston, L. J., Wojtys, E. M., & Ashton-Miller, J. A. (2008). Effect of varying hamstring tension on anterior cruciate ligament strain during in vitro impulsive knee flexion and compression loading. *The Journal of Bone and Joint Surgery-American Volume, 90*(4), 815-823.

Woo, S., Abramowitch, S. D., Kilger, R., & Liang, R. (2006). Biomechanics of knee ligaments: injury, healing, and repair. *Journal of Biomechanics, 39*(1), 1-20.

Wright, R. W., Haas, A. K., Anderson, J., Calabrese, G., Cavanaugh, J., Hewett, T. E., . . . Group, M. (2015). Anterior cruciate ligament reconstruction rehabilitation: MOON Guidelines. *Sports Health, 7*(3), 239-243.

Xu, H., Bloswick, D., & Merryweather, A. (2015). An improved OpenSim gait model with multiple degrees of freedom knee joint and knee ligaments. *Computational Methods in Biomechanics and Biomedical Engineering, 18*(11), 1217-1224.

Yamazaki, J., Muneta, T., Ju, Y. J., & Sekiya, I. (2010). Differences in kinematics of single leg squatting between anterior cruciate ligament-injured patients and healthy controls. *Knee Surgery, Sports Traumatology, Arthroscopy, 18*(1), 56-63.

Yoo, Y., Jeong, W., Shetty, N. S., Ingham, S. J., Smolinski, P., & Fu, F. H. (2010). Changes in ACL length at different knee flexion angles: an in vivo biomechanical study. *Knee Surgery, Sports Traumatology, Arthroscopy, 18*(3), 292-297.

Yu, B., & Garrett, W. E. (2007). Mechanisms of non-contact ACL injuries. *British Journal of Sports Medicine, 41*(Supplement 1), 47-i51.

Zabala, M. E., Favre, J., & Andriacchi, T. P. (2015). Relationship between knee mechanics and time since injury in ACL-deficient knees without signs of osteoarthritis. *The American Journal of Sports Medicine, 43*(5), 1189-1196.

Zajac, F. E. (1989). Muscle and tendon: properties, models, scaling and application to biomechanics and motor control. *Critical Reviews in Biomedical Engineering, 17*, 359-411.

9.0 Appendix

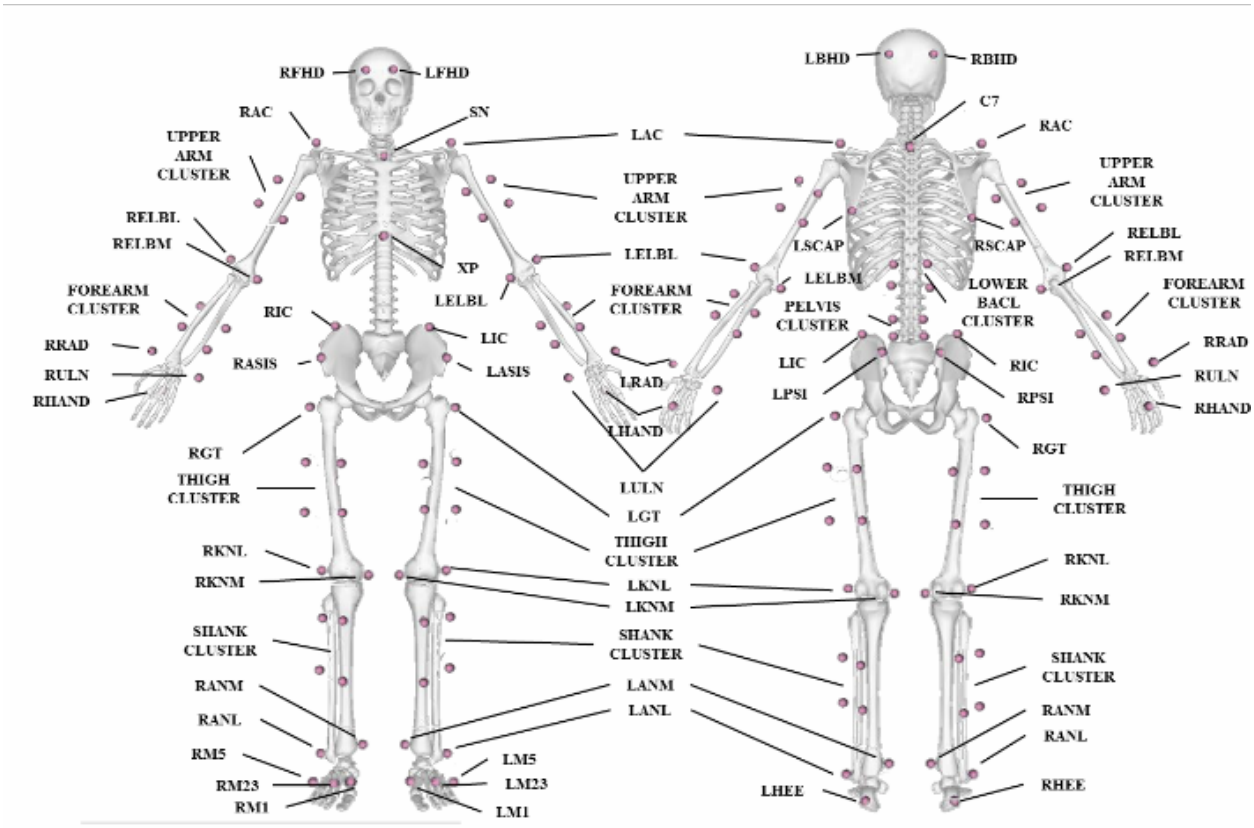

Figure A 9.1: CBRU motion tracking markers used in data collections, from Mantovani & Lamontagne 2017.